The influence of uniform and non-uniform fluid oscillations on particle settling and migration behavior

R.G. van de Wetering

March 2016

Delft University of Technology

TU Delft Delft University of Technology

Challenge the future

The influence of uniform and non-uniform fluid oscillations on particle settling and migration behavior

by

R.G. van de Wetering

in partial fulfilment of the requirements for the degree of

Master of Science
in Offshore & Dredging Engineering (ODE)
- track Dredging Engineering

at the Delft University of Technology, Faculty of Mechanical, Maritime and Materials Engineering
to be defended publicly on Wednesday March 30, 2016 at 02:00 PM.

Student number:	4256182	
Supervisor:	Prof. dr. ir. C. van Rhee	TU Delft
Thesis committee:	Dr. ir. A.M. Talmon	TU Delft
	Dr. ir. C. Chassagne	TU Delft
	Ir. R.H.A. Kuypers	Royal IHC
	Ir. E.C. van der Blom	Royal IHC
	Drs. N. Stam	Stamsolve

TU Delft Delft University of Technology

IHC

Preface

This thesis report is the final result of my Master of Science (MSc) project. This project was the last step to be taken in fulfilment of the MSc program Offshore and Dredging Engineering (ODE) at Delft University of Technology (DUT).

The project was provided by Royal IHC, located at Kinderdijk in the Netherlands. Throughout my thesis project I received help and guidance from both my supervisor at Royal IHC as well as my professor and daily supervisor from the University. Their help and guidance enabled me to write this thesis. I would like to use this section of the report to express my gratitude towards everybody.

First of all, I would like to thank my colleagues at Royal IHC, in particular my supervisor Ron Kuypers and chief Erik van der Blom. Throughout the entire project Ron was always present to discuss certain issues and available to read my report, ensuring the quality of my work. Besides being serious and thinking about the subject, there was also room to have a laugh. Especially at times when papers needed to be read daily, it helped me to relax and find the inspiration to keep on going. Erik offered me the chance to graduate on this interesting subject within Royal IHC, for which I'm truly thankful.

Secondly, I would like to thank Nijs Stam, as he can be seen as the founding father of this thesis project. Without Nijs' first hypothesis, I would not have done this interesting and challenging research as my thesis project.

From the Delft University of Technology, I would like to thank my professor, Cees van Rhee and daily supervisor Arno Talmon for the academical guidance. The monthly meetings helped me in decision making and improved the quality of my work.

Last, but not least, I would like to thank my mother and brothers for supporting me and listening to my attempts explaining what I'm doing during the project.

I hope you all enjoy reading this document.

Best regards,
Rick van de Wetering

March 18, 2016

Abstract

In 2006, N. Stam (Stamsolve) performed small scale experimental research (settling tube with internal diameter $D \approx 120\,mm$) to investigate whether the hindered settling process could be improved for silt and fine sand fractions ($d = 170 - 15\ \mu m$). Hindered settling (Richardson and Zaki, 1954) causes the average settling velocity of the solid particles to decrease due to the presence of neighboring particles (Winterwerp, 2002). N. Stam visually observed that the presence of a repeating shock wave through a settling mixture could influence the hindered settling process such that the average settling velocity increased (or the negative influence of the hindered settling process decreased). A shock wave was defined as a single input of energy which creates a propagating pressure wave.

Two hypotheses were created based on different physical processes. N. Stam's hypothesis was based on the dissipation of return flow energy by applying a shock wave perpendicular to the settling direction (Stam, 2007). J. van Wijk's hypothesis did not include an increase in hindered settling velocity, but mentioned that only compaction of the bed layer would occur (Van Wijk, 2013). A collaboration between Royal IHC and Stamsolve resulted in small scale and semi-industrial scale model experiments to investigate N. Stam's hypothesis. During the experiments, inconsistencies in observed settling behavior caused only partially satisfactory results. It was therefore concluded that the physical processes were not fully understood.
To investigate these physical processes, this thesis project was created, starting with an elaborate literature study (Van de Wetering, 2015b). The hypothesis by Van Wijk (2013) was concluded to be correct and some boundary conditions were established. Regarding the hypothesis by Stam (2007), it was concluded that shock waves do not effect the hindered settling velocity positively. A velocity field perpendicular to the settling direction causes a higher drag force and a longer traveling distance for the particles to settle. However, during the literature study an interesting technique was found, where non-uniform (sawtooth-like) fluid oscillations proved to be capable of levitation solid spherical particles against gravity (Van Oeveren and Houghton, 1971). The particle response motion to a non-stagnant fluid could be described using a differential equation suggested by Boussinesq (1885), Basset (1888) and Oseen (1927). This equation is referred to as the *BBO-equation*.

The goal of this thesis is to theoretically and numerically investigate whether the hindered settling influences can be decreased by an oscillatory motion of the fluid. This oscillatory motion can either be *uniform* or *non-uniform*.

Uniform oscillations are described by a *sinusoidal* fluid displacement whereas non-uniform fluid oscillations are described by a *sawtooth* wave fluid displacement. The BBO-equation was adjusted to account for fluid oscillations and implemented in MATLAB. Two different scenarios which could lead to a possible increase in the average hindered settling velocity were developed.

The first scenario is based on the "vein-like" principle described by Kuenen (1968). He found that particles have a natural tendency to fall in vertically oriented clusters or "veins", creating drainage paths to dissipate the pore water (horizontal density gradient). This phenomenon is called *settling convection* and decreases the hindered settling effects (Kranenburg and Geldof, 1974). These findings, combined with the BBO-equation, were implemented in MATLAB and solved for the particle response velocities as function of the fluid oscillations. It was found that non-uniform oscillations are indeed capable of migrating a single solid particle horizontally, artificially creating Kuenen's veins. Using a fluid amplitude of $5\ mm$ and a frequency of $40\ Hz$, an average horizontal relative particle velocity of approximately two times the terminal settling velocity was found, using a particle diameter $d = 100\ \mu m$. It is important to note that these findings are highly theoretical, as the sawtooth wave shape used as fluid displacement input will be extremely hard to reproduce in practice due to system properties such as friction and inertia.

The direction of migration was found to be dependent on the direction of the highest velocity, caused by the differentiated sawtooth fluid displacement. Although the model does not take concentration into account, it strongly suggests that two veins (horizontal density gradient) can be created using this technique. One of the veins will contain the migrated particles, so the mixture density will be high. The other vein will act as the drainage path, dissipating the water and creating a convection flow, increasing the average hindered settling velocity.

The second scenario is also based on experimental results published by Van Oeveren and Houghton (1971). As mentioned, they experimentally demonstrated that it is possible to make particles hover or even rise against gravity using vertically non-uniform oscillations with the highest velocity of the sawtooth-wave pointed upwards. Hence, the non-uniform oscillations produce a resultant force upwards which is larger than the downward gravity force. So, simply reversing the direction of the highest velocity resulted in a predicted increase in settling velocity of a single solid particle. Using an equal oscillation frequency and amplitude as during the first scenario, an increase of two and a half times the terminal settling velocity was predicted by the model.

The particle response behavior is described using an amplitude ratio (A_p/A_f) and a phase angle (φ). The response behavior was found to be dependent on the ratio between viscous forces and inertial forces. A force analysis for both mentioned scenarios showed that the viscous forces (history force and Stokes drag force) were *always* dominant, using the particle sizes of interest. When the viscosity was neglected (inviscid model), it was found that the decoupled motion (amplitude ratio) is dependent on the inertial differences between fluid and particle and no phase angle would occur. The addition of viscosity showed that the decoupled motion decreased with respect to the inviscid model and a phase difference between particle and fluid arose. In the upper limit of viscosity, it was proven that also no phase angle would occur, i.e. $\varphi = 0$. These observations together with more calculations showed that the phase angle is maximum if the ratio between viscous and inertial forces is approximately unity.

Regarding the fluid oscillations properties, it was found that the fluid amplitude more dominant than oscillation frequency if particle migration is desired.

Contents

Nomenclature viii

Introduction 1

1 Literature study review 5
- 1.1 Research Objectives . . . 5
- 1.2 Summary . . . 6
- 1.3 Conclusions . . . 8
- 1.4 Recommendations . . . 11

2 Thesis Outline 13
- 2.1 Thesis project . . . 13
- 2.2 Hypotheses . . . 14

3 Derivation inviscid & viscous models 17
- 3.1 Oscillatory Translation of Spheres in Inviscid Fluids . . . 18
- 3.2 Oscillatory Translation of Spheres in Viscous Fluids . . . 20

4 Modelling the nonlinear BBO-equation 25
- 4.1 Assumptions and simplifications . . . 25
- 4.2 Solution method . . . 26
  - 4.2.1 Particle geometry and properties . . . 26
  - 4.2.2 Oscillating fluid properties . . . 27
  - 4.2.3 ODE45 Solver . . . 33
  - 4.2.4 Decoupling and phase angle . . . 34
- 4.3 Validation . . . 35
  - 4.3.1 Herringe (1976) . . . 35
  - 4.3.2 Takahashi (1992) . . . 40

5 Inviscid particle motion results 45
- 5.1 Horizontal oscillations . . . 45
  - 5.1.1 Uniform oscillations . . . 45

5.1.2 Non-uniform oscillations . . . 48
5.2 Vertical oscillations . . . 51
5.2.1 Uniform oscillations . . . 51
5.2.2 Non-uniform oscillations . . . 53

6 Viscous particle motion results **55**
6.1 Horizontal oscillations . . . 55
6.1.1 Uniform oscillations . . . 55
6.1.2 Non-uniform oscillations . . . 58
6.1.3 Decoupling dependency on frequency . . . 60
6.1.4 Phase angle dependency on frequency . . . 62
6.1.5 Decoupling dependency on viscosity . . . 63
6.1.6 Phase angle dependency on viscosity . . . 65
6.1.7 Particle migration . . . 67
6.1.8 Force analysis . . . 70
6.2 Vertical oscillations . . . 77
6.2.1 Uniform oscillations . . . 77
6.2.2 Non-uniform oscillations . . . 79
6.2.3 Particle retardation and levitation . . . 82
6.2.4 Force analysis . . . 83

7 Conclusions & Recommendations **91**
7.1 Conclusions . . . 92
7.1.1 Increased settling velocity using horizontal fluid oscillations . . . 92
7.1.2 Increased settling velocity using vertical fluid oscillations . . . 92
7.1.3 General . . . 93
7.2 Recommendations . . . 95

A MATLAB code **97**

B Dataset Herringe (1976) **109**

C Dataset Takahashi (1992) **111**

List of Figures **114**

Bibliography **117**

Nomenclature

Acronyms

BBO	Boussinesq (1885), Basset (1888) and Oseen (1927)
CPT	Cone Penetration Test
DFT	Discrete Fourier Transform
DNS	Direct Numerical Simulation
DUT	Delft University of Technology
EOM	Equation Of Motion
FFT	Fast Fourier Transform
MSc	Master of Science
ODE	Offshore and Dredging Engineering
ODE	Ordinary Differential Equation
PRT	Particle Response Time
PSD	Particle Size Distribution
RHS	Right Hand Side
SHS	Smart Hopper Settling
TSHD	Trailing Suction Hopper Dredger

Symbols

Latin Symbols

Notation	Description	Units
a	Fourier series coefficient	$[-]$
A	Amplitude	$[\mathrm{m}]$
Ac	Acceleration number	$[-]$
Acc	Fluid acceleration parameter Herringe (1976)	$[-]$
b	Fourier series coefficient	$[-]$
$b0$	Retardation coefficient uniform oscillations	$[-]$
$b1$	Retardation coefficient non-uniform oscillations	$[-]$
c	Concentration	$[-]$
C	Coefficient	$[-]$
d	Particle diameter	$[\mathrm{m}]$
dt	Time step	$[\mathrm{s}]$
D	Settling tube diameter	$[\mathrm{m}]$
e	Void ratio	$[-]$
f	Frequency	$[\mathrm{s}^{-1}]$
F	Force	$[\mathrm{N}]$
g	Gravitational constant	$[\mathrm{m\,s}^{-2}]$
k	Slope estimation equation Runge-Kutta method	[r.u.*]
ki	Shape factor non-uniform wave (input)	$[-]$
ko	Shape factor non-uniform wave (output)	$[-]$
L	Length	$[\mathrm{m}]$
m	Mass	$[\mathrm{kg}]$
n	Exponent nonlinear drag law	$[-]$
r	Particle radius	$[\mathrm{m}]$
Re	Reynolds number	$[-]$
s	Fluid displacement (uniform oscillations)	$[\mathrm{m}]$
S	Fluid velocity (uniform oscillations)	$[\mathrm{m\,s}^{-1}]$
Sl	Strouhal number	$[-]$
St	Stokes number	$[-]$
t	Wall thickness	$[\mathrm{m}]$
t	Time	$[\mathrm{s}]$
T	Temperature	$[^{\circ}\mathrm{C}]$
u	Horizontal particle velocity	$[\mathrm{m\,s}^{-1}]$
v	Vertical particle velocity	$[\mathrm{m\,s}^{-1}]$
V	Volume	$[\mathrm{m}^3]$
w	Empirical variable	$[-]$
y	Certain variable in differential equation	[r.u.]

* r.u. = relative units.

Greek symbols

Notation	Description	Units
β	Amplitude scale	$[-]$
γ	Density ratio	$[-]$
δ	Inverse Stokes number	$[-]$
Δ	Relative density	$[-]$
Θ	Particle settling parameter	$[-]$
μ	Dynamic viscosity	$[\mathrm{Pa\ s}]$
μ	Micro	$[-]$
ν	Kinematic viscosity	$[\mathrm{m^2\ s^{-1}}]$
π	Pi	$[-]$
ρ	Density	$[\mathrm{kg\ m^{-3}}]$
τ	Dummy variable	$[-]$
τ	Time scale	$[\mathrm{s}]$
ϕ	Empirical correction factor to Stokes drag force	$[-]$
φ	Phase shift	$[\mathrm{rad}]$
ω	Angular frequency	$[\mathrm{rad}]$
Ω	Dimensionless frequency	$[-]$

Mathematical symbols

Notation	Description	Units
$d(...)/d(...)$	Specified derivative of certain parameter	$[-]$
$\bar{x}$	Mean value	$[-]$
$\int_x^y$	Bounded integral	$[-]$
∞	Infinity	$[-]$
$\lvert ... \rvert$	Absolute value	$[-]$
$\log_{10}$	Logarithm	$[-]$
$\sum_{x=1}^{\infty}$	Summation from 1 to infinity	$[-]$
$f(...)$	Function of certain parameters	$[-]$

Subscripts

Notation	Description	Units
0	Starting point Fourier Series	$[-]$
1	Empirical value Odar and Hamilton (1964)	$[-]$
1	Empirical value Ferguson and Church (2004)	$[-]$
1	First slope estimation value	$[\mathrm{r.u.}]$
2	Empirical value Ferguson and Church (2004)	$[-]$
2	Second slope estimation value	$[\mathrm{r.u.}]$
3	Third slope estimation value	$[\mathrm{r.u.}]$
4	Fourth slope estimation value	$[\mathrm{r.u.}]$
a	Added mass	$[-]$
b	Buoyancy	$[-]$
bed	Bed	$[-]$
d	Drag	$[-]$
f	Fluid	$[-]$
g	Gravity	$[-]$
h	History or Basset	$[-]$
h	Horizontal	$[-]$
$inertial$	Collection of all inertial forces	$[\mathrm{N}]$
m	Added mass	$[-]$
m	Mixture	$[\mathrm{kg\,m^{-3}}]$
$mean$	Mean or average	$[-]$
n	Amount of sine waves	$[-]$
p	Particle	$[-]$
p	Pore	$[-]$
p	Pressure	$[\mathrm{N\,m^{-2}}]$
pot	Potential theory	$[-]$
res	Resultant	$[-]$
s	Soil	$[-]$
S	Fluid velocity (uniform oscillations)	$[\mathrm{m\,s^{-1}}]$
t	Terminal	$[-]$
t	Total	$[-]$
v	Vertical	$[-]$
v	Viscous	$[-]$
v	Volumetric	$[-]$
$viscous$	Collection of all viscous forces	$[\mathrm{N}]$
w	Non-uniform oscillation	$[-]$
wx	Horizontal displacement non-uniform oscillations	$[\mathrm{m}]$
x	Horizontal displacement uniform oscillations	$[\mathrm{m}]$
y	Vertical displacement uniform oscillations	$[\mathrm{m}]$

Introduction

In the dredging industry Trailing Suction Hopper Dredgers (TSHD) are deployed to transport large quantities of sand or silt ($\sim 1.500 - 46.000\, m^3$). This can either be from the open sea to a deposit area (land reclamation) or from harbors to the open sea (maintenance work). As the name suggests, the vessel uses a suctionhead or *draghead* to create a mixture of sand and water (called a slurry) at the seabed (Figure 1). Without water being added to the sand, what is also known as *fluidization*, the sand would not be pumpable by the on board *dredgepumps*. These are centrifugal pumps that create the needed suction and discharge pressure to pump the slurry into the hopper.

Figure 1: TSHD (`http://atozhub.weebly.com/mechanical-engineers/dredging`)

The hopper can be seen as a temporary storage area where the slurry mixture is separated again by the fact that without any kinetic energy input, creating turbulence (a highly chaotic process needed to suspend the sand particles), solid particles will *settle* under the influence of gravity (*gravitational separation*). Slurry mixtures are rarely uniformly graded, which means that a lot of different particle sizes are present in the mixture. All these different sizes have different settling velocities, varying from minutes to even days. The water, which has now become of no use, is redirected overboard through the *overflow*. All the particles which did not settle, or feel sufficient horizontal force due to the flow towards the overflow, will be washed or eroded overboard.

This phenomenon of losing production (the solid material is desired) through the overflow is known as *overflow losses* and is undesired in multiple ways. Economically for the dredging operator, it will require longer dredging times to fill the hopper entirely. Environmentally it has some consequences as well: the carbon footprint per dredge cycle increases and because the overflow exits at the bottom of the vessel, a so-called *dredgeplume* emerges.

Figure 2: Overflow inside the hopper and dredgeplume behind the THSD

Considering Figure 2, the overflow is located at the bottom left, whereas the dredgeplume is visible at the top right of the figure. The presence of (usually fine) particles in the sea or harbor where the dredger is operating, creates a high *turbidity* area where low amounts of light can penetrate. Furthermore, the fine particles eventually form a "blanket" over the seabed. Both of these can be harmful for the underwater flora and fauna.

Clean water through the overflow would therefore be the ultimate goal. This means that all the different particle sizes which enter the hopper need to settle before they can reach the overflow. Extensive research has already been performed to all the physical processes which determine the overflow losses, such as; *hindered settling* (Richardson and Zaki, 1954; Van Rhee, 2002; Dankers, 2006; Te Slaa et al., 2012), eroding of particles due to horizontal currents, particle behavior in turbulent flows etc. If we neglect the turbulence and horizontal currents, than hindered settling is a very important process, which occurs when a concentration of particles settle in a fluid. This process can be compared with the velocity of multiple cars on the highway. If the amount of cars (concentration) increases, the average velocity of all cars will decrease. This principle also holds for solid particles. During this thesis project, especially the particle fractions in the range of $170 - 15\ \mu m$ are of interest (fine sand to medium silt (Matousek, 2004)), because of their low terminal settling velocities.

In 2006, N. Stam from Stamsolve performed small scale experimental research (settling tube with an internal diameter $D \approx 120\ mm$) to investigate whether the hindered settling process could be improved. He visually observed that the presence of a repeating shock wave through the settling mixture could influence the hindered settling process such that the average settling velocity increased (or the negative influence of the hindered settling process decreased).

Subsequently, N. Stam built a small model scale hopper (1:100) in which a slender vertical plate was placed. This plate added the shock wave through the settling mixture by a small but highly accelerated horizontal displacement. The obtained results from a series of experiments were partially satisfactory. A stable but relatively low improvement of the settling velocity was achieved ($\sim 3\%$) by measuring the bed growth velocity. A more dominant observation however, proved that the soil surrounding the vertical plate got compacted.

Using the visual observations, N. Stam stated the following hypothesis (Stam, 2007):

"The addition of a shock wave in a settling mixture dissipates the energy of the upward return flow in such a way that the particles no longer feel the presence of this return flow. The energy of the shock wave itself should be small enough to not be the driving force for the particles to stay longer in suspension than without any".

The term "shock wave" was defined as a single energy input which creates a horizontally propagating pressure wave through the settling mixture. The addition of a shock wave and its visible influence N. Stam called: *Smart Hopper Settling* (SHS).

Besides N. Stam, J. van Wijk from MTI Holland B.V. also created a hypothesis based on the same visual observations. His hypothesis is based on a different physical process and was described as follows (Van Wijk, 2013):

"When the sand settles naturally under the influence of gravity, a loosely packed layer is created (bed layer). By the addition of repeating shock waves this layer is compacted: the particle-particle interaction strongly increases. At the transition between hindered settling and the bed layer it is difficult to visually determine the governing process".

In 2011, a collaboration between Royal IHC and Stamsolve was established to experimentally investigate Stam's hypothesis on a larger model scale (1:4). This semi-industrial scaled hopper did not provide the satisfactory results concerning the increase of the average settling velocity. Uncertainties in obtaining a more or less homogeneous mixture and measuring the bed growth velocity, influenced the measurements such that no quantitative conclusion could be made. Compaction however, was proven to be found over the entire length of the hopper ($11m$). Still, unanswered questions remained. In order to answer these questions and achieve higher consistency, an additional small scale hopper (1:55) was built. In contrast to the previous scale models, the third scale model was made of transparent Perspex with a relatively large wall thickness (instead of thin steel walls). Again, the vertically placed plate was used to horizontally excite the settling mixture. The addition of shock waves in the settling mixture proved to have no influence on the settling velocity in this case. Furthermore, the compaction as found during previous scale experiments, was also concluded not to be present as severely as previously found.

It was concluded that the hindered settling process in combination with shock waves (fluid oscillations) was not fully understood. To better understand the physics behind this combination, this thesis project was created, starting with an elaborate literature study.

In Chapter 1 a summary of the performed literature study (Van de Wetering, 2015b) is presented. Chapter 2 will discuss the thesis outline together with the hypotheses created in response to the literature study, which will form the basis of this thesis. Chapter 3 provides an explanation and derivation of inviscid and viscous models (the BBO-equation), together with some adjustments to specific force terms, in order to increase the validity range of the viscous model. These models are used to numerically investigate the mentioned hypotheses. In Chapter 4 the numerical model created to solve the BBO-equation is presented, together with assumptions and simplifications made in order to do so. A validation study using experimental data from literature is performed, to examine the usability and accuracy of the numerical model. The particle response motion results, using the inviscid model, are presented in Chapter 5. Chapter 6 presents the particle response motion results using the viscous model. Here, multiple parameters are varied to find relations between particle response behavior and different fluid oscillation properties. Finally, in Chapter 7 conclusions regarding the hypotheses are drawn, together with some general conclusions and recommendations regarding future work.

CHAPTER 1

Literature study review

This chapter presents an overview of the literature study, which was performed to theoretically determine the influences of shock waves (fluid oscillations) on the settling behavior of solid particles. First, the research objectives are discussed, which formed the basis of the literature study. Subsequently, a summary of the literature study is presented, together with the conclusions and recommendations towards the thesis.

1.1 Research Objectives

The main research question of the thesis literature study was:

Do shock waves influence the hindered settling process and the amount of deposited material in time?

As mentioned, the definition of a shock wave reads: *a single input of energy which creates a propagating pressure wave with certain amplitude and frequency.* To answer the main research question, a number of research objectives were created:

1. What kind of natural sediment distribution, i.e. particle size and concentration as function of height (under the influence of gravity and kinetic energy) is found when no kinetic energy is added to a fluidized mixture?
2. What is the influence of a shock wave through the naturally obtained layer system?
3. How does a shock wave influence the settling velocity and the amount of deposited material?
4. What physical process governs the transitional area between the suspended layer and the deposited bed layer?
    (a) **Liquefaction** where the effective stress $\sigma' = 0$? Terzaghi's effective stress principle: $\sigma' = \sigma - p$ describes the relation between total stress (σ) and pore pressure (p). The effective stress describes the amount of contact force between the particles. When the effective stress equals zero, the pressure in the pores is equal to the present normal and shear stresses. In this case the soil acts like a liquid (quicksand) (Verruijt, 2011).

(b) **Hindered settling** principle (Richardson and Zaki, 1954) still applies? In this case the transitional area is considered to be a slowly settling layer where the terminal settling velocity is strongly dependent on the concentration.

(c) **Consolidation/compaction** of the loosely packed layer? The loosely packed layer is still suspended and settles very slowly by the gravitational force combined with a submerged weight, squeezing out the pore water uniformly over the entire surface.

(d) **Channel/cloud formation** applies? A hypothesis suggested by prof. C. van Rhee where a similar process described by (c) takes place. The only difference is the fact that the outflow of the pore water is not uniformly distributed, certain channels are created by the pore water choosing the path with the least resistance.

5. If either one or more of the hypotheses is correct then what are the boundary conditions?

Both the main research question and the research objectives aim to examine the hypotheses by N. Stam and J. van Wijk.

1.2 Summary

The literature study starts at the very basics by describing soil classification and properties. This is more or less a summary of the soil mechanics book of Verruijt (2011). Important parameters describing the gradation of the soil are given in order to distinguish different soil mixtures. Furthermore, it is described which stresses occur when the transition between settling and forming a grain skeleton takes place. This is important when considering the transitional layer as described in the research objectives.

The second chapter of the literature study goes into depth about the settling velocity of a single solid particle in a stagnant fluid. General settling velocity equations are given for different flow regimes together with visual representations. It was found that different equations still predict relatively large differences ($\sim 30\%$) in terminal settling velocity (v_t). As this project focuses at particles in the range of $170 - 15\ \mu m$, the equations by Ferguson and Church (2004) and Stokes (1851) are used during the modelling. Using the equation of motion (EOM) by Van Rhee (2002), it was found that the particle response time (PRT) is in the order of milliseconds. This proves that the particle settling in a stagnant fluid, travels almost instantaneously at its terminal settling velocity.

In chapter three a concentration of particles is considered instead of a single one. This can either be a mono-sized mixture (rarely found in practice) or a multi-sized mixture. First, an elaborate description of the hindered settling process is given, starting with the definition (Winterwerp, 2002):

hindered settling is the reduced sedimentation rate of a concentrated suspension of particles, caused by the influence of neighboring particles on the settling velocity of an individual particle within a suspension.

The presence of a concentration of particle causes seven different interaction processes to occur: return flow and wake formation, dynamic flow effect, collisions, particle-particle interaction, effective viscosity, reduced gravity and settling convection. It was found that settling convection is the only positive interaction process, named after Kuenen (1968). It describes the tendency of particles to settle in groups (clusters), temporary increasing the settling velocity.

The hindered settling velocity as function of concentration can be calculated with the well known equation from Richardson and Zaki (1954), using the exponent m from Rowe (1987). It was found that the settling velocity decreased with approximately 80%, using a volumetric concentration $c_v = 0.3$ and particle sizes $d < 100\ \mu m$.

Te Slaa et al. (2012) discussed the settling velocity of silt water mixtures using non-cohesive sediment with particle sizes $d = 2 - 63\ \mu m$. They found that the particle flux can be divided into three phases: a hindered settling phase and two consolidation phases. The hindered settling phase will evolve to the first consolidation phase when a volumetric concentration $c_v \approx 0.4$ is reached. At this concentration, a structure between the solid particles is created. At the first consolidation phase *permeability* and *effective stress* are dominant until the volumetric concentration of the structure increases to approximately $c_v \approx 0.55$ (this increase is created by the outflow of pore water). Now, the second consolidation phase starts, where *compaction* and *creep* are dominant.

Because of the mentioned *settling convection* process being a positive side effect from having a concentration of particles, the behavior of particles settling in a cluster is the last subject of the third chapter. Kuenen (1968) experimentally showed that two types of settling convection can occur: a *chaotic*-type or a *vein*-type.
Kajishima and Takiguchi (2002) showed that *wake-induced clusters* are predicted using a Direct Numerical Simulation (DNS) method, at relatively low volumetric concentrations $c_v \approx 0.002$ using relatively heavy particles $(\rho_p/\rho_f \approx 10)$. The clustering process is mentioned to be a cycle between cluster formation, break-up and reforming. All three mentioned cluster types cause the settling velocity to temporary (in the order of PRT) increase due to the increased weight. Increasing shear stresses eventually break up the formed clusters.

The fourth chapter of the literature study is about the effects of shock waves (fluid oscillations) through a settling or settled mixture of solid particles within a fluid. First the properties of acoustic waves through suspensions are covered. It is found that the velocity of sound waves increases with increasing solids fraction (dependent on particle size). Subsequently, the wave propagation velocity in slurry pipe flow and porous granular material is discussed.
When the mixture is settled, it is interesting to determine the effects of shock waves through the bed layer. It was found that two types of compaction are often used in the dredging industry: *Dynamic impact compaction* and *vibratory compaction.* The first method uses a pounder (heavy weight), dropped form a certain height to introduce a shock wave through the soil, which is almost exactly equal to the slender vertical plate used by Kuypers et al. (2011); Kuypers and Stam (2013a,b, 2014). This shock wave results in compression of the soil together with partial liquefaction and the creation of drainage paths. An empirical relation was found to predict the depth of influence (Mayne et al., 1984). The second method uses continuous vibrations to compact the soil. The vibration frequency has to be at the resonance frequency $(15 - 20\,Hz)$ of the soil in order to compact the soil effectively.

Chapter four closes with two interesting techniques using continuous oscillations (both fluid and acoustic) to manipulate solid particles, suspended in a fluid. The technique which uses fluid oscillations is described by Houghton (1963, 1966); Baird et al. (1967). Vertical sinusoidal (uniform) fluid oscillations were used to retard solid spherical particles from traveling at their terminal settling velocity. Furthermore, Van Oeveren and Houghton (1971) experimentally showed that the use of non-uniform oscillations (sawtooth-like wave shape) in vertical direction were capable of levitating solid particles against gravity. They used the *nonlinear Langevin equation* in order to predict the measured data, but found that the retardation could not be accurately predicted.

The second technique uses ultrasonic standing-waves to migrate solid particle toward the antinodes (Whitworth et al., 1991; Whitworth and Coakley, 1992; Benes et al., 2001). This causes the particles to form clusters in a vertical string configuration (similar to the vein-type settling convection as described by Kuenen (1968)). After the formation of the vertical string of clusters, the transducer (which creates the ultrasonic standing-waves either by reflection or a second transducer) is turned off. The string of clusters will start to settle under the influence of gravity, resulting in an increased settling velocity by a factor 1000. Unfortunately, this technique limited because of scaling possibilities.

The fifth and last chapter in the literature study discusses the hypotheses (Stam, 2007; Van Wijk, 2013) and the physical SHS experiments, performed a few years ago. At first, the theory used at that time was analyzed and it was found that certain aspects were not interpreted correctly. During the experiments, it was found that a three layer system would occur (dependent on concentration). The SHS technology focused on the so-called "soup-layer" which could not be described using *hindered settling*. This layer did already become a part of the bed layer, but remained liquefied due to the high pore pressure and low permeability because *segregation* was present. The addition of shock waves to this layer causes the particles to rearrange, creating drainage paths to dissipate the pore water and therefore *compacting* the bed layer. Furthermore, it was thought that hindered settling would only occur when the solids mixture was *well-graded*, which is not the case (Winterwerp, 2002).

1.3 Conclusions

The conclusions made at the end of the literature study, answering the main research question and the research objectives, are repeated here. First, the main research question as formulated at the start of the literature study is repeated and answered:

Do shock waves influence the hindered settling process and the amount of deposited material in time?

The shock waves, as applied during the SHS experiments, do indeed influence the hindered settling process (hereafter sedimentation process). By introducing a velocity field perpendicular to the sedimentation direction in the form of a single oscillation (uniform or non-uniform), it is expected that the drag coefficient C_d will increase up to $2C_d$. This expectation is based on experiments where vertical retardation of multiple spherical particles was found as a result of oscillatory fluid motion (Houghton, 1963, 1966; Baird et al., 1967; Houghton, 1968). The results of these experiments were theoretically examined using the *Langevin equation*. Because of the particle sizes used during the experiments, in combination with the amplitude of the shock wave, it is expected that the particles will follow the horizontal oscillation. This causes the overall distance, which has to covered to settle completely, to increase. The amount of deposited material as function of time t will therefore decrease as well.

As for the research objectives, these will be answered in the same order as they have been described:

1. **What kind of natural sediment distribution, i.e. particle size and concentration as function of height (under the influence of gravity and kinetic energy) is found when no kinetic energy is added to a fluidized mixture?**

   In the dredging industry, typically found mixture densities (ρ_m) are in the range $1100 - 1600\ kg/m^3$. Corresponding volumetric concentrations c_v are found to be in the range $0.1 - 0.4$. Besides the amount of particles, the Particle Size Distribution (PSD) is of importance. Obviously, when considering a narrow graded (or mono-sized) mixture, the particle size and concentration are **not** a function of the height of the settled bed.

   In the case of a well-graded mixture, the particle size and concentration are found to be a function of the height of for instance the settling column or hopper (Ooijens et al.). Until the concentration of the mixture reaches approximately the concentration of the bed $c_v = c_{bed}$ which is found to be approximately $c_v = c_{bed} \approx 0.45$, a physical process called *segregation* will be present. Segregation is caused by the weight differences between the various particle sizes found in a well-graded mixture. Because of these weight differences, larger particles will travel faster than smaller particles. If volumetric concentrations are as high as the bed concentration, segregation is reduced, as measurements showed reduced vertical concentration gradients (Te Slaa et al., 2012).

   In this specific situation, the largest particles will be found at the bottom, while the smallest particles will be found at the top of the settled bed. Therefore, there can be concluded that the particle size as well as the concentration and permeability are a function of the height of bed layer. The volumetric concentration will increase with increasing height of the bed layer, while the permeability will decrease with increasing height of the bed layer.

2. **What is the influence of a shock wave through the naturally obtained layer system?**

   The influence of a shock wave through the naturally obtained layer system can be compared with a pounder (weight) being dropped from a certain height. This technique is used to compact granular soil and is also known as *dynamic impact compaction.*

   The shock or compression waves and high stresses induced by dropping the pounder result in compression of the soil, together with partial liquefaction and the creation of preferential drainage paths through which pore water can be dissipated. The dissipation of pore water automatically lowers the pore pressure, leading to an increase in effective stress. Furthermore, the *void ratio* ($e = V_p/V_s$) reduces, resulting in compaction of the soil (Mayne et al., 1984; Pan and Selby, 2002; Gupta et al., 2013).

   As mentioned in the previous research objective (1), segregation often occurs when typical dredging concentrations are used. The segregation process has a negative influence on the compaction effect, as the permeability decreases with increasing height of the bed. In the PSD used to perform the SHS experiments a clay fraction was present, which created an impermeable layer on top of the bed because of segregation.

3. **How does a shock wave influence the settling velocity and the amount of deposited material?**

   During the literature study, no publication or paper was found where the exact influence or relation of a shock wave on the terminal settling velocity was described. In all cases, a continuous input of vibratory energy was used instead of a single input. Publications were found describing the influence of a suspension on pressure and acoustic wave propagation, velocity and attenuation (Paterson, 1956; Atkinson and Kytömaa, 1992; Wenliang et al., 1998).

   On the other hand, publications were found describing the influence of acoustic waves on the solid phase of the suspension (particles). Using ultrasonic standing-waves it was showed that settling convection after Kuenen (1968) could be created and manipulated. Experiments were performed using multiple particle sizes (spherical and non-spherical) and a theory was created for the use of acoustic radiation forces (Whitworth et al., 1991; Whitworth and Coakley, 1992; Benes et al., 2001). On a small scale it was even showed that it would be possible to use this technique during a continuous flow situation. By the growing of clusters mechanism using ultrasonic standing-waves, clusters become large and heavy enough to settle by gravity against the continuous flow (Hawkes and Coakley, 1996; Prest et al., 2015).

   Besides the use of high frequency (ultrasonic) standing-waves, research was performed using low frequency, vertically oscillating fluids in which particles were led to settle (Houghton, 1963, 1966; Baird et al., 1967; Houghton, 1968). It was found that uniform and non-uniform vertically oscillating fluids cause retardation in the terminal settling velocity. Increasing frequency and amplitude could even make particles hover ($v_t \approx 0$) or rise against gravity (non-uniform oscillations). The occurrence of the retarded motion was theoretically explained by an increase in drag coefficient C_d and the drag exponent n of the nonlinear drag law, using the *nonlinear Langevin equation*.

   By introducing a velocity field perpendicular to the sedimentation direction in the form of a single oscillation (uniform or non-uniform), it is expected that the drag coefficient C_d will increase up to $2C_d$. Furthermore, because of the particle sizes used during the experiments, in combination with the amplitude of the shock wave, it is expected that the particles will follow the horizontal oscillation. This causes the overall distance, which has to covered to settle completely, to increase. The amount of deposited material as function of time t will therefore decrease as well.

4. **What physical process governs the transitional area between the suspended layer and the deposited bed layer?**

   The transitional area (or soup-layer according to Stam (2007)) is not governed by a single physical process. As the hindered settling process reaches its final stage, only the very small particles (fine silt and clayey particles) are found in the transitional layer. Visually no signs of hindered settling can be observed any more, as a structure has been formed ($c_v \approx 0.4$). When segregation was present due to a regular volumetric particle concentration, the *permeability* of the layer is found to be a function of its height. Two *consolidation* phases can be distinguished (Te Slaa et al., 2012). During the first consolidation phase the governing physical processes are *permeability* and *effective stress*. As time proceeds, a second consolidation phase will start at a volumetric concentration $c_v \approx 0.55$. From here the governing physical processes were found to be *compaction* and *creep*. The initial volumetric concentration (when all the solid particles are still in suspension) determines if segregation will take place and how the sedimentation process looks like (Kynch, 1952).

5. **If either one or more of the hypotheses is correct then what are the boundary conditions?**

   The hypothesis by Van Wijk (2013) about compacting the naturally formed bed layer, was proven to be correct. It was found that indeed compaction had taken place during the SHS experiments conducted by Kuypers and Stam. Boundary conditions of compaction were mentioned by Massarsch (1991) with the use of a compactibility graph, which can only be determined by performing a Cone Penetration Test (CPT).

   Furthermore, Mayne et al. (1984) compared 128 sites to create an empirical equation which approximates the depth of influence as function of the amount of energy per blow. The used SHS energy proved to be too low to influence the settled mixture over the entire length of the industrial scaled hopper. It was therefore concluded that the walls of the hopper played an important role during the performed experiments (Kuypers et al., 2011; Kuypers and Stam, 2013a,b, 2014). Because of the enclosure by thin steel walls, the shock wave could be transferred over the entire length. In the case of the small scaled Perspex hopper, this process could not occur by the much larger wall thickness over the length (t/L) ratio. Further boundary conditions were left untouched, as compaction is not the main interest.

   As for the hypothesis by Stam (2007), it was already mentioned that no direct validation could be made with the use of literature. The conclusions stated by Houghton (1966); Baird et al. (1967); Van Oeveren and Houghton (1971) created the expectation that the addition of a shock wave in horizontal direction, perpendicular to the settling direction, creates a higher drag force. Furthermore, the particle sizes used during the experiments, were relatively small compared with the used amplitudes of the shock wave. It is expected that the particles will follow the horizontal fluid oscillation causing the overall distance, which has to covered by the particles to settle completely, to increase. This retards the particle instead of improve its settling velocity.

1.4 Recommendations

The mentioned technique by Van Oeveren and Houghton (1971) of using non-uniform fluid oscillations to make solid spherical particles with a density greater than that of the fluid $(\rho_p > \rho_f)$ hover (no absolute vertical displacement) or even levitate (absolute vertical motion against gravity), proved to be very interesting.

After reading more articles using the same technique, it was found that these fluid oscillations could be uniform (Odar and Hamilton, 1964; Odar, 1966; Baird et al., 1967; Tunstall and Houghton, 1968; Houghton, 1968; Herringe, 1976; Takahashi et al., 1992; Abbad and Souhar, 2004a,b) or non-uniform (Van Oeveren and Houghton, 1971; Boyadzhiev, 1973; Maxey and Riley, 1983).
In most cases the oscillations were applied in vertical direction, whereas only a few were applied in horizontal direction (Weinstein, 2008). One extreme case even reported physical experiments where the fluid oscillations were applied in in two directions simultaneously (Herringe, 1977). The mentioned *nonlinear Langevin equation* proved to be a simplification of the complete equation to predict the resulting particle motion vertically (*settling or rising*) and horizontally (*migration*) due to the fluid oscillations. It was found that the complete equation was derived by Boussinesq (1885), Basset (1888) and Oseen (1927), which is known as the *BBO-equation*.

It is therefore recommended to solve the BBO-equation numerically, to simulate whether it would be possible to increase the hindered settling velocity by using non-uniform fluid oscillations.

CHAPTER 2

Thesis Outline

As explained in the introduction, the ultimate goal would be to have zero production losses and thus find clean water in the overflow. By finding the mentioned technique of using non-uniform oscillatory fluid motions to manipulate and control particle motion, two possible scenario's were developed in which the hindered settling velocity may actually be increased. This chapter provides a general overview of the thesis project together with the hypotheses which this thesis aims to prove by a theoretical and numerical approach.

2.1 Thesis project

To provide a clear overview of the entire thesis project, Figure 2.1 was created.

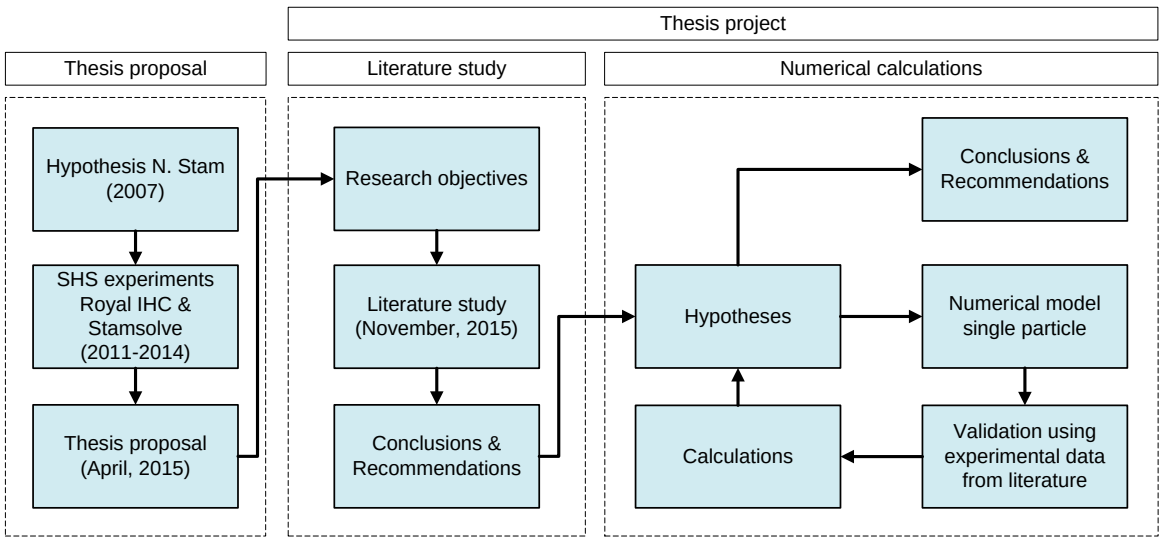

Figure 2.1: Outline of the entire thesis project

As shown, the thesis project is divided in two phases. The thesis proposal was created prior to the thesis project in a preliminary phase Van de Wetering (2015a). Here, the main research question and research objectives were created which were aimed to be answered by the first phase: the literature study Van de Wetering (2015b). An thorough review of the literature study was given in Chapter 1. The conclusions and recommendation found during the literature study, resulted in two hypotheses. This thesis aims to prove these hypotheses theoretically and numerically, using the second phase of the thesis project. Both hypotheses will be presented together with a short discussion on the execution of the second phase.

2.2 Hypotheses

Increased settling velocity using horizontal fluid oscillations

When a graded concentration of solid particles, up to approximately 45% by volume ($c_v \approx 0.45$), is settling under gravity, a process known as *segregation* occurs (Te Slaa et al., 2012). During this process, the larger and therefore heavier particles (assuming similar particle density) travel faster than the smaller fractions. It was found that the smaller fractions tend to fall in the wake of the larger particles (Minkov et al., 2015), creating a so-called *vein-like* system (Kuenen, 1968). This process is also known as *settling convection* and is the only one out of seven processes occurring during *hindered settling* (Winterwerp, 2002; Dankers, 2006), which causes an increase in average settling velocity. Because of the veins, paths are being created to dissipate the water. The first hypothesis uses this vein-like principle of dissipating pore water to increase the hindered settling velocity:

"Using non-uniform fluid oscillations in horizontal direction causes solid spherical particles to migrate in the direction of oscillation, creating a horizontal density gradient which introduces a convection flow and therefore increases the average settling velocity"

Van Oeveren and Houghton (1971) showed experimentally that solid particles could be made hovering or even levitated against gravity using non-uniform fluid oscillations, with the highest velocity directed upwards. Non-uniform fluid oscillations are defined as a *sawtooth wave* inputs for the fluid displacement whereas uniform fluid oscillations are defined as a *sinusoidal wave* inputs. If a vertical particle motion against gravity can be achieved, than horizontal migration of particles should also be possible.
This horizontal migration creates a horizontal density gradient (two "veins") at which particles will gather in the direction of oscillation and the carrier fluid will flow in the opposite direction.

Let's consider a rectangular settling tube in which a mixture has been created of solid spherical particles having a density larger than the carrier fluid ($\rho_p > \rho_f$) and being mixed more or less homogeneously (Figure 2.2, left). The particles will settle by gravity in downward direction, forcing the water to flow through the particles upwards (indicated by the black arrow). This is known as the *return flow* phenomenon during the hindered setting process.

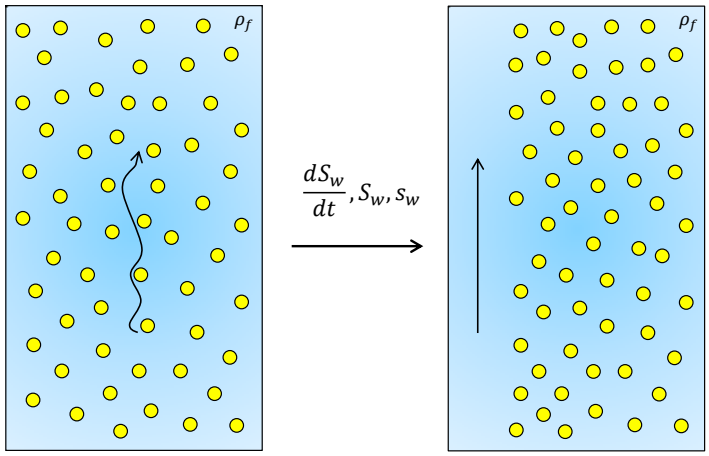

Figure 2.2: Creating a horizontal density gradient using horizontal non-uniform oscillations

Non-uniform oscillations are applied to the settling tube in horizontal direction, indicated by a fluid displacement s_w, a fluid velocity S_w and an fluid acceleration dS_w/dt. The particles migrate in the direction of the highest velocity, creating a vein with a higher density and a vein where the water can flow upwards freely (Figure 2.2, right). A density driven convection flow is expected to occur, which is known from inclined settling tubes.

Increased settling velocity using vertical fluid oscillations

As mentioned in the previous section, Van Oeveren and Houghton (1971) made solid spherical particles with a density greater than the carrier fluid, move against gravity by applying non-uniform fluid oscillations with the highest velocity in upward direction. Perhaps a more convenient way of increasing the average hindered settling velocity would be to just reverse the direction of the highest velocity of the fluid:

"Using non-uniform fluid oscillations in vertical direction with the highest velocity faced downwards, causes solid spherical particles to settle with increased average settling velocity"

This hypothesis is supported by the theoretical work of Boyadzhiev (1973). He showed, with a slightly different force-balance model than used in the *BBO-equation*, that it would be theoretically possible to either levitate particles against gravity or accelerate particles in the gravitational direction. This particle motion behavior was found to be dependent on the direction of the highest velocity of a *saw-tooth wave* input for displacement. The force-balance used in the calculations was mentioned to be taken from Houghton (1963), which is in fact a simplified modification of the general BBO-equation.

As mentioned and shown at Figure 2.1, MATLAB will be used to create a numerical model which solves the BBO-equation in two separate directions. The model predicts the particle response behavior to the fluid oscillations for a single, solid, spherical particle. Therefore, only a qualitative conclusion can be made regarding the both hypotheses. In order to fully prove the hypotheses, the addition of a the volumetric concentration in the BBO-equation is required. A validation study using available experimental data from literature is performed in order to investigate the usability and accuracy of the model. Subsequently, calculations will be performed in order to find relations between different parameters and determine (qualitatively) whether the hypotheses can be proven.

CHAPTER 3

Derivation inviscid & viscous models

There is an enormous amount of existing literature in the field of solid particle dynamics in stagnant fluids. However, this number decreases significantly when only oscillatory motion in translation is considered as mentioned by Weinstein (2008) and experienced by the author during this research. Weinstein (2008) gave a visual representation of his estimation on relative articles, considering bubbles and solid particles:

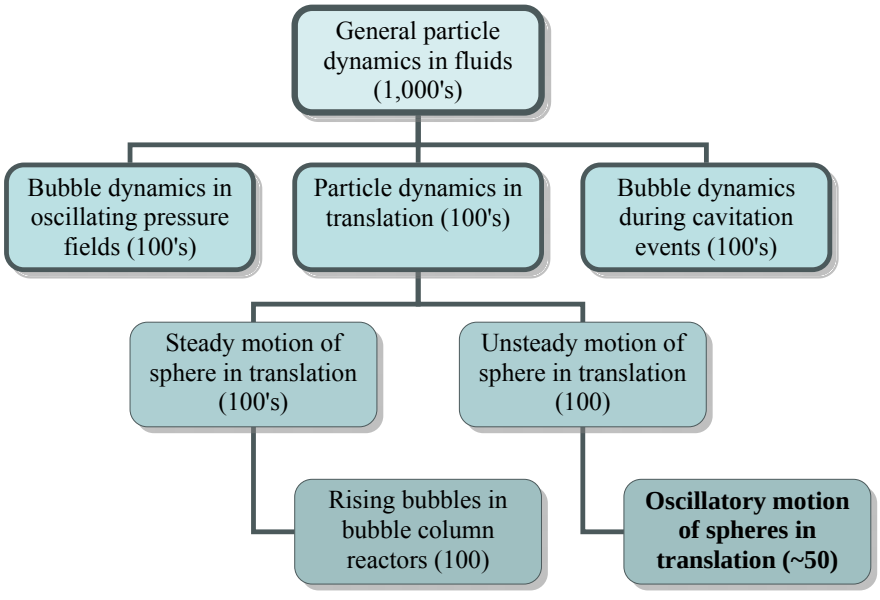

Figure 3.1: Estimation of articles on the oscillatory motion in translation (Weinstein, 2008)

The amount of articles decreases even further when the oscillatory motion of spheres becomes non-uniform. In this section, available literature on solid particle behavior, in both uniformly and non-uniformly oscillating fluids, is reviewed. The review is used to derive the inviscid and viscous models which will be solved using MATLAB.

3.1 Oscillatory Translation of Spheres in Inviscid Fluids

Let's start by examining the problem of a rigid spherical particle falling in an unsteady velocity field by assuming an inviscid fluid. Using this assumption and neglecting heat transfer, the Navier-Stokes equations simplify to the so-called Euler equations. Using potential flow theory (inviscid and irrotational flow field), the solution of the Euler equations provides the necessary equations of motion (EOM) for this particular problem (Weinstein, 2008).
The particle response velocity to the unsteady velocity field is affected by an added mass (F_a) and a pressure force (F_p) in horizontal direction, whereas gravity (F_g) and buoyancy forces (F_b) need to be added in vertical direction. Here, it is assumed that particle and fluid move in a single direction only, resulting in a pure *rectilinear* motion. We are interested in the force balance in both directions, yielding for the horizontal force balance:

$$F_{h,t} = F_a + F_p, \tag{3.1}$$

$$F_{h,t} = \frac{1}{2}\,\rho_f V_p \left(\frac{dS}{dt} - \frac{du_{pot}}{dt}\right) + \rho_f V_p \frac{dS}{dt}, \tag{3.2}$$

where the volume of the particle is written as:

$$V_p = \frac{4}{3}\pi r^3. \tag{3.3}$$

For the vertical direction the force balance becomes:

$$F_{v,t} = F_a + F_p + F_g, \tag{3.4}$$

$$F_{v,t} = \frac{1}{2}\,\rho_f V_p \left(\frac{dS}{dt} - \frac{dv_{pot}}{dt}\right) + \rho_f V_p \frac{dS}{dt} + V_p\, g\,(\rho_f - \rho_p)\,. \tag{3.5}$$

Here, S is the fluid velocity and u_{pot} & v_{pot} are the particle response velocities in horizontal and vertical direction, respectively. The density is described using ρ where the subscript p or f refers to particle or fluid. Equation 3.2 and Equation 3.5 are visualized using Figure 3.2:

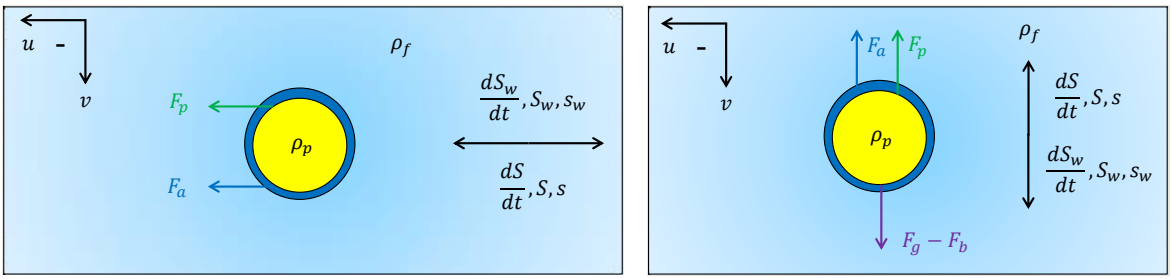

(a) Forces in horizontal direction

(b) Forces in vertical direction

Figure 3.2: Visual representation of all the forces in the inviscid model in two directions

At both Figure 3.2(a) and Figure 3.2(b), the black arrow at the right side indicates the fluid oscillations. These are described using the fluid displacement, velocity and acceleration for both uniform and non-uniform oscillations. This will discussed thoroughly in Subsection 4.2.2.

Considering Equation 3.2, the first force on the right hand side (RHS) accounts for the added mass effect (F_a) which is caused by the acceleration of the surrounding fluid due to the spherical particle which is constantly displacing fluid as it moves through the flow field. The added mass force is determined by the shape of the object, which is described using an added mass coefficient (C_a). In the case of objects with an asymmetrical arbitrary shape, this coefficient can be hard to obtain and will be dependent on the orientation at which the object is placed in the flow field. Luckily, in the case of a symmetrical sphere this coefficient is independent of orientation and found to be one half of the mass of the displaced fluid $C_a = \frac{1}{2}$ (Weinstein, 2008). The second force in Equation 3.2 is an inertial, buoyancy-like force caused by the acceleration of the fluid relative to an inertial frame. The acceleration of the fluid causes a pressure gradient over the particle which produces the pressure force term (F_p). For Equation 3.5 the first two terms are the same as for Equation 3.2, with the addition of a combined gravity force (F_g) and buoyancy force (F_b) term. Newton's second law of motion can be applied to obtain a differential equation for particle motion. With the mass of the sphere times its acceleration on the left and the sum of the force on the right, Equation 3.2 becomes:

$$V_p\,\rho_p\,\frac{du_{pot}}{dt} = \frac{1}{2}\,\rho_f V_p\left(\frac{dS}{dt} - \frac{du_{pot}}{dt}\right) + \rho_f V_p \frac{dS}{dt}. \tag{3.6}$$

Rewriting gives:

$$\left(1 + \frac{2\rho_p}{\rho_f}\right)\frac{du_{pot}}{dt} = 3\,\frac{dS}{dt}. \tag{3.7}$$

Applying the same method to Equation 3.5 in the case of vertical direction:

$$V_p\,\rho_p\,\frac{dv_{pot}}{dt} = \frac{1}{2}\,\rho_f V_p\left(\frac{dS}{dt} - \frac{dv_{pot}}{dt}\right) + \rho_f V_p \frac{dS}{dt} + V_p\,g\,(\rho_f - \rho_p)\,. \tag{3.8}$$

Again, rewriting yields:

$$\left(1 + \frac{2\rho_p}{\rho_f}\right)\frac{dv_{pot}}{dt} = 3\,\frac{dS}{dt} + 2\,g\left(1 - \frac{\rho_p}{\rho_f}\right). \tag{3.9}$$

Equation 3.7 indicates that for a particle of negligible density (bubble) in water ($\rho_p \ll \rho_f$) the particle will have three times the acceleration of the fluid. Integrating the equation twice shows that the particle travels three times as far as the fluid per oscillation of the settling tube. A particle having the same density as water (droplet) ($\rho_p = \rho_f$) will have the same position, velocity and acceleration responses as the fluid. If the particle is more dense than the fluid ($\rho_p \gg \rho_f$), then the fluid will experience greater acceleration than the particle.

The fluid phase is assumed to be incompressible and generally to move directly with the tube as a rigid body (Weinstein, 2008). It is clear from Equation 3.7 that the density ratio is the most important parameter for the potential flow analysis of decoupling, as it completely determines the amplitude ratio (A_p/A_f) of the two phases. As would be expected, we find that the inertial difference between the two phases drives the relative acceleration and causes decoupling (Chapter 5).

3.2 Oscillatory Translation of Spheres in Viscous Fluids

Stokes (1851) was the first who investigated harmonic and rectilinear oscillations of a sphere, cylinder and an infinitely long flat plate in a viscous fluid. He neglected the nonlinear (inertia) terms in the Navier-Stokes equations and derived expressions for the forces exerted by the fluid on these objects. One of these is the widely known *Stokes drag force* (F_d).

Later, Boussinesq (1885), Basset (1888) and Oseen (1927) (BBO) independently studied the rectilinear motion of a sphere which has a rapid but arbitrary acceleration in a viscous fluid. They neglected the nonlinear terms in the Navier-Stokes equations as well, when the force expressions were derived. It was agreed however, that the force on a sphere not only depends on its instantaneous velocity and acceleration, but also on a force term which describes the effect of its entire history of acceleration. This term is knows as the history or Basset term (F_h).

In order to accurately predict the particle motion behavior, it is necessary to extend the potential flow theory described in the previous section by incorporating viscous effects. The viscous model includes two extra forces: the Stokes drag force (F_d) and the history or Basset force (F_h). By addition of these forces, it is expected that decoupling between the phases decreases (especially at higher viscosity). It is also expected that the motion between particle and fluid will be out of phase because of the lag in acceleration and deceleration of the particle, caused by the addition of the drag force.

Because of the addition of the above mentioned drag and history force, it instantly becomes more difficult to predict the oscillatory motion of a particle in a fluid. In a stagnant fluid, a viscous wake region develops behind the particle, as fluid flows past it and boundary separation occurs. However, in an oscillating fluid, the particle oscillates back and forth through its own wake, making it more difficult to correctly predict its behavior.

Through solution of the unsteady Stokes equations, Basset determined the expression for particle motion with no-slip boundary condition in horizontal direction to be:

$$V_p\,\rho_p\,\frac{du}{dt} = F_d + F_h + F_a + F_p, \tag{3.10}$$

or in its complete form:

$$\begin{aligned} V_p\,\rho_p\,\frac{du}{dt} \;=\; & 6\pi\mu_f\,r(S-u) + \\ & 6\,r^2\sqrt{\pi\mu_f\rho_f}\int_{-\infty}^{t}\left(\frac{dS}{d\tau}-\frac{du}{d\tau}\right)\frac{1}{\sqrt{t-\tau}}d\tau + \\ & \frac{2}{3}\pi\rho_f\,r^3\left(\frac{dS}{dt}-\frac{du}{dt}\right) + \\ & \frac{4}{3}\pi\rho_f\,r^3\,\frac{dS}{dt}, \end{aligned} \tag{3.11}$$

and in vertical direction:

$$V_p\,\rho_p\,\frac{dv}{dt} = F_g + F_d + F_h + F_a + F_p, \tag{3.12}$$

or in its complete form:

$$\begin{aligned} V_p\,\rho_p\,\frac{dv}{dt} &= V_p\,g(\rho_f-\rho_p)+ \\ &\quad 6\pi\mu_f\,r(S-v)+ \\ &\quad 6\,r^2\sqrt{\pi\mu_f\rho_f}\int_{-\infty}^{t}\left(\frac{dS}{d\tau}-\frac{dv}{d\tau}\right)\frac{1}{\sqrt{t-\tau}}d\tau+ \\ &\quad \frac{2}{3}\pi\rho_f\,r^3\left(\frac{dS}{dt}-\frac{dv}{dt}\right)+ \\ &\quad \frac{4}{3}\pi\rho_f\,r^3\,\frac{dS}{dt}, \end{aligned} \tag{3.13}$$

where r, ρ_p, ρ_f, μ_f are particle radius, particle density, fluid density and fluid viscosity (dynamic), respectively. Both equations are essentially Newton's second law of motion. Considering the RHS of Equation 3.13, the first force term occurs due to gravity and buoyancy acting on the particle, the second term describes the Stokes drag law, whereas the third term describes the history or Basset force which accounts for the effects of the past motion of the particle. The forth and fifth term again describe the added mass force and buoyancy-like pressure force, respectively.

Visually, all the different forces can be distinguished using Figure 3.3.

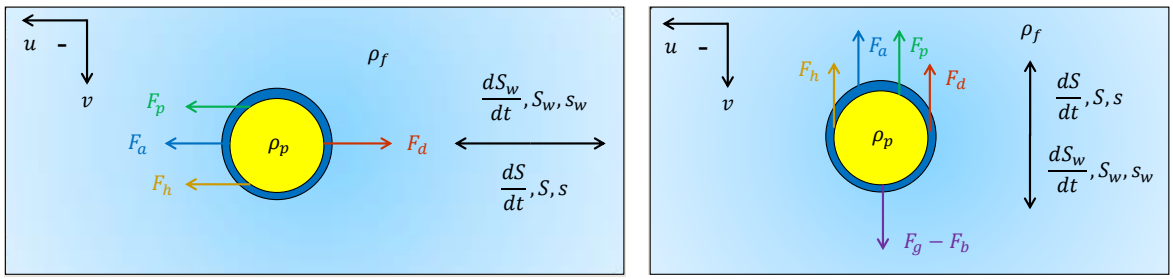

(a) Forces in horizontal direction

(b) Forces in vertical direction

Figure 3.3: Visual representation of all the forces in the BBO-equation in two directions

The Stokes drag force as presented in Equation 3.11 and Equation 3.13 is limited to very low particle Reynolds numbers i.e. $Re_p < 0.1$ (Odar and Hamilton, 1964; Herringe and Flint, 1974), which is in vertical direction defined to be:

$$Re_p = \frac{2\,r\,|S-v|}{\nu_f}, \tag{3.14}$$

where the kinematic fluid viscosity (ν_f) is obtained by the ratio of the dynamic fluid viscosity (μ_f) over the fluid density (ρ_f):

$$\nu_f = \frac{\mu_f}{\rho_f}. \tag{3.15}$$

To examine the acceleration effects on the motion of the particle, Odar and Hamilton (1964); Odar (1966) experimentally studied the oscillations of a *guided* sphere in oil for particle Reynolds numbers up to 62. A modification of the BBO-equation was proposed by multiplying the Stokes drag force, the added mass force and the history force with the empirical coefficients C_1, C_m and C_h respectively. These coefficients depend on the particle Reynolds number and the acceleration number:

$$Ac = \frac{2\,r}{|S-v|^2}\left|\frac{dS}{dt} - \frac{dv}{dt}\right|, \tag{3.16}$$

and are given by:

$$C_1 = 1 + 0.15Re_p^{0.687}, \qquad C_m = 2.1 - \frac{0.132Ac^2}{(1+0.12Ac^2)}, \qquad C_h = 0.48 + \frac{0.52Ac^3}{(1+Ac)^3}. \tag{3.17}$$

Based on the resulting equation of motion proposed by Odar and Hamilton (1964), several studies were carried out to simulate the motion of a sphere at higher particle Reynolds numbers. Karanfilian and Kotas (1978) conducted similar experiments at $10^2 < Re_p < 10^4$ and found that the coefficients proposed by Boussinesq (1885), Basset (1888) and Oseen (1927) are still valid ($C_m = C_h = 1$). It must be noted that these experiments were performed using relatively high amplitudes (up to 60 mm) and relatively low frequencies (up to 0.4 Hz).

To adjust the Stokes drag force for higher particle Reynolds numbers, an empirical correction factor $\phi(Re_p)$ has been determined from the results of experiments by Clift et al. (1978). Using this coefficient the drag force is accurate in steady flow up to particle Reynolds numbers of 1500.

The final form of the drag force term (F_d) becomes:

$$F_d = 6\pi\mu_f\, r(S-v)\phi(Re_p), \tag{3.18}$$

where:

$$\phi(Re_p) = 1 + \left(\frac{3}{16}\right)Re_p, \qquad 0 < Re_p \leq 0.01 \tag{3.19}$$

$$\phi(Re_p) = 1 + 0.1315Re_p^{0.82-0.05w}, \qquad 0.01 < Re_p \leq 20 \tag{3.20}$$

$$\phi(Re_p) = 1 + 0.1935Re_p^{0.6305}, \qquad 20 < Re_p \leq 260 \tag{3.21}$$

$$\phi(Re_p) = 1.8335(Re_p)\,10^{-1.1242w+0.1558w^2}, \qquad 260 < Re_p \leq 1500 \tag{3.22}$$

and where:

$$w = \log_{10}(Re_p). \tag{3.23}$$

Figure 3.4 shows how the correction factor for the Stokes drag law varies with the particle Reynolds number. In the lower limit, $\phi(Re_p)$ is unity, where the Stokes drag low does not need correction. In the limit of particle Reynolds numbers up to 1500 the value of $\phi(Re_p)$ increases to about 27.

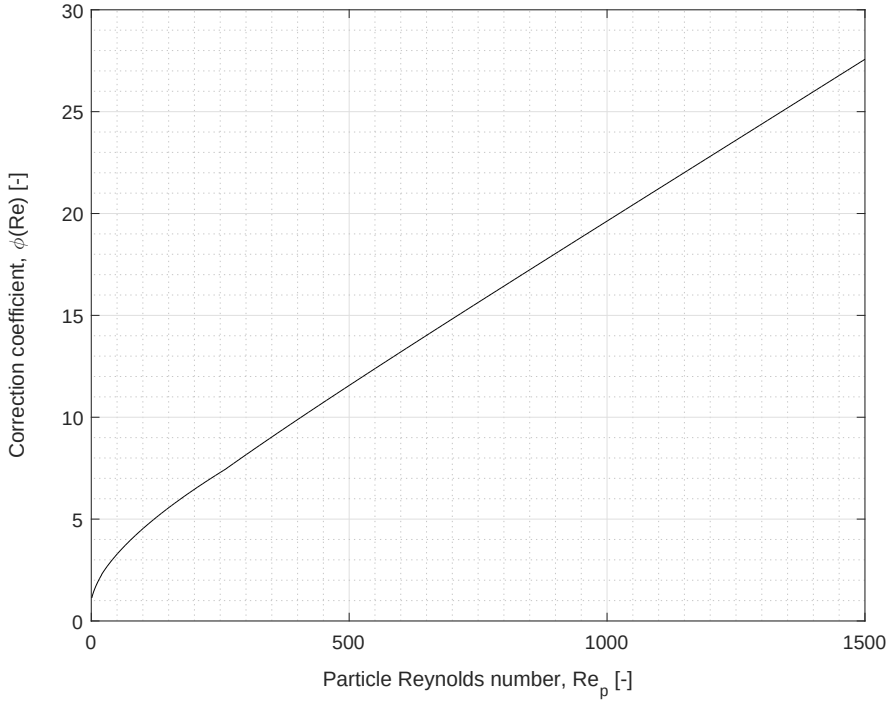

Figure 3.4: Correction to the Stokes drag law at high particle Reynolds numbers

As mentioned previously, the work of Karanfilian and Kotas (1978) showed that the added mass and history force are more or less independent of the particle Reynolds number and therefore do not need correction.

It is however presented by Coimbra et al. (2004) that the history force depends on the dimensionless frequency, defined as:

$$\Omega = Sl\ Re_p = \frac{r^2\omega}{9\nu_f}, \tag{3.24}$$

Where Sl is also known as the Strouhal number, given by:

$$Sl = \frac{\omega\, r}{|S - v|}. \tag{3.25}$$

This dimensionless parameter represents a ratio of the viscous diffusion time to the oscillation time. When the diffusion time is similar to the oscillation time, vorticity generated on the surface of the sphere is especially important and history effects are significant. When the dimensionless frequency is much greater than unity, inviscid added mass effects dominate and when it is small, the Stokes drag force dominates.

Considering Equation 3.11 and Equation 3.13, it shows a complex and numerically intensive integral form of the history force (F_h), which takes into account the entire history of the relative acceleration between the fluid and particle.

Fortunately, the integral form of the history force can be simplified to an explicit form for the case of quasi-steady oscillations and the no-slip boundary condition, as presented by Abbad and Souhar (2004a):

$$F_h = 6\pi\mu_f\, r \left[\frac{S-v}{\delta} + \frac{\delta\tau_v}{2} \left(\frac{dS}{dt} - \frac{dv}{dt} \right) \right], \tag{3.26}$$

where the dimensionless parameters δ and τ_v are defined as:

$$\delta = \sqrt{\frac{2\nu_f}{r^2\omega}}, \tag{3.27}$$

and:

$$\tau_v = \frac{r^2}{\nu_f}. \tag{3.28}$$

The dimensionless parameter δ is also known as the *inverse Stokes number*. It represents a ratio of the oscillation time to the viscous diffusion time scale. The second dimensionless parameter (τ_v), describes the viscous diffusion time scale. The explicit form of the history force as presented by Abbad and Souhar (2004b) is experimentally proven to be accurate for particle Reynolds numbers $Re \leq 2.5$ and Strouhal numbers $1 \leq Sl \leq 20$. Later, Weinstein (2008) showed that the Strouhal validity range could be extended to $1 < Sl < 45$.

With the addition to the Stokes drag force by Clift et al. (1978) and the explicit form of the history force by Abbad and Souhar (2004a), the final form of the BBO-equation in both horizontal and vertical direction becomes:

$$\begin{aligned} V_p\, \rho_p\, \frac{du}{dt} \;=\; & 6\pi\mu_f\, r(S-u)\phi(Re_p) + \\ & 6\pi\mu_f\, r \left[\frac{S-u}{\delta} + \frac{\delta\tau_v}{2} \left(\frac{dS}{dt} - \frac{du}{dt} \right) \right] + \\ & \frac{2}{3}\pi\rho_f\, r^3 \left(\frac{dS}{dt} - \frac{du}{dt} \right) + \\ & \frac{4}{3}\pi\rho_f\, r^3\, \frac{dS}{dt}, \end{aligned} \tag{3.29}$$

and:

$$\begin{aligned} V_p\, \rho_p\, \frac{dv}{dt} \;=\; & V_p\, g(\rho_f - \rho_p) + \\ & 6\pi\mu_f\, r(S-v)\phi(Re_p) + \\ & 6\pi\mu_f\, r \left[\frac{S-v}{\delta} + \frac{\delta\tau_v}{2} \left(\frac{dS}{dt} - \frac{dv}{dt} \right) \right] + \\ & \frac{2}{3}\pi\rho_f\, r^3 \left(\frac{dS}{dt} - \frac{dv}{dt} \right) + \\ & \frac{4}{3}\pi\rho_f\, r^3\, \frac{dS}{dt}. \end{aligned} \tag{3.30}$$

CHAPTER 4

Modelling the nonlinear BBO-equation

In this chapter the solution method for the particle motion in uniformly and non-uniformly oscillating fluids is described. First the assumptions and simplifications are discussed, after which the model is explained in detail. In Section 4.3 we close this chapter with a discussion on the validity and accuracy of the model, using datasets from literature.

4.1 Assumptions and simplifications

Certain assumptions and simplifications had to be made in order to create the model. A very important note to the BBO-equation is that it is a *rectilinear model*, meaning it is only found to be valid when the particle motion is in the direction of oscillation. In the case of a particle falling in a vertically oscillating settling tube, this condition is always satisfied. However, when a solid particle is falling through a horizontally oscillating settling tube, the model can loose its validity. In recent work from Weinstein (2008) the BBO-equation was found to be in good agreement with the experiments of solid particles, settling in a horizontally oscillating tube, when the following condition is satisfied:

$$\Theta = \frac{v_t}{2\,r\,\omega} \leq 0.4. \tag{4.1}$$

This dimensionless parameter compares the distance traveled vertically by the particle in one cycle to the particle diameter. Furthermore, it is assumed that the explicit form of the history force, suggested by Abbad and Souhar (2004a) is valid for higher particle Reynolds numbers and Strouhal numbers. Karanfilian and Kotas (1978) have showed that the added mass coefficient and the history force coefficient both can be kept approximately unity ($C_a = C_h = 1$) but they did not use this explicit form. Also, the fluid phase is assumed to be incompressible and *moves directly* with the settling tube as a *rigid body*.
Regarding the solid particle, it is assumed that it is perfectly spherical and that it will settle in a *two dimensional space* where no wall-effects will be present as long as the distance to the wall is $\geq 8d$ (Abbad and Souhar, 2004b; Weinstein, 2008). As for now, the model will only calculate the motion of a *single particle*, so concentrations can not be simulated.

4.2 Solution method

A MATLAB model has been developed which allows the user to obtain the particle motion in an oscillating fluid over a wide range of particle and fluid conditions. These will be discussed separately in this section.

4.2.1 Particle geometry and properties

The model starts by setting the particle properties. As mentioned in Section 4.1, the model will only calculate the motion for a single particle in a two dimensional space. At first, the radius (r) must be set to a certain value. Subsequently, the particle volume is calculated by:

$$V_p = \frac{4}{3}\pi\, r^3. \tag{4.2}$$

By setting the density of the particle (ρ_p) to a certain value (often the density of quartz sand $\approx 2650\ kg/m^3$ is used), the mass of the particle is calculated using:

$$m_p = \rho_p\, V_p. \tag{4.3}$$

By setting these properties, the model calculates the terminal settling velocity in a stagnant fluid using the equation by Stokes (1851) as function of the particle diameter $(d = 2r)$:

$$v_s = \frac{\Delta g d^2}{18\nu_f}, \tag{4.4}$$

where g describes the gravitational constant $(\approx 9.81\ m/s^2)$ and Δ the relative density, defined by:

$$\Delta = \frac{\rho_p - \rho_f}{\rho_f}. \tag{4.5}$$

Because of the very limited validity of the *Stokes equation* $(d \leq 0.1mm)$, the equation for the terminal settling velocity proposed by Ferguson and Church (2004) is also added to the model:

$$v_p = \frac{\Delta g d^2}{C_1\nu_f + \sqrt{0.75 C_2 \Delta g d^3}}. \tag{4.6}$$

For spherical particles the coefficients C_1 and C_2 are given to be 18 and 0.44, respectively. In case of natural sands these coefficients were determined to be $C_1 = 18$ and $C_2 = 1$. In the model only the coefficients for the spherical particles are included.

4.2.2 Oscillating fluid properties

To simulate an oscillating fluid, first the fluid properties have to be determined. In the dredging industry the fluid used to create a pumpable mixture will always be fresh or salt water. The model always assumes fresh water. The properties of water are temperature dependent, so the first parameter to set is the temperature (T). This being done, the model uses the following equation to approach the temperature dependent fluid density (ρ_f) (Matousek, 2004):

$$\rho_f = 999.7 - 0.10512(T-10) - 0.005121(T-10)^2 + 0.00001329(T-10)^3. \tag{4.7}$$

The viscosity (both dynamic and kinematic) depends on the temperature (T) as well. The kinematic viscosity is calculated using the approximation of Van Rhee (2002):

$$\nu_f = \frac{40 \times 10^{-6}}{20 + T}. \tag{4.8}$$

Using both Equation 4.7 and Equation 4.8, the dynamic viscosity can be determined using:

$$\mu_f = \rho_f \, \nu_f. \tag{4.9}$$

These three equations are valid in a temperature range of 5 °C $<$ T $<$ 105 °C. Once the fluid properties have been determined, the oscillation properties need to be set. The model enables the user to set a fluid oscillation amplitude (A_f) and frequency (f) which are needed to calculated the fluid displacement, velocity and acceleration. First, the angular frequency is calculated using the user defined frequency:

$$\omega = 2\pi f. \tag{4.10}$$

Let's now consider a settling tube which oscillates uniformly. To initiate the sinusoidal motion, a displacement has to be generated by some sort of driver (solenoid, camshaft etc.). The obtained fluid displacement (which is assumed to be exactly equal to the settling tube) can be described as:

$$s = A_f \sin(\omega t). \tag{4.11}$$

By differentiating Equation 4.11 twice, the fluid velocity (S) and acceleration (dS/dt) are found:

$$S = A_f \, \omega \cos(\omega t), \tag{4.12}$$

$$\frac{dS}{dt} = -A_f \, \omega^2 \sin(\omega t). \tag{4.13}$$

The fluid displacement, velocity and acceleration as described above are independent of direction, so they will be used to solve the inviscid and viscous model (BBO-equation) in both horizontal and vertical direction. It is expected that the particle responds to the inviscid uniform fluid oscillations with an equal frequency (ω) and a response amplitude (A_p) and can be described for both horizontal and vertical direction as:

$$[u, v] = A_p \, \omega \cos(\omega t). \tag{4.14}$$

In case of the viscous fluid oscillations a phase lag (φ) is expected to occur:

$$[u, v] = A_p \, \omega \cos(\omega t + \varphi). \tag{4.15}$$

Considering the hypotheses presented in Chapter 1, we are especially interested in the particle response behavior using non-uniform fluid oscillations. Unfortunately this is not as straightforward as the previously described uniform oscillations. Let's again consider a settling tube which oscillates around the zero axis, but this time having a *sawtooth* like displacement. The sawtooth wave is a *discontinuous* or *piecewise continuous* function. This means that between certain points, the function does not exist.

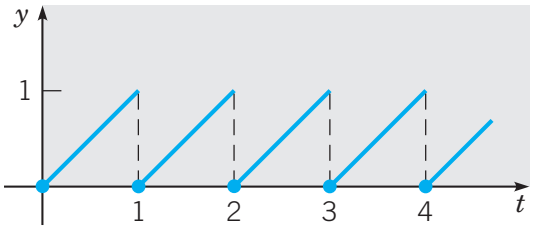

Figure 4.1: Piecewise continuous sawtooth function (Boyce et al., 1969)

Because the sawtooth wave will be used for the displacement, it has to be differentiated twice to find the velocity and acceleration. This can only be done if the function is continuous, which is be solved by using a *Fourier series* to approximate the sawtooth wave. The Fourier series uses a summation of multiple sinusoidal waves to approach for instance a sawtooth wave or square wave. The general form of the Fourier series expansion is known as:

$$a_0 + \sum_{n=1}^{\infty} a_n \cos(n\omega t) + b_n \sin(n\omega t). \tag{4.16}$$

As said earlier, the sawtooth wave needs to oscillate around the zero axis and start at the origin for the fluid displacement, similar to the sinusoidal wave. These boundary conditions determine that $a_0 = 0$ and $a_n = 0$. To describe the sawtooth wave using the Fourier series, the b_n term was found to be:

$$b_n = \frac{-2(-1)^n ki^2}{n^2(ki-1)\pi^2} \sin\left(\frac{n(ki-1)\pi}{ki}\right). \tag{4.17}$$

Here, the factor n determines the amount of sinusoidal functions which will be used to approach the piecewise continuous function that is required. In the case of the MATLAB model this variable has been set to be $n = 40$ by trial and error, but can be adjusted if needed. The shape factor ki enables the user to adjust the steepness of the sawtooth wave. This factor was described by Van Oeveren and Houghton (1971) to be the ratio between the downstroke duration and the upstroke duration and determines the shape of the wave:

$$ki = \frac{\text{downstroke duration}}{\text{upstroke duration}}. \tag{4.18}$$

This ki factor can be varied between unity (1) and infinity (∞) the way it is programmed in the model. The final form of the sawtooth wave fluid displacement can thus be approximated using:

$$s_w = A_f \sum_{n=1}^{40} \frac{-2(-1)^n ki^2}{n^2(ki-1)\pi^2} \sin\left(\frac{n(ki-1)\pi}{ki}\right) \sin(n\omega t). \tag{4.19}$$

This form is easily differentiable and by again differentiating twice with respect to t, the fluid velocity and acceleration are found:

$$S_w = (A_f\, n\, \omega) \sum_{n=1}^{40} \frac{-2(-1)^n ki^2}{n^2(ki-1)\pi^2} \sin\left(\frac{n(ki-1)\pi}{ki}\right) \cos(n\omega t), \tag{4.20}$$

$$\frac{dS_w}{dt} = \left(-A_f\, n^2\, \omega^2\right) \sum_{n=1}^{40} \frac{-2(-1)^n ki^2}{n^2(ki-1)\pi^2} \sin\left(\frac{n(ki-1)\pi}{ki}\right) \sin(n\omega t). \tag{4.21}$$

Using Equation 4.11, Equation 4.19 and the built-in MATLAB function to generate sawtooth waves for the fluid displacement resulted in Figure 4.2. Here, the following settings were applied; a frequency of $f = 1\ Hz$, a fluid amplitude $A_f = 1\ mm$ and a shape factor $ki = 1$.

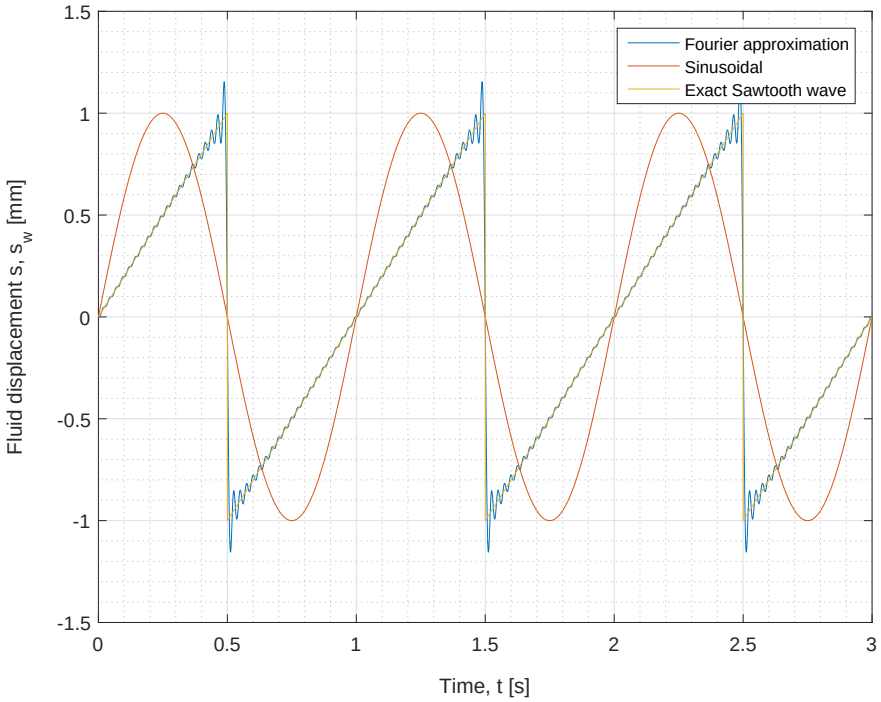

Figure 4.2: Fluid displacement using uniform and non-uniform oscillations $(ki = 1)$

Comparing the exact sawtooth wave generated by MATLAB with the Fourier series approximation, it is clearly visible that the Fourier series approximation has some overshoot at the locations where the sawtooth wave has a sharp transition in direction. This is know as the *Gibbs phenomenon*. Using the current settings, the overshoot error was determined to be $\sim 15\%$ for the fluid displacement. However, examining the fluid velocity (S_w) and fluid acceleration (dS_w/dt) this error rapidly increases to $\sim 80\%$, which dramatically decreases the accuracy.

Fortunately, it was found that the Gibbs phenomenon could significantly be decreased by adjusting the range of the shape factor (ki). Limiting the shape factor in the range $ki = 1.05 - 21$ gives a slightly less perfect sawtooth wave, but gains a large improvement in overshoot.
Setting the shape factor at $ki = 1.05$, Figure 4.3 was created. In this case the largest velocity is pointed in downward direction. As can be seen, the approximation and exact solution are hardly to distinguish and the resulting overshoot error was determined to be $< 1\%$.

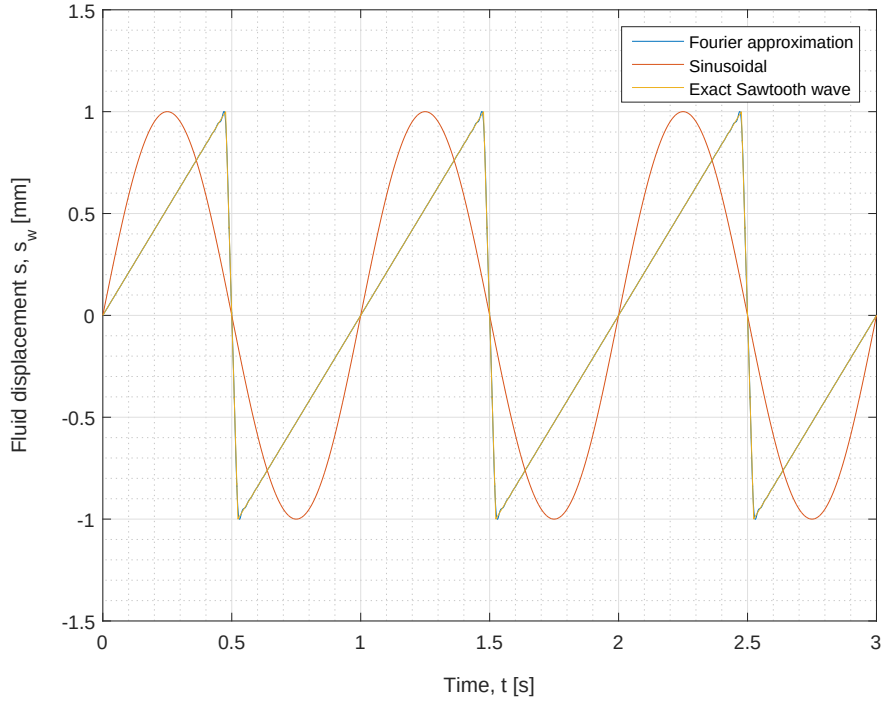

Figure 4.3: Fluid displacement using uniform and non-uniform oscillations ($ki = 1.05$)

The other limiting value of the shape factor ($ki = 21$) has its largest velocity in upward direction and looks as follows:

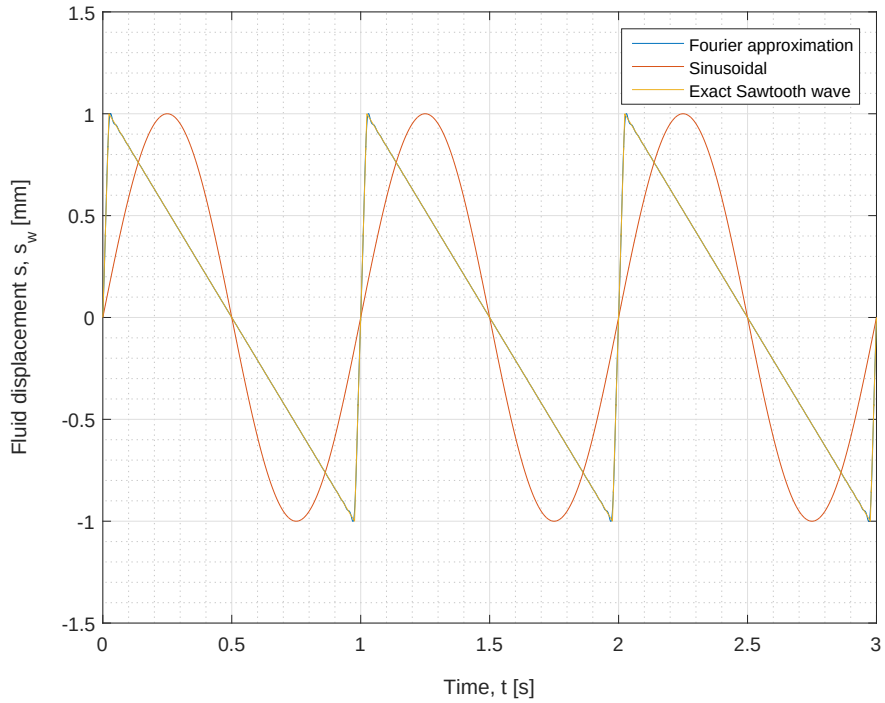

Figure 4.4: Fluid displacement using uniform and non-uniform oscillations ($ki = 21$)

The other possibilities within the shape factor range adjust the sawtooth wave within these extremes.

The fluid velocity S and S_w resulting from differentiating Figure 4.3 and Figure 4.4 look as follows:

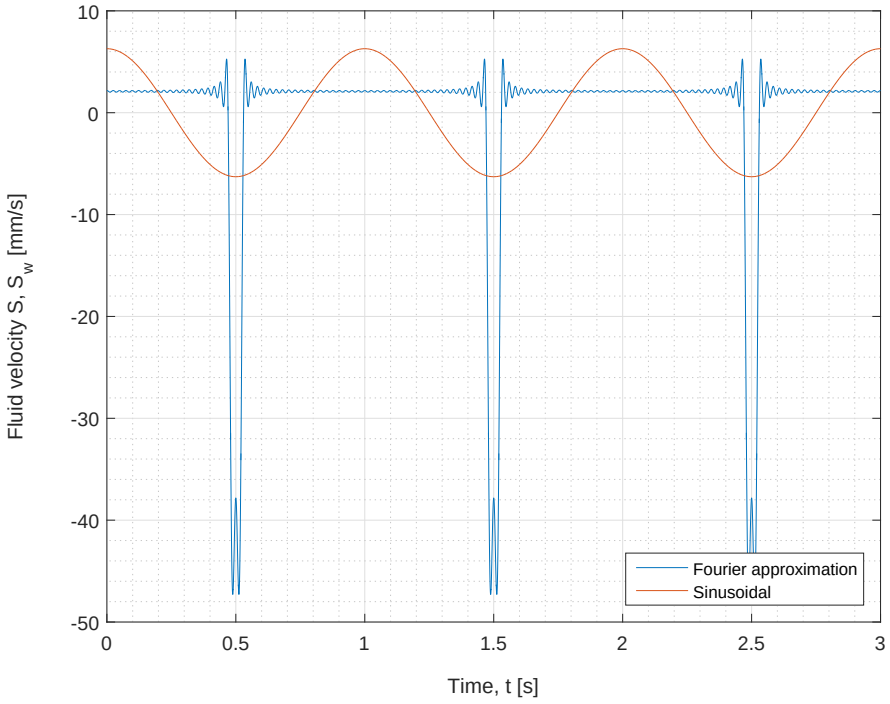

Figure 4.5: Fluid velocity using uniform and non-uniform oscillations ($ki = 1.05$)

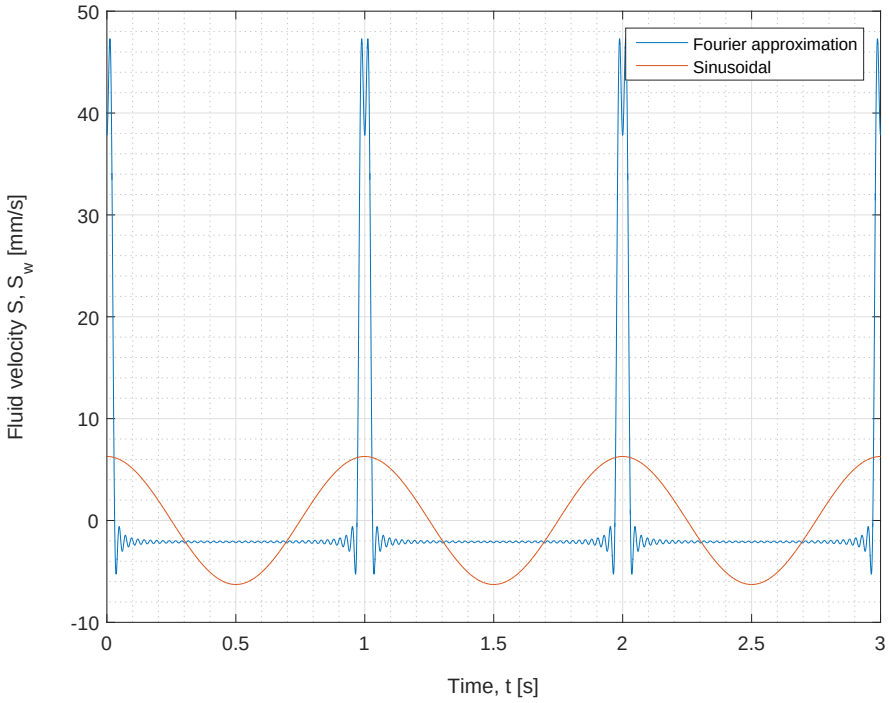

Figure 4.6: Fluid velocity using uniform and non-uniform oscillations ($ki = 21$)

And the fluid acceleration dS/dt and dS_w/dt resulting from differentiating Figure 4.5 and Figure 4.6 look as follows:

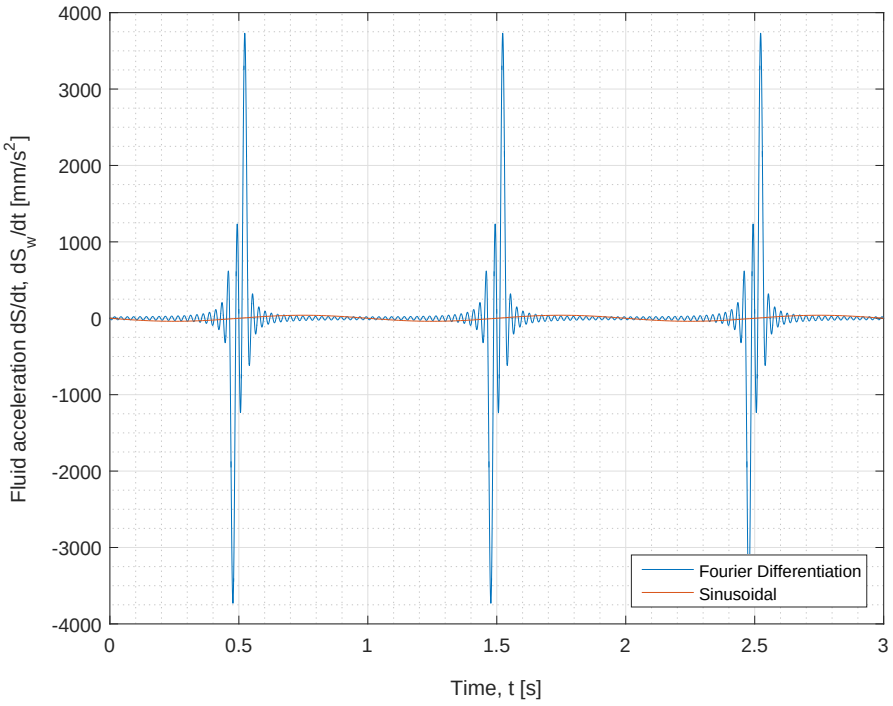

Figure 4.7: Fluid acceleration using uniform and non-uniform oscillations ($ki = 1.05$)

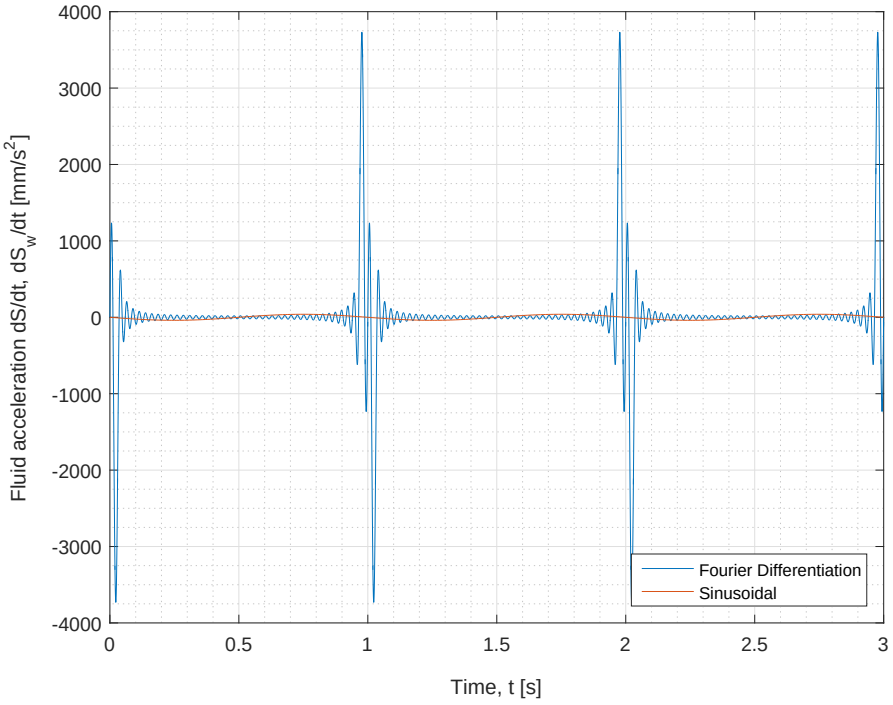

Figure 4.8: Fluid acceleration using uniform and non-uniform oscillations ($ki = 21$)

4.2.3 ODE45 Solver

The equations of motion (inviscid and viscous model) for a solid, spherical particle in an uniformly or non-uniformly oscillating fluid are solved in MATLAB. The built-in ODE45 solver is used to solve the particle response velocities in horizontal direction u and u_w and vertical direction v and v_w. This built-in solver is convenient for solving non-stiff, first order differential equations, as it uses an explicit fourth order Runge-Kutta method. Its most general form will be explained shortly in this section. First an ordinary differential equation is defined:

$$\frac{dy(t)}{dt} = f(y(t), t) \qquad \text{with} \qquad y(t_0) = y_0. \tag{4.22}$$

The Runge-Kutta method involves the weighted average of values of $f(y(t), t)$ at different points in the interval $t_0 \leq t \leq t_0 + dt$. It is given by :

$$y(t_0 + dt) = y(t_0) + \frac{(k_1 + 2k_2 + 2k_3 + k_4)\, dt}{6}, \tag{4.23}$$

where:

$$\begin{aligned}
k_1 &= f(y(t_0), t_0), \\
k_2 &= f\left(y(t_0) + k_1 \frac{dt}{2}, t_0 + \frac{dt}{2}\right), \\
k_3 &= f\left(y(t_0) + k_2 \frac{dt}{2}, t_0 + \frac{dt}{2}\right), \\
k_4 &= f(y(t_0) + k_3 dt, t_0 + dt).
\end{aligned}$$

Here, dt is defined to be the stepsize, which is set at $1/5000$, but can be adjusted by the user. The sum $(k_1 + 2k_2 + 2k_3 + k_4)/6$ can be interpreted as an average slope. Note that k_1 is the slope at the left end of the interval, k_2 is the slope at the midpoint using the Euler formula to go from t_0 to $t_0 + dt/2$, k_3 is a second approximation to the slope at the midpoint and k_4 is the slope at $t_0 + dt$ using the Euler formula and the slope k_3 to go from t_0 to $t_0 + dt$ (Boyce et al., 1969). In our case $y(t_0 + dt)$ represents the velocity being updated to the next time step.

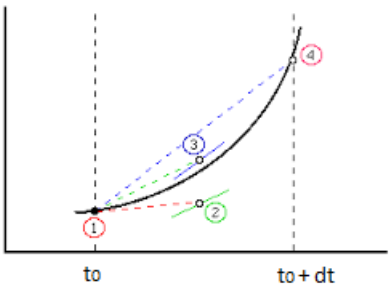

Figure 4.9: Fourth order Runge-Kutta method

Two important parameters which can be set by the user, are the relative and absolute accuracy tolerances. By default these are set to be 10^{-3} and 10^{-6}, respectively. To obtain more accurate values and because the built-in solver is very time efficient, these values were set to 10^{-7} and 10^{-9}, respectively.

4.2.4 Decoupling and phase angle

After the particle velocity is calculated numerically using the fourth order Runge-Kutta solver, the next step is to determine the amplitude ratio (decoupling) and phase angle between the particle and fluid. The amplitude ratio describes the response amplitude of the particle (A_p) as function of the imposed fluid amplitude (A_f). The phase angle described whether the particle is lagging behind (negative) the fluid motion or is leading (positive) with respect to the fluid motion. When the particle and fluid are in phase, i.e. $\varphi = 0$, the particle will follow the fluid motion one to one.

The amplitude ratio and phase angle are both used to describe the particle response behavior. As mentioned previously, it is expected that the particle will respond to the fluid oscillations having the same frequency as the fluid (ω), a particle response amplitude (A_p) and a phase angle (φ) (Equation 4.15). The amplitude ratio is defined as:

$$\text{Decoupling} = \frac{A_p}{A_f}. \tag{4.24}$$

To determine the amplitude ratio and phase angle, first a built-in Fast Fourier Transform (FFT) algorithm is used to calculate the Discrete Fourier Transform (DFT). As input, both the fluid velocity (S, S_w) and the particle response velocities u, u_w and v, v_w are used. To find the magnitude of the desired amplitudes, the absolute value is determined after which MATLAB calculates the maximum of the fluid velocity and particle response velocity signals. Both magnitudes are then divided using Equation 4.24.

To find the phase difference in radians (rad), the built-in MATLAB function "angle" is applied at the transformed signals. The fluid phase $(\varphi_S, \varphi_{Sw})$ and response phases φ_u, φ_{uw} and φ_v, φ_{vw} are determined and subtracted to find the final phase angle:

$$\begin{aligned} \varphi &= \varphi_u - \varphi_S, \\ \varphi &= \varphi_{uw} - \varphi_{Sw}, \\ \varphi &= \varphi_v - \varphi_S, \\ \varphi &= \varphi_{vw} - \varphi_{Sw}. \end{aligned} \tag{4.25}$$

4.3 Validation

The goal of this section is to validate the numerical model and its performance. Within this thesis project no physical experiments were performed because of the tight schedule. Fortunately, two datasets were found during the literature study, enabling detailed comparison.

4.3.1 Herringe (1976)

The first dataset was published by Herringe (1976) and is added in Appendix B. Herringe varied the particle density between glass ($\rho_p \approx 2960\ kg/m^3$), steel ($\rho_p \approx 7800\ kg/m^3$) and lead ($\rho_p \approx 11400\ kg/m^3$) and used two fluid amplitudes ($A_f \approx 1\ \&\ 3\ mm$). Four parameters were defined:

$$\text{Amplitude scale :} \quad \beta = \frac{A_f}{d}, \tag{4.26}$$

$$\text{Density ratio :} \quad \gamma = \frac{\rho_p}{\rho_f}, \tag{4.27}$$

$$\text{Stokes number :} \quad St = \sqrt{\frac{\nu_f}{\omega d^2}}, \tag{4.28}$$

$$\text{Fluid acceleration :} \quad Acc = \frac{A_f \omega^2}{g}. \tag{4.29}$$

These four parameters were used to investigate their dependency on the retardation ($b0 = \bar{v}/|v_t|$), amplitude ratio (A_p/A_f) and phase lag (φ). Particle retardation is defined as the ratio between the mean oscillating settling velocity ($\bar{v}$) and the absolute terminal settling velocity $|v_t|$. The experimental retardation is plotted against the *inverse Stokes number* using a particle density variation (Figure 4.10) and a fluid amplitude (A_f) variation (Figure 4.11), indicated by the colorbar.

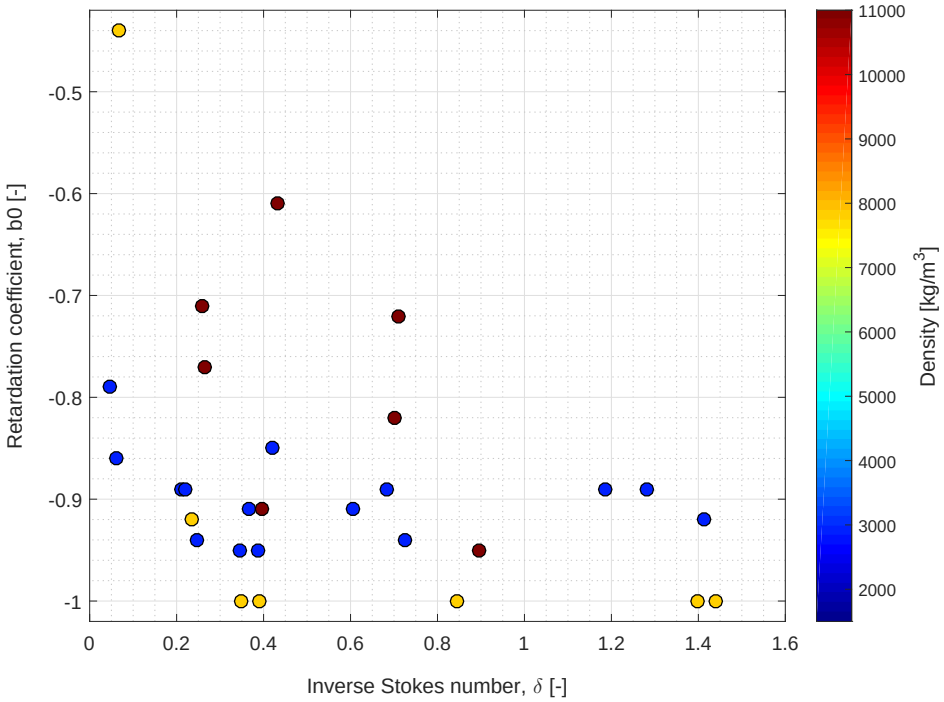

Figure 4.10: Retardation versus inverse Stokes number (δ), particle density variation

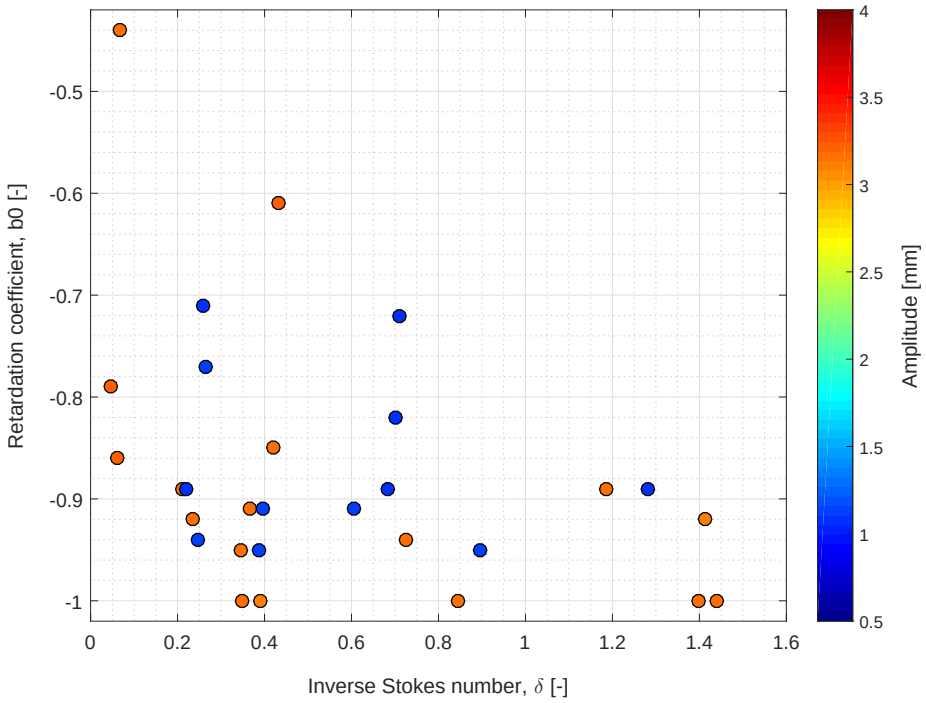

Figure 4.11: Retardation versus inverse Stokes number (δ), fluid amplitude variation

It's important to note that *uniform* oscillations were used during all Herringe's experimental runs. Furthermore, Herringe defined a Stokes number, whereas in Figure 4.10 and Figure 4.11 (and coming figures) the inverse Stokes number (δ) has been used. This is done in order to compare the results with more recent studies (Abbad and Souhar, 2004b; Weinstein, 2008) where the inverse Stokes number is used. Another important parameter is the ratio between the settling tube diameter (D) and the particle diameter (d). As mentioned in Section 4.1, no wall-effects will occur as long as the distance between the particle and the wall is larger than eight times the particle diameter $(\geq 8d)$. This results in:

$$D/d \geq 16. \tag{4.30}$$

Even considering the largest particle used during the experiments, this condition is easily satisfied. Herringe explicitly mentioned the phase angle to be *lagging* because he found that a solid particle having a larger density than the carrier fluid will always lag behind on the fluid oscillation (this will be discussed more thoroughly in Chapter 6).

During the analysis of the provided dataset, it was found that Herringe did not include the density ratio. Although the kinematic viscosity (ν_f) could be calculated using the provided Stokes number (St), the fluid density could not be determined. This proved to be a major issue when reproducing his physical experiments by the numerical model, because the model needs the fluid density as input parameter. The fluid used, was mentioned to be a *glycerol-water* solution of which the mixture ratio was varied. Using another paper (Herringe, 1977) and an online calculator, the fluid density as function of glycerol fraction could be approximated (Figure 4.12). It is assumed that all the experiments were performed at a constant fluid temperature $T \approx 15$ °C.

The online calculator: `http://www.met.reading.ac.uk/~sws04cdw/viscosity_calc.html`.

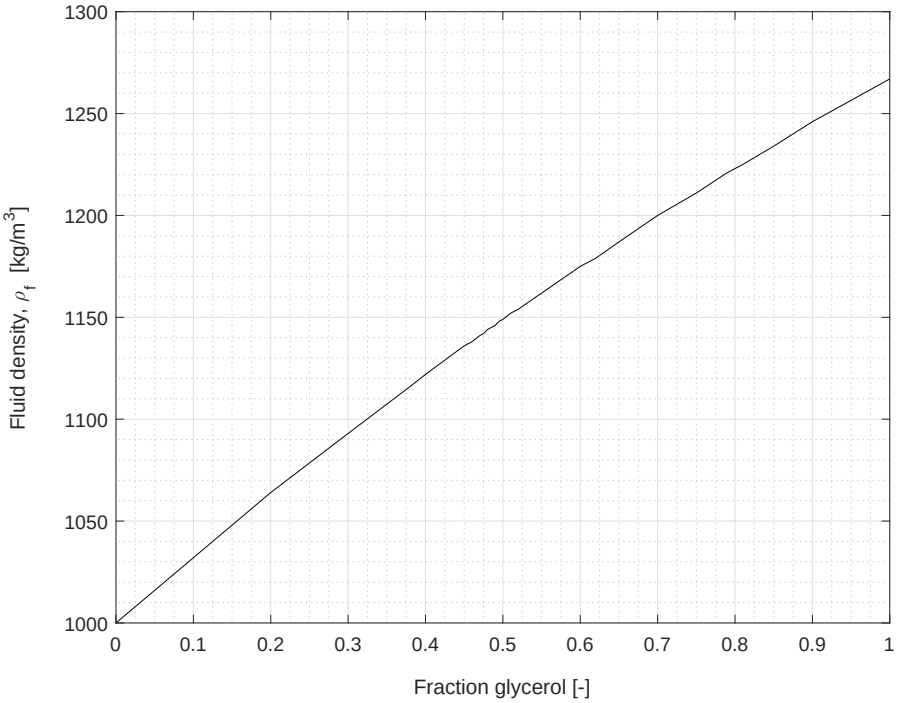

Figure 4.12: Fluid density (ρ_f) as function of glycerol fraction with $T \approx 15$ °C

After approximating the fluid density (ρ_f) calculations were conducted, resulting in Figure 4.13.

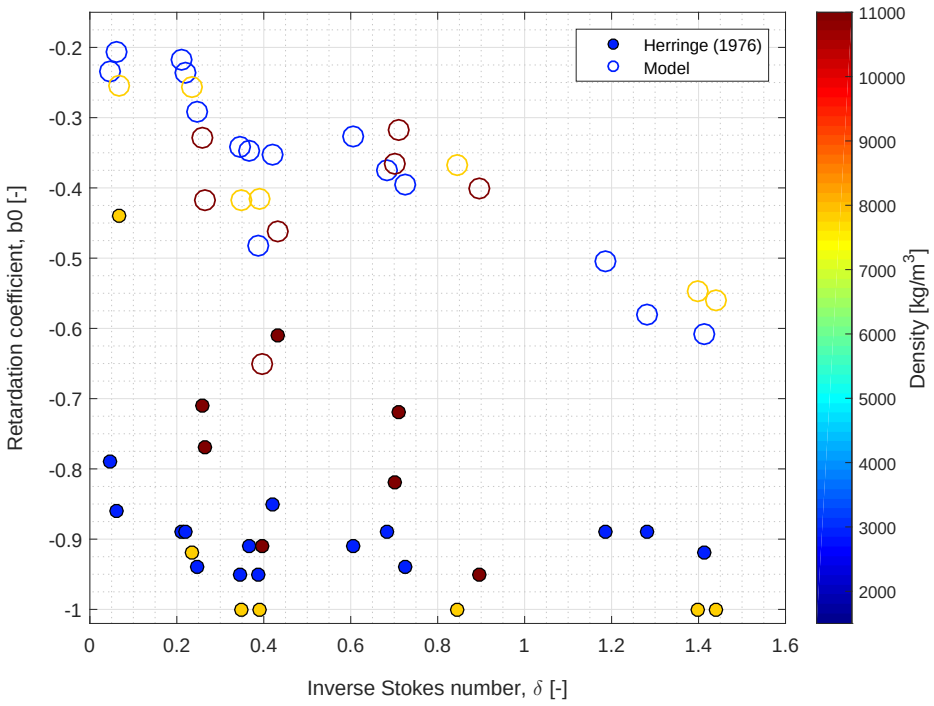

Figure 4.13: Retardation validation using experimental data

When the retardation coefficient is found to be -1, the average oscillating settling velocity $(\bar{v})$ is approximately equal to the terminal settling velocity $|v_t|$. In this case, the particle is hardly influenced by the presence of the fluid oscillations. On the other hand, when the retardation coefficient goes to zero, the particle is made hovering due to the vertically oscillating settling tube. Analyzing Figure 4.13, it is found that the predicted retardation is much greater than experimentally measured. Herringe also concluded this, but his numerical model (using a different form of the drag force (F_d) and history force (F_h)) seems to be 50% more accurate. In our comparison, an average discrepancy of 55% was found, whereas Herringe found a discrepancy of 26%. Great care has been taken to eliminate the possibility that the found discrepancy was being caused by the experimental apparatus. He concluded it had to be a shortcoming of the theory rather than some error in the imposed motion. The force terms causing this discrepancy were mentioned to be the Stokes drag force and the history force, because of their limited and unknown validity at higher particle Reynolds numbers. In the model, the Stokes drag force has been corrected to account for particle Reynolds numbers up to 1500 and besides three experimental runs, the model fell within that range. This leaves the unknown factor to be the history force (F_h). There can be concluded that the numerical model does not provide satisfactory results in this region of inverse Stokes numbers.

Fortunately, the comparison with the amplitude ratio (A_p/A_f) showed a better result. An average discrepancy of 13% was found, mostly caused by the lead particles (Figure 4.14). This conclusion was also found by Herringe, as he found an average discrepancy of 5.7%. Herringe also concluded that the discrepancy between model and theory was larger for the lead particles. Possible reasons were given to be the likelihood of the lead particles being non-spherical and the higher relative velocity due to the much larger density ratio.

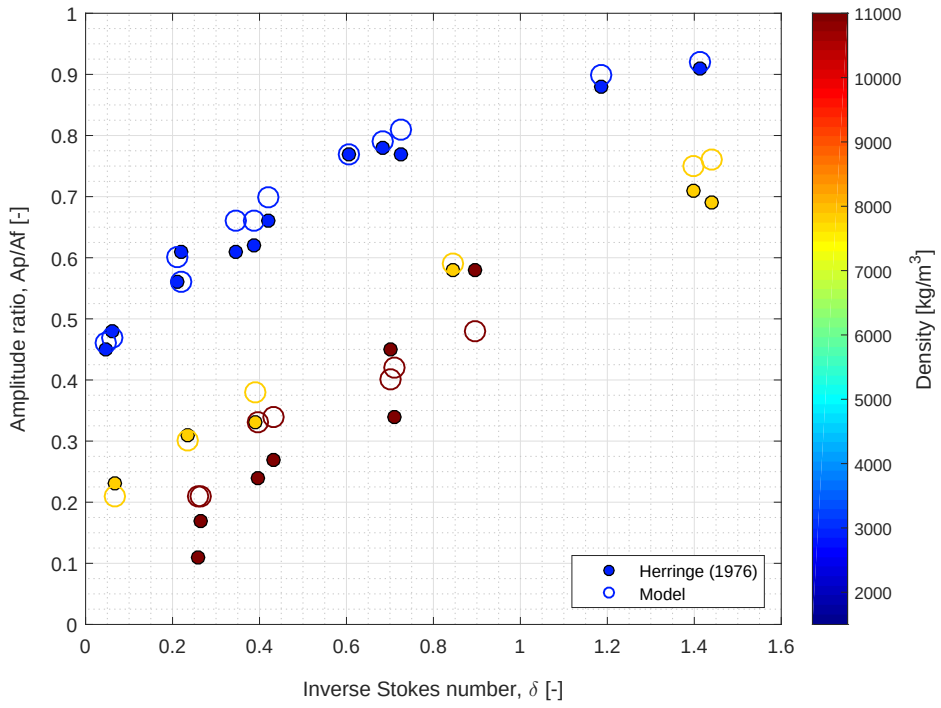

Figure 4.14: Amplitude ratio validation using experimental data

An increase in inverse Stokes number indicates an increase in viscosity or decrease in particle size, which makes it physically logical that the amplitude ratio goes to unity as shown in Figure 4.14.

Regarding the phase angle (φ) comparison between the model and experimental data, a discrepancy of 60.7% was found. This again indicates that the model would not be accurate, as Herringe found a discrepancy of 17.1% between the experimental data and his model. However, analyzing Figure 4.15 does not result in such an inaccuracy.

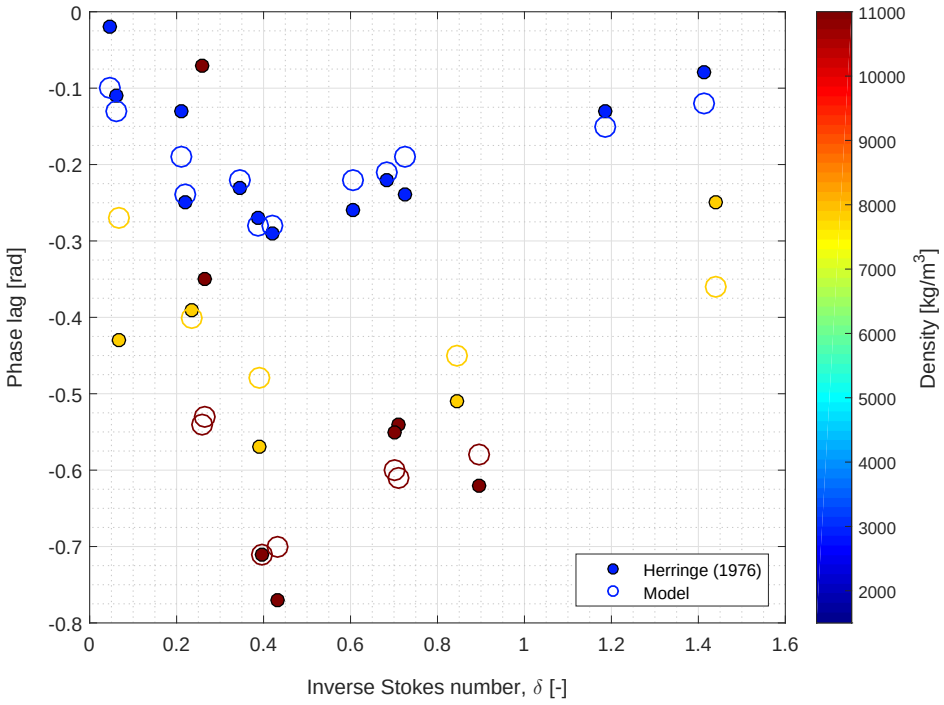

Figure 4.15: Phase lag validation using experimental data

It must be noted that two runs presented by Herringe (1976) were odd compared with the rest. These runs gave the largest discrepancy with the model, which were up to two orders of magnitude larger. Ignoring these two runs, the average discrepancy between model and experiments dropped to 10% for the amplitude ratio and 17.6% for the phase lag. Combined with the uncertainty of the fluid density approximation, it seems that the model is able to predict the phase lag and amplitude ratio reasonably well. The retardation coefficient in the used range of inverse Stokes numbers however, is significantly overestimated.

As mentioned earlier, Herringe used four parameters to study the influence on the retardation coefficient. He found that the (inverse) Stokes number (St), is a major factor affecting the amplitude ratio (A_p/A_f) and phase lag (φ). The amplitude scale (β) and density ratio (γ) were concluded to have a significant influence on the retardation coefficient $(b0)$. Regarding the fluid acceleration parameter (Acc) it was noted that it influenced the retardation coefficient the least.

4.3.2 Takahashi (1992)

The second dataset was published by Takahashi et al. (1992) and is added in Appendix C. A more systematic approach was used, compared with the experiments of Herringe (1976). Three different particle sizes were used: $d = 8, 12.7$ and $15.9\ mm$ having densities of $\rho_p = 1380, 1350$ and $1250\ kg/m^3$, respectively. Fluid amplitudes $A_f = 13.6, 23.6$ and $40.8\ mm$ were used in combination with eight different frequencies, varying between $f = 0.8 - 2.2\ Hz$. The experiments were conducted using fresh water at a constant fluid temperature $T \approx 20$ °C. Two figures were created where the retardation is plotted against the inverse Stokes number applying a particle density variation (Figure 4.16) and fluid amplitude variation (Figure 4.18), indicated by the colorbar.

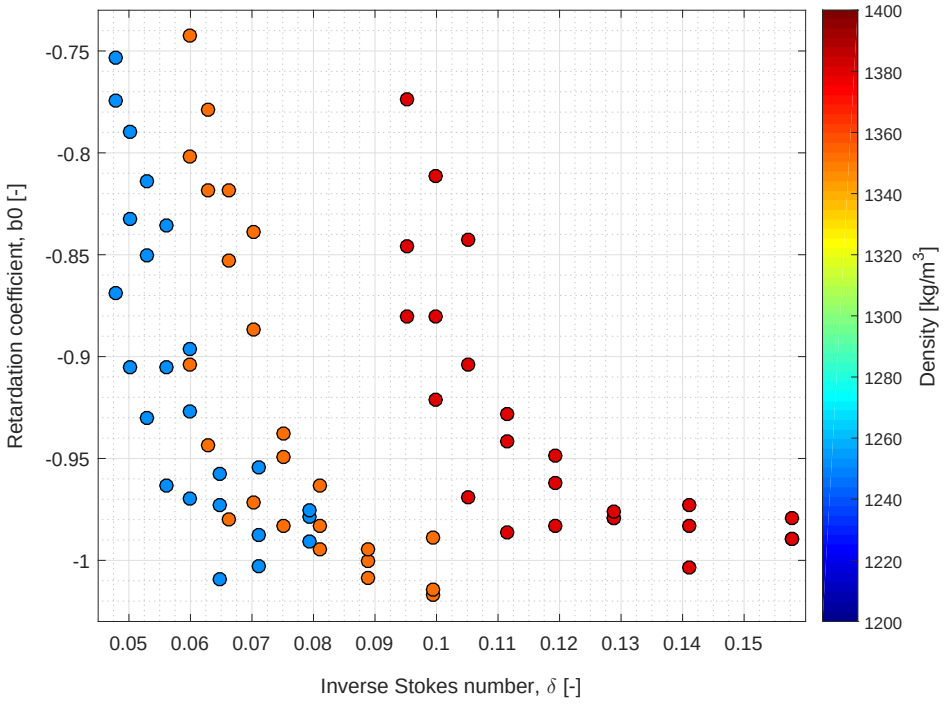

Figure 4.16: Retardation versus inverse Stokes number, particle density variation

Again, it must be noted that all the experiments were performed using *uniform* fluid oscillations. Unfortunately it was found that, because of the relatively large and dense particles used, the particle Reynolds numbers are *not* within the validity range of our model. Furthermore, during the analysis of the experimental apparatus using Equation 4.30, it turned out that the ratio between the settling tube diameter (D) and largest particle diameter (d) was too small:

$$D/d \approx 4. \tag{4.31}$$

This means that wall-effects could have been present during the experiments. It is not mentioned whether Takahashi et al. (1992) took wall-effects into account. Analyzing Figure 4.16, it can be seen that all the different particle densities used during the experiments are more or less sorted into groups. It must be noted that this is *not* because of the different densities of the particles, but because every density has its own particle size. Some of the experiments also show an increase in settling velocity $(b0 < -1)$, which is not expected. Considering Figure 4.17, these measurements show a reasonably large standard deviation.

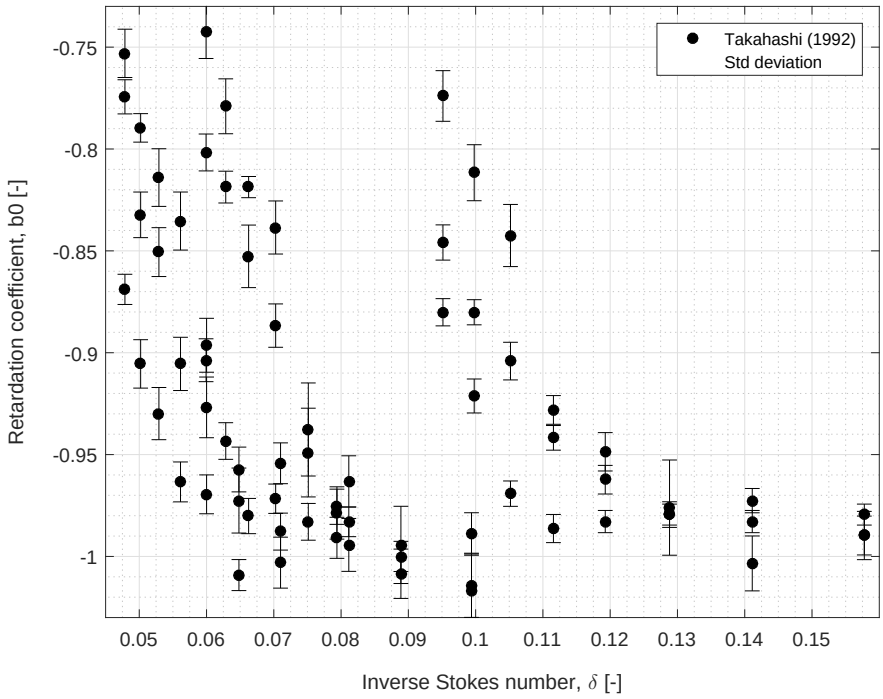

Figure 4.17: Retardation versus inverse Stokes number, standard deviation included

When the distinction between measuring points is changed from density to amplitude, a more interesting behavior is found:

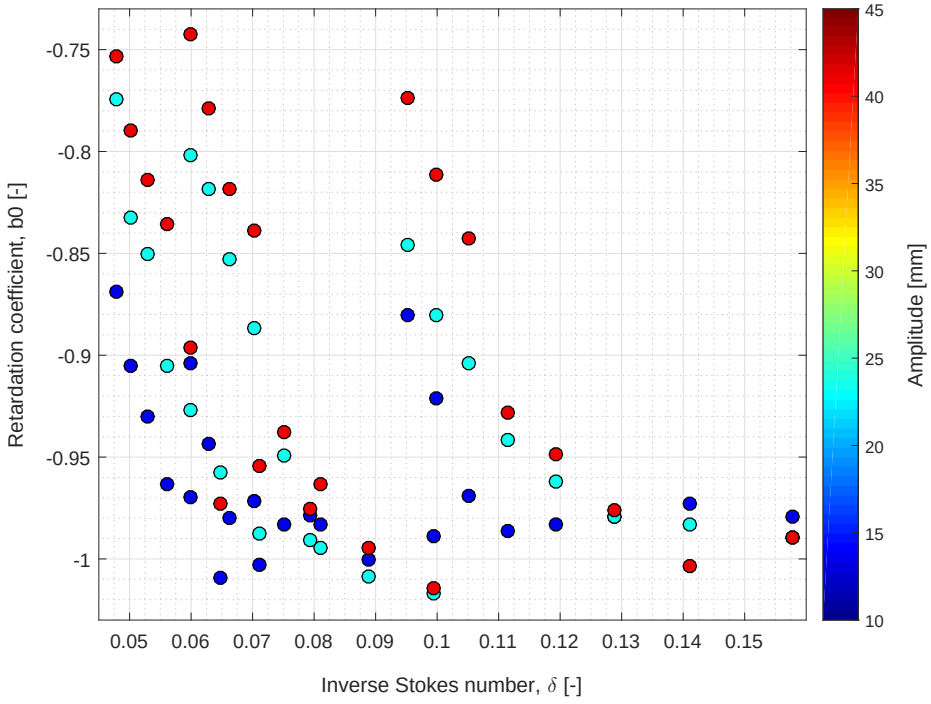

Figure 4.18: Retardation versus inverse Stokes number, fluid amplitude variation

If we now isolate certain measuring series ($d = 8\ mm$ & $\rho_p = 1380\ kg/m^3$) at which we vary the fluid amplitude and the inverse Stokes number (δ), the following is found:

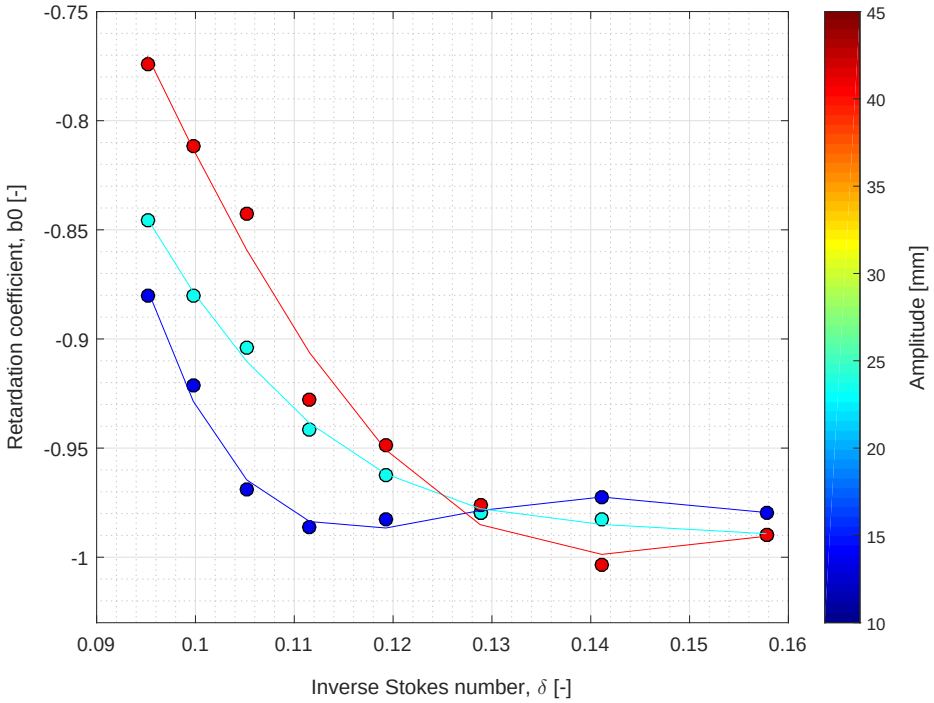

Figure 4.19: Retardation versus inverse Stokes number, fluid amplitude variation

Lower inverse Stokes numbers indicate a higher frequency (f), larger particle size (d) or lower fluid viscosity. In Figure 4.19 the particle size was kept constant together with the fluid viscosity, resulting in only a frequency dependency between the individual points per measurement series. It can be seen that a lower inverse Stokes number (and thus higher frequency) generally results in a higher retardation coefficient ($b0$). Using a standard fitting tool in MATLAB, a line (polynomial) is curve fitted through the measuring points per measuring series. Between the series, only the fluid amplitude is varied as indicated by the colorbar.

When the inverse Stokes number increases (thus the frequency decreases), the retardation coefficient ($b0$) goes to minus one (or actually unity (1) because the sign only indicates direction). This is expected behavior: as the frequency approaches zero, the terminal settling velocity in stagnant water should be found. Figure 4.19 shows that the retardation coefficient depends on both the oscillation frequency and fluid amplitude, but also suggests that the amplitude might have a larger influence than the frequency. This will be discussed thoroughly in Chapter 4.

Again plotting all the measured data (without standard deviation to increase clarity of the figure), together with the numerical calculations, resulted in Figure 4.20.

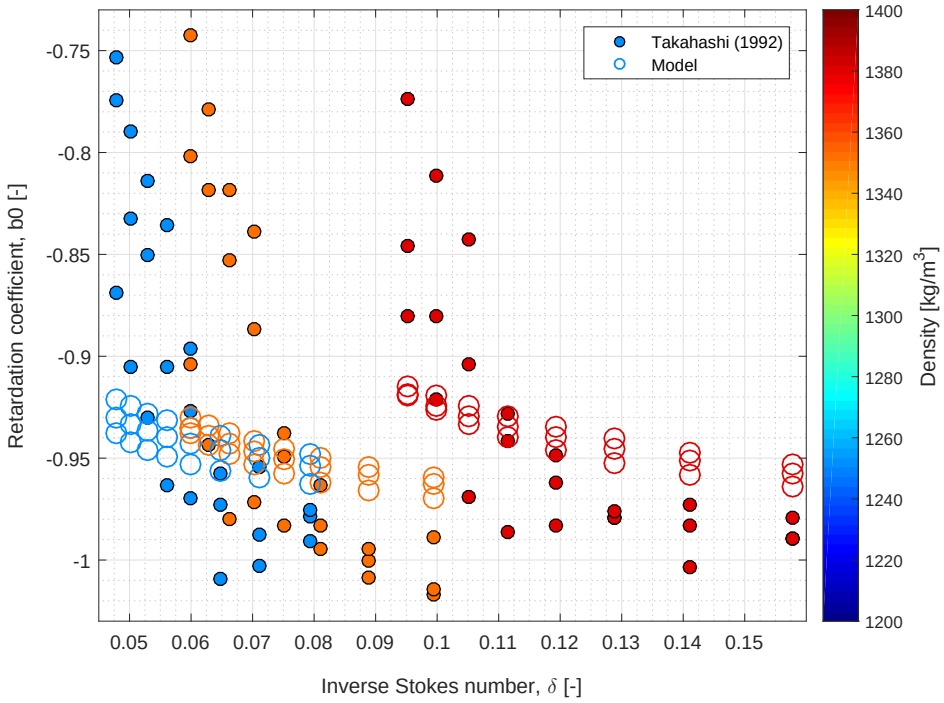

Figure 4.20: Retardation validation using experimental data

At first glance the model does not seem to fit the data very well. However, considering the scale of the y-axis it was found that the fit was actually reasonably good. An average discrepancy of only 6.4% was found. This is interesting, taking into account that the particle Reynolds numbers are well above the maximum of 1500 and that the used Inverse Stokes numbers are one order of magnitude smaller compared with the data from Herringe (1976). The largest discrepancy between the Ferguson and Church (2004) equation Equation 4.6 and the measured terminal settling velocity (v_t) by Takahashi et al. (1992) was found to be 4.3%. This discrepancy thus influenced the overall error significantly.

Furthermore, it was found that increasing the fluid amplitude, particle size (Herringe's parameter $\beta = A_f/d$) and the frequency during specific measurement series, the discrepancy between experiments and numerical model increased up to 30%. It is expected to be caused by the increase in relative velocity between particle and fluid (Herringe, 1976) together with the mentioned the Stokes drag force (F_d) being outside the validity range. Unfortunately, Takahashi et al. (1992) did not measure the decoupling and phase angle during their experiments.

Summarizing:
From the validation study it can be concluded that the phase angle (φ) and decoupling (A_p/A_f) are reasonably well predicted by the numerical model, having a accuracy of 17.6% and 10%, respectively. The retardation coefficient $(b0)$ however, proved to be significantly overestimated at the higher inverse Stokes numbers $(0.2 < \delta < 1.6)$ in combination with particle Reynolds numbers within the validity range. When the particle Reynolds numbers went well outside the validity range, but the inverse Stokes number were low $\delta < 0.16$, it was found that the retardation coefficient could be estimated within 6.4% accuracy. However, the retardation behavior at higher frequencies was underestimated.

CHAPTER 5

Inviscid particle motion results

In this chapter the particle response motions due to inviscid fluid oscillations are presented. As mentioned, it is expected that no phase angle will occur because of the lag of viscosity. Uniform as well as non-uniform fluid oscillations are examined in order to determine whether a difference in particle response behavior will occur. Besides this, the particle response motions are separated in horizontal and vertical direction to study the hypotheses (Chapter 2).

5.1 Horizontal oscillations

5.1.1 Uniform oscillations

Let's consider a horizontally oscillating settling tube, the horizontal force balance (as derived in Chapter 3), yields:

$$V_p \, \rho_p \, \frac{du_{pot}}{dt} = \frac{1}{2} \, \rho_f V_p \left(\frac{dS}{dt} - \frac{du_{pot}}{dt} \right) + \rho_f V_p \frac{dS}{dt}. \tag{5.1}$$

Rewriting the force balance shows that the inviscid particle acceleration only depends on the density ratio ($\gamma = \rho_p / \rho_f$):

$$\frac{du_{pot}}{dt} = \frac{3 \, (dS/dt)}{1 + 2(\rho_p / \rho_f)}. \tag{5.2}$$

Substituting the uniform fluid acceleration (dS/dt) and integrating with respect to t yields the particle response velocity in horizontal direction (u_{pot}):

$$u_{pot} = \frac{3 \, A_f \, \omega}{1 + 2(\rho_p / \rho_f)} \cos(\omega t). \tag{5.3}$$

Plotting Equation 5.3 and the uniform fluid velocity (S) where $\rho_p > \rho_f$, results in the following figure:

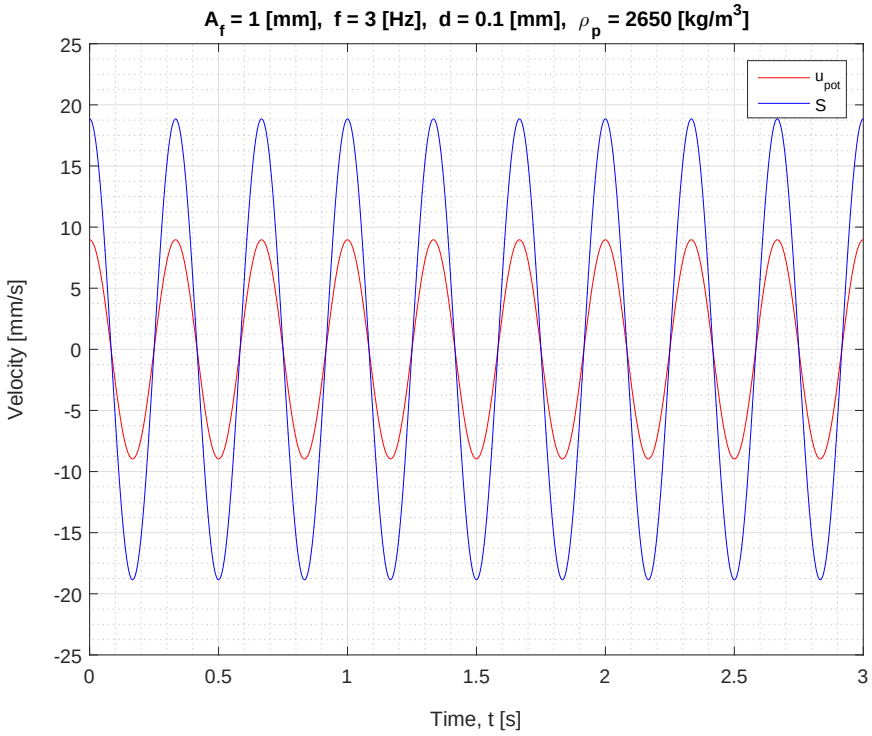

Figure 5.1: Horizontal particle response velocity u_{pot}, uniform oscillations $\gamma > 1$

When the particle is less dense than the fluid, i.e. $\rho_p < \rho_f$, the following figure is obtained:

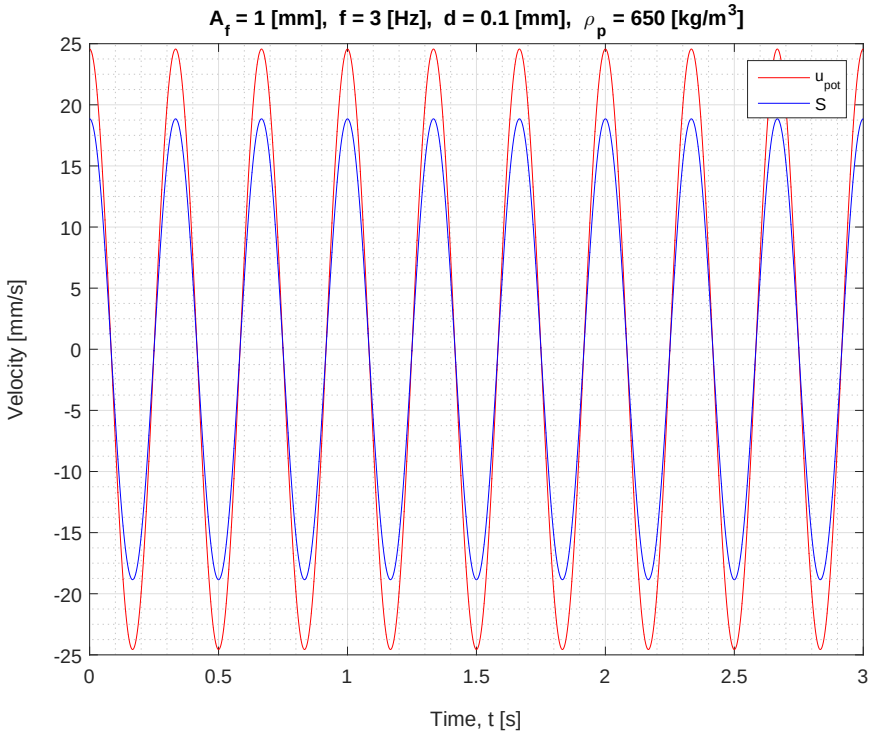

Figure 5.2: Horizontal particle response velocity u_{pot}, uniform oscillations $\gamma < 1$

Both Figure 5.1 and Figure 5.2 clearly show the decoupled motion between the fluid and the particle. The results are as discussed in Section 3.1, where it was expected that a relative motion would occur when the particle is more or less dense than the fluid. The fluid density was chosen to be $\rho_f \approx 998\ kg/m^3$ (fresh water) whereas the density of the particle was either quartz sand ($\rho_p \approx 2650\ kg/m^3$) or a random material ($\rho_p \approx 650\ kg/m^3$). In both figures the fluid amplitude (A_f) was kept constant. For a solid particle with a larger density than the fluid the response amplitude is lower than that of the fluid, i.e. $A_p/A_f < 1$ (Figure 5.1) and for a less dense solid particle the response amplitude is higher, i.e. $A_p/A_f > 1$ (Figure 5.2).

As described in Chapter 3, using Equation 3.7 (which is repeated at the beginning of this subsection), it is expected that for very low particle densities ($\rho_p \ll \rho_f$) the particle acceleration will be at maximum three times as high as the fluid acceleration. By integrating twice, it is found that this is also the case for the particle velocity and displacement. The amplitude ratio (A_p/A_f) as function of the density ratio ($\gamma = \rho_p/\rho_f$), is presented in Figure 5.3:

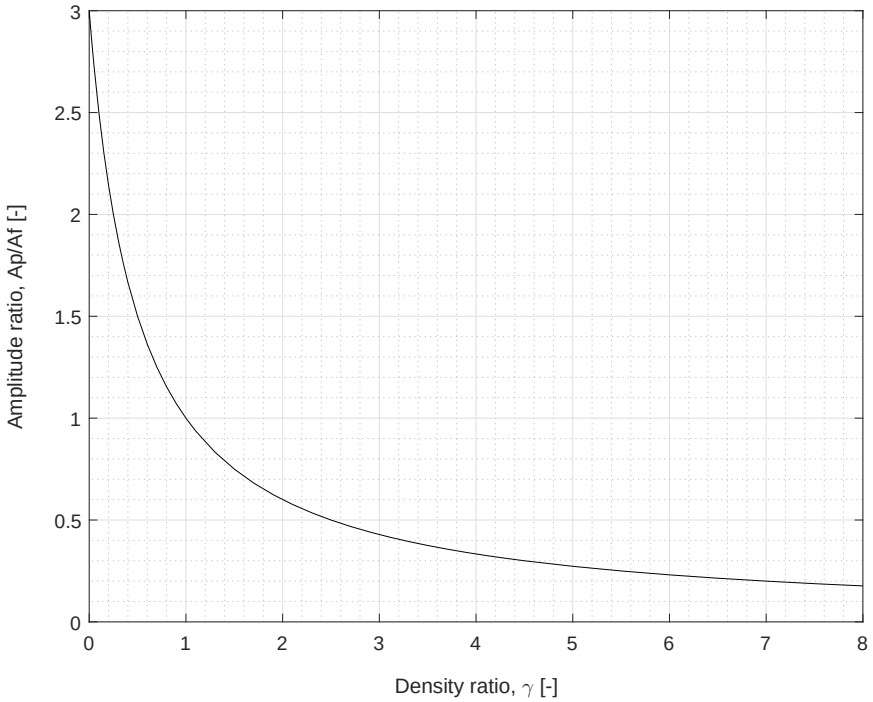

Figure 5.3: Decoupling as function of density ratio (γ) for the inviscid model

It is nicely shown that in the lower limit of the density ratio, i.e. $\rho_p \ll \rho_f$ the amplitude ratio is maximal three and when the density ratio becomes large ($\rho_p \gg \rho_f$) the amplitude ratio goes to zero (A_p eventually becomes zero). Furthermore, when the density ratio is unity ($\rho_p = \rho_f$) the amplitude ratio is also unity, ensuring the particle motion to be exactly equal to the fluid motion.

Besides the decoupled motion it was also expected that the particle would oscillate in phase with the fluid because of the neglected drag and history force. This expectation is also clearly shown in both Figure 5.1 and Figure 5.2. The particle oscillates at the drive frequency of the fluid, which is assumed to be exactly equal to the frequency of the settling tube.

5.1.2 Non-uniform oscillations

Until now, only uniform oscillations were used to excite the settling tube. In case of non-uniform fluid oscillations, the horizontal particle acceleration is defined as:

$$\frac{du_{w,pot}}{dt} = \frac{3\,(dS_w/dt)}{1+2(\rho_p/\rho_f)}, \tag{5.4}$$

where dS_w/dt is the non-uniform fluid acceleration (as derived in Subsection 4.2.2). Again the particle velocity and displacement are found by integrating twice with respect to t. Unfortunately, no simple equation is obtained by substituting the non-uniform fluid velocity (S_w), so in final form, the horizontal particle velocity using non-uniform inviscid fluid oscillations yields:

$$u_{w,pot} = \frac{3\,S_w}{1+2(\rho_p/\rho_f)}. \tag{5.5}$$

It is expected that Figure 5.3 will also hold for Equation 5.5. Solving for the particle velocity using the same settings as for the uniform fluid oscillations, except the shape factor (ki) results in:

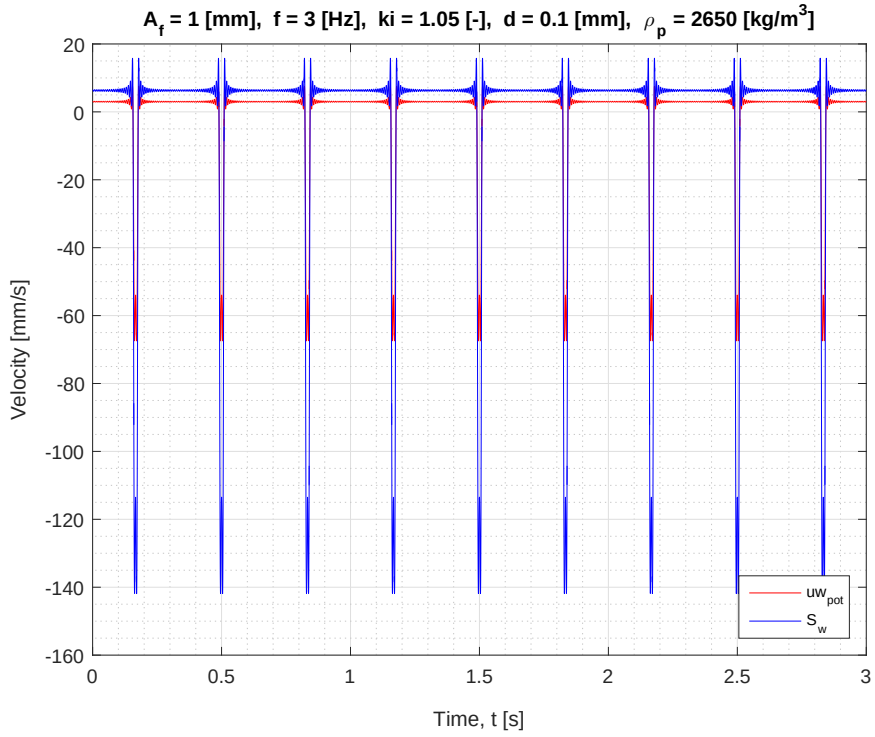

Figure 5.4: Horizontal non-uniform particle response velocity $u_{w,pot}$, $ki = 1.05$

This fluid velocity profile is obtained by using a sawtooth-like fluid displacement where $ki = 1.05$ (Figure 4.3). Because of the greater steepness incorporated into the sawtooth wave fluid displacement, the fluid velocities found by differentiating are also an order of magnitude larger compared with uniform oscillations (both the fluid and the particle response velocity). Because of the approximation using the Fourier series, the fluid displacement, velocity and acceleration will never show exact straight lines. Especially in the discontinuous regions the approximation comes up short. To clarify the fluid and particle response motion, Figure 5.5 was added.

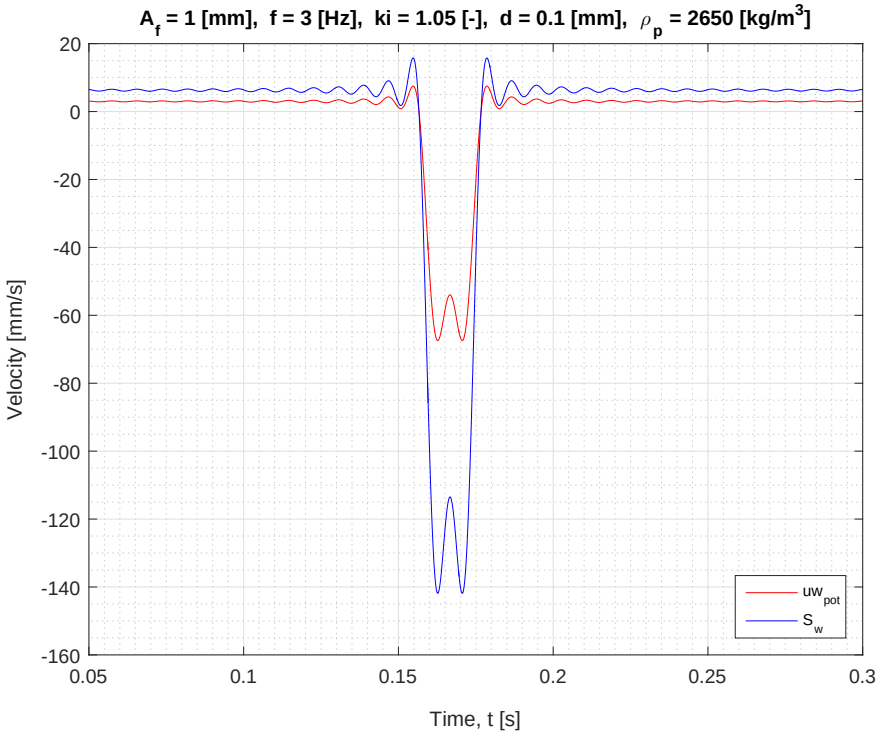

Figure 5.5: Horzontal non-uniform particle response velocity $u_{w,pot}$, single wave

Changing the shape factor to its upper limit $(ki = 21)$ results in mirrored velocity profiles:

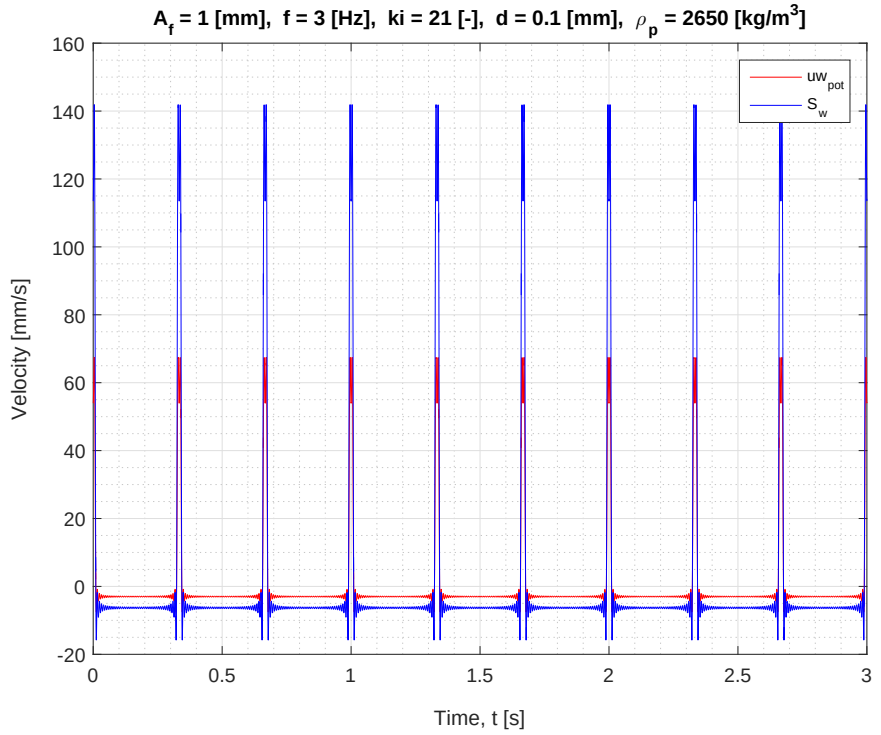

Figure 5.6: Horizontal non-uniform particle response velocity $u_{w,pot}$, $ki = 21$

Performing calculations with the particle being less dense than the fluid, resulted in the same particle motion behavior as shown at Figure 5.2 (also identical for both shape factors). Therefore, it was chosen to show the difference in shape factor (Figure 5.6) instead of the difference in particle density. Analyzing the shape factor $ki = 21$, it is shown that the fluid velocity profile mirrors over the x-axis. This results from the fluid displacement sawtooth wave having its steepest incline in an upward direction.

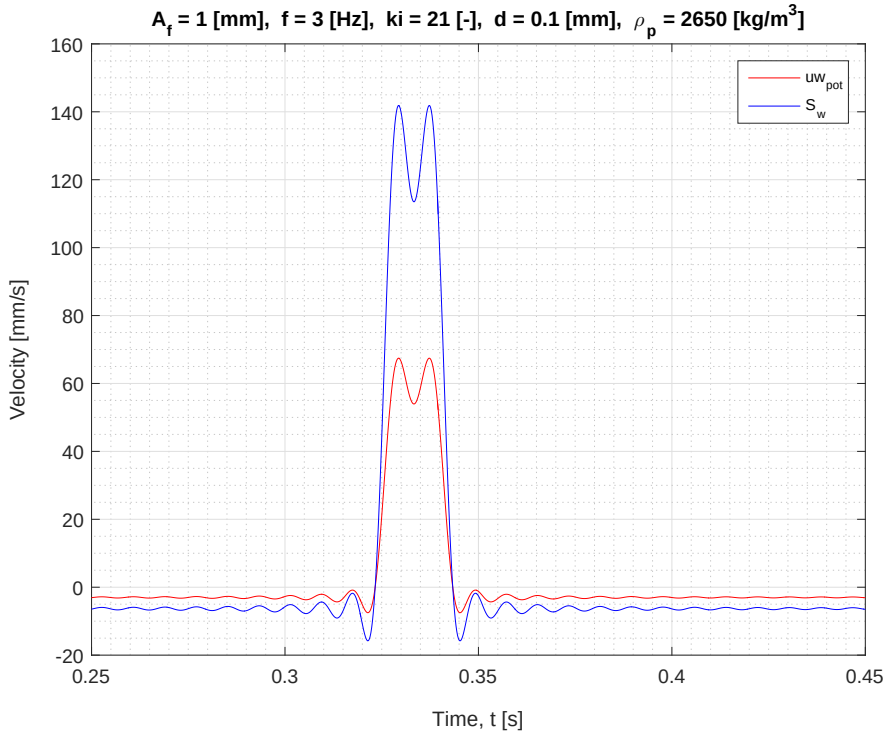

Figure 5.7: Horizontal non-uniform particle response velocity $u_{w,pot}$, single wave

Furthermore, it is shown that the average particle response velocity using a shape factor $ki = 1.05$ (Figure 5.5) is positive, whereas the high velocity peak is in the left direction. This behavior is due to the sawtooth wave shape presented in Subsection 4.2.2. Again, changing the shape factor to $ki = 21$, this behavior is exactly mirrored over the x-axis.

5.2 Vertical oscillations

5.2.1 Uniform oscillations

Let's now consider a vertically oscillating settling tube, the vertical force balance (Chapter 2), yields:

$$V_p\,\rho_p\,\frac{dv_{pot}}{dt} = \frac{1}{2}\,\rho_f V_p\left(\frac{dS}{dt} - \frac{dv_{pot}}{dt}\right) + \rho_f V_p \frac{dS}{dt} + V_p\,g\,(\rho_f - \rho_p). \tag{5.6}$$

Rewriting gives:

$$\frac{dv_{pot}}{dt} = \frac{3\,(dS/dt)}{1 + 2(\rho_p/\rho_f)} + \frac{2g(\rho_f - \rho_p)}{(\rho_f + 2\rho_p)}. \tag{5.7}$$

Substituting the uniform fluid acceleration (dS/dt) and integrating with respect to t yields the particle response velocity in vertical direction (v_{pot}):

$$v_{pot} = \frac{3\,A_f\,\omega}{1 + 2(\rho_p/\rho_f)}\cos(\omega t) + \frac{2g(\rho_f - \rho_p)}{(\rho_f + 2\rho_p)}. \tag{5.8}$$

Plotting Equation 5.8 and the uniform fluid velocity (S) where $\rho_p > \rho_f$, results in:

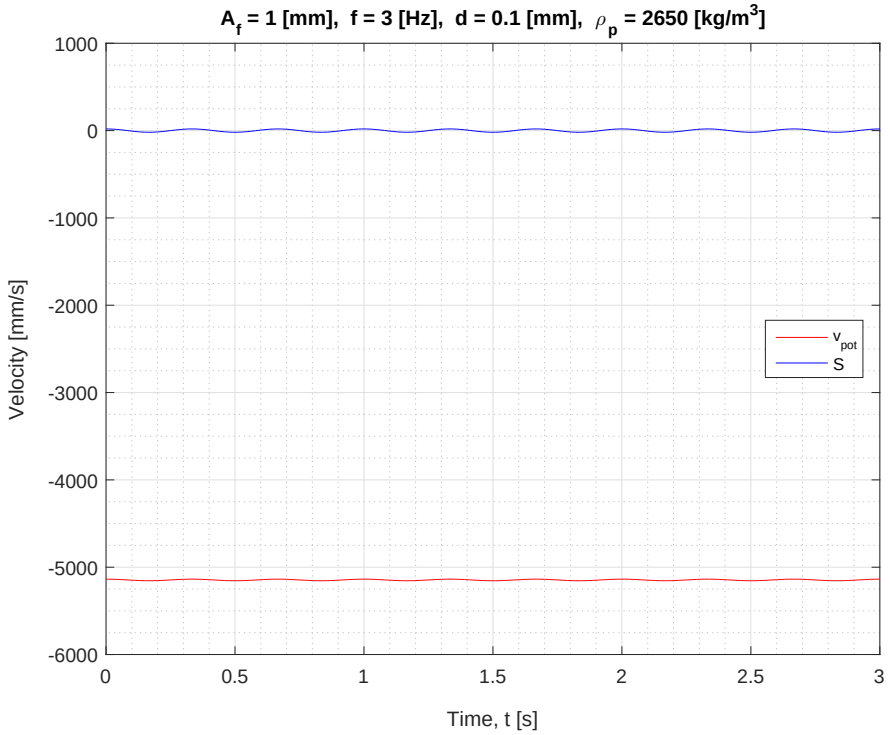

Figure 5.8: Vertical particle response velocity v_{pot}, $\gamma > 1$

To compare Figure 5.8 to Figure 5.1, equal settings were applied (shown at the top of the figure). Clearly the gravity term in Equation 5.8 is more dominant than the combined pressure and added mass term. Slight oscillatory motion of the particle is visible, but at these settings the terminal settling velocity is much larger than the particle response velocity to the vertical uniform fluid oscillations. Increasing both the frequency and amplitude, results in:

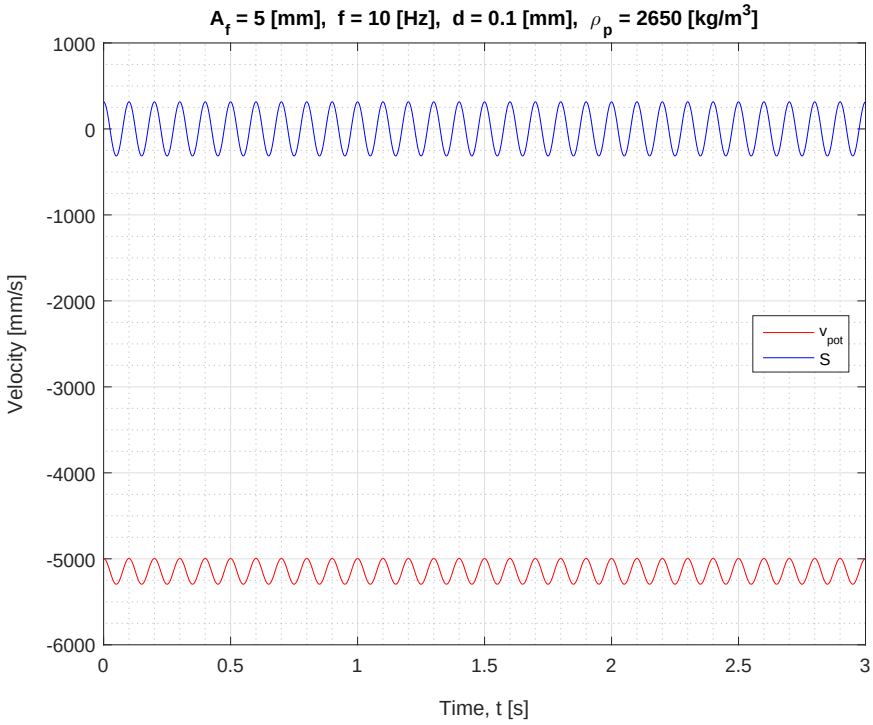

Figure 5.9: Vertical particle response velcoity v_{pot}, $\gamma > 1$

Lowering the particle density to $\rho_p = 650\ kg/m^3$, yields:

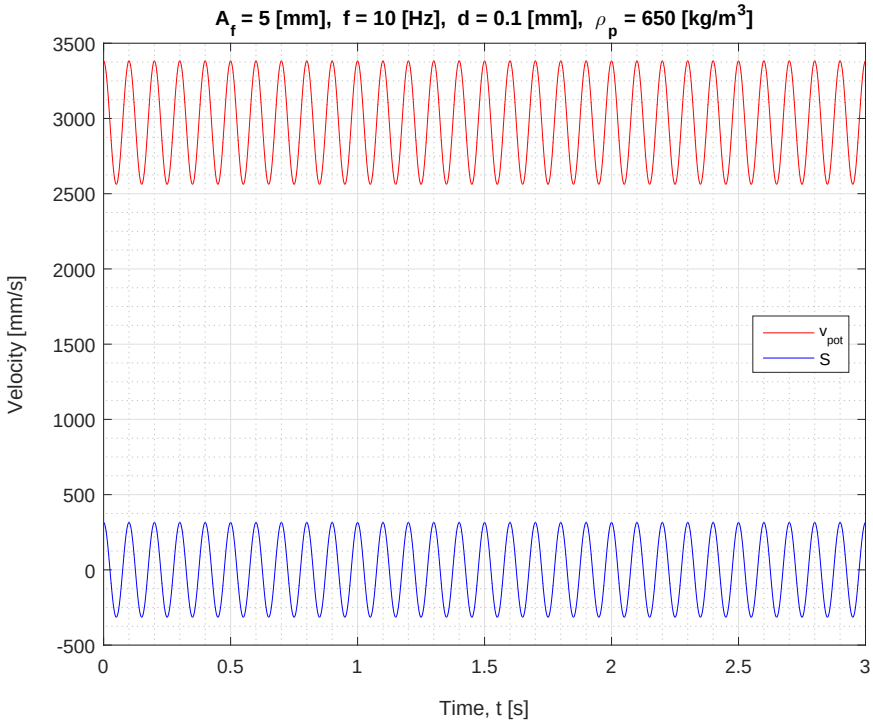

Figure 5.10: Vertical particle response velcoity v_{pot}, $\gamma < 1$

Using a oscillation frequency $f = 10Hz$ and amplitude $A_f = 5mm$, results in a more visible particle response motion. The particle density being larger than the fluid density again results in a amplitude ratio $A_p/A_f < 1$, as expected (Figure 5.9).

Conducting more calculations (Figure 5.10) showed that a density ratio $\gamma < 1$, thus the fluid being more dense than the particle, resulted in a decoupling ratio $A_p/A_f > 1$ with a maximum ratio of 3. This proved that Figure 5.3 is also valid in the case of vertical oscillations. If the fluid is more dense than the particle, then the particle velocity is also found to be oscillating in the positive quadrant because it will rise instead of settle. Furthermore, it may be harder to see immediately, but again the fluid and particle oscillate in phase $(\varphi = 0)$ at the same driving frequency.

5.2.2 Non-uniform oscillations

Considering non-uniform fluid oscillations to excite the settling tube, first the equation for the vertical particle response acceleration is defined:

$$\frac{dv_{w,pot}}{dt} = \frac{3\,(dS_w/dt)}{1 + 2(\rho_p/\rho_f)} + \frac{2g(\rho_f - \rho_p)}{(\rho_f + 2\rho_p)}, \tag{5.9}$$

Integrating with respect to time (t) yields the non-uniform vertical particle response velocity:

$$v_{w,pot} = \frac{3\,S_w}{1 + 2(\rho_p/\rho_f)} + \frac{2g(\rho_f - \rho_p)}{(\rho_f + 2\rho_p)}. \tag{5.10}$$

Plotting Equation 5.10 and the non-uniform fluid velocity (S_w) where $\rho_p > \rho_f$, using both shape factors $ki = 1.05$ and $ki = 21$ results in Figure 5.11 and Figure 5.12, respectively.

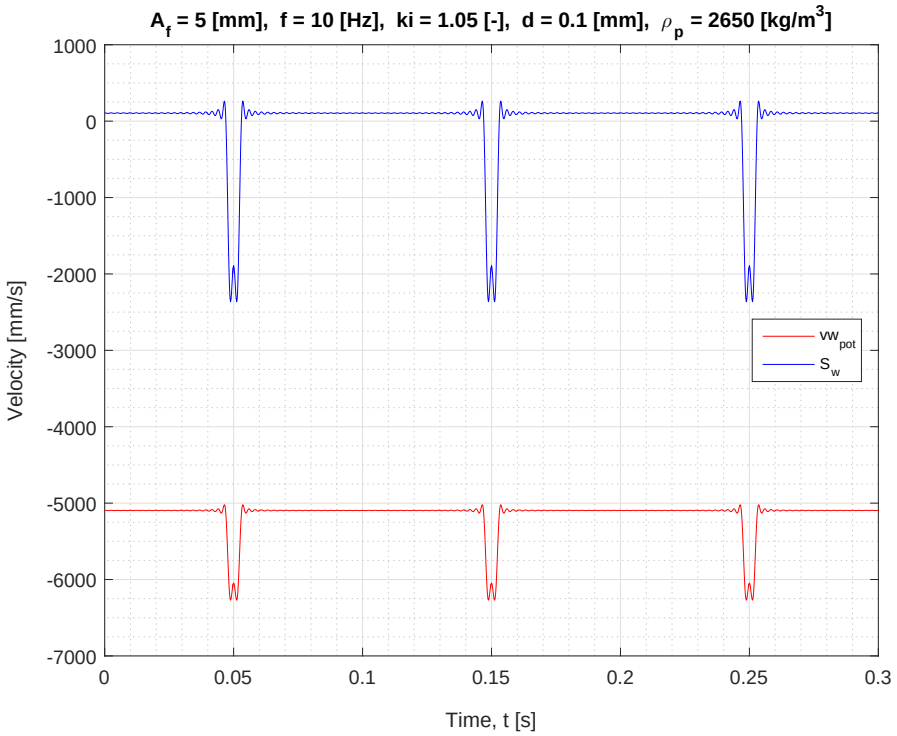

Figure 5.11: Vertical non-uniform particle response velocity $v_{w,pot}$, $ki = 1.05$

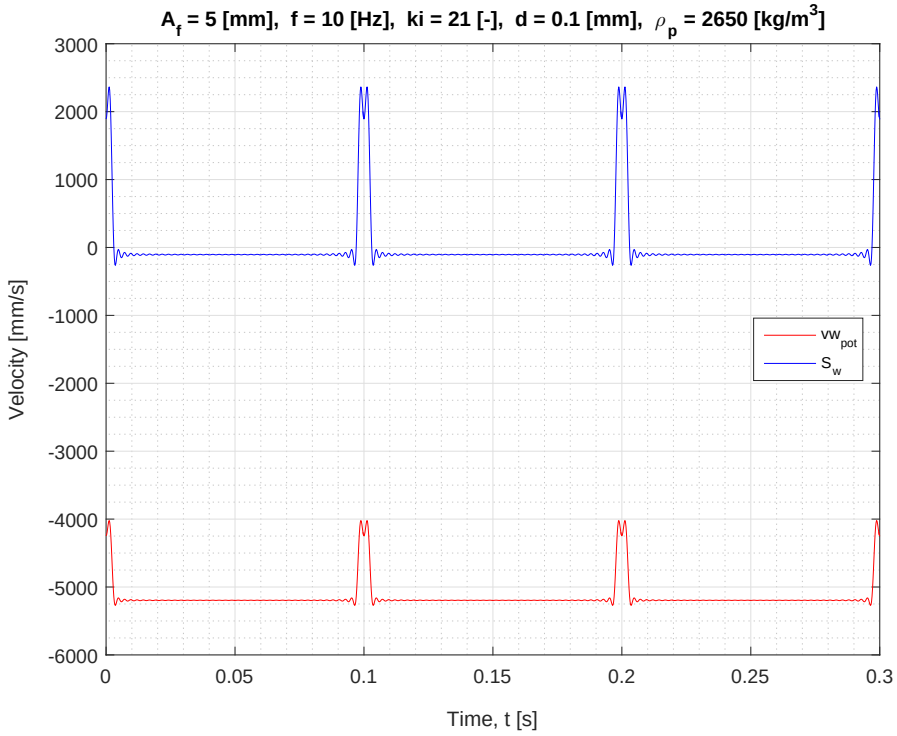

Figure 5.12: Vertical non-uniform particle response velocity $v_{w,pot}$, $ki = 21$

After calculating the particle response velocity using a density ratio $\gamma < 1$, it was again concluded that similar particle behavior was found in the case of non-uniform oscillations (A_p/A_f). These figures will not be shown.

Analyzing the average vertically oscillating particle velocity, combined with the particle size (d) in either the uniform or the non-uniform inviscid fluid oscillations $(\bar{v_{pot}}$ & $\bar{v_{w,pot}})$, it is noted that the fall velocity under gravity is extremely high. This is caused by the lag of the Stokes drag force and history force. As mentioned, it is expected that the decoupled motion between the particle and the fluid will decrease when the fluid becomes viscous (with addition of the Stokes drag force (F_d) and history force (F_h)) and the history force is added. The addition of these forces will presumably also cause a phase difference between the fluid and particle. This phase difference is expected to depend on the density ratio (γ), as the decoupled motion also showed this dependency.

The inviscid model has clearly shown that the inertial difference between the particle and the fluid is essentially the driving force for the decoupled motion. However, due to the viscosity being neglected, this model cannot be used to predict a possible relative velocity between particle and fluid.

CHAPTER 6

Viscous particle motion results

From this point forward, the fluid is considered to be viscous, ensuring the Stokes drag force (F_d) and history or Basset force (F_h) to be non-zero. During the calculations, the fluid density and viscosity are calculated for fresh water having a temperature $T = 20$ °C. Dependency between fluid oscillation frequency (f), amplitude ratio (A_p/A_f), phase difference (φ), shape factor (ki) and particle migration or settling velocity (u, u_w, v, v_w) for uniform and non-uniform fluid oscillations is examined. First, the horizontal direction is discussed, for both uniform and non-uniform fluid oscillations. Subsequently, the vertical direction is covered for both oscillations types.

6.1 Horizontal oscillations

6.1.1 Uniform oscillations

Let's again consider a horizontally oscillating settling tube, using uniform fluid oscillations. The exact same settings are used as shown in Figure 5.1, except for the model. The viscous model (BBO-equation) is repeated here for convenience:

$$\begin{aligned} V_p\,\rho_p\,\frac{du}{dt} &= 6\pi\mu_f\,r(S-u)\phi(Re_p) + \\ &\quad 6\pi\mu_f\,r\left[\frac{S-u}{\delta}+\frac{\delta\tau_v}{2}\left(\frac{dS}{dt}-\frac{du}{dt}\right)\right] + \\ &\quad \frac{2}{3}\pi\rho_f\,r^3\left(\frac{dS}{dt}-\frac{du}{dt}\right) + \\ &\quad \frac{4}{3}\pi\rho_f\,r^3\,\frac{dS}{dt}. \end{aligned} \tag{6.1}$$

Solving for the viscous particle response velocity (u), using the same oscillation frequency and amplitude as in Figure 5.1, results in the following figure:

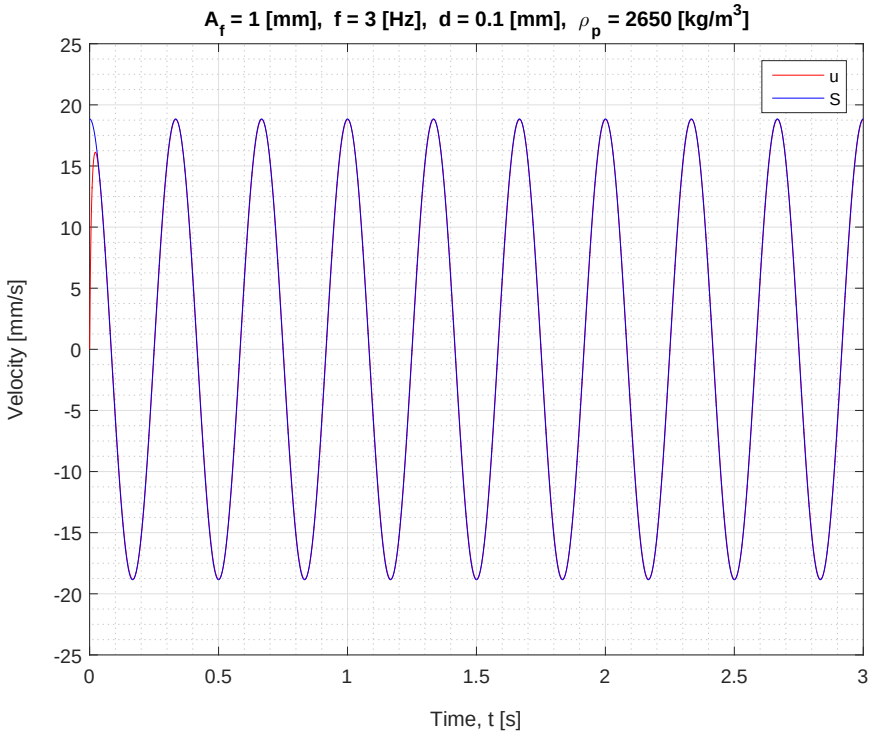

Figure 6.1: Horizontal particle response velocity u, uniform oscillations $\gamma > 1$, $d = 0.1\ mm$

Analyzing Figure 6.1, there is hardly any observable difference between the fluid motion and the particle response motion. As expected, the addition of drag causes the decoupling between the particle and fluid to decrease compared to the particle motion results presented in Figure 5.1. In combination with a relatively small particle $(d = 0.1\ mm)$, the particle will follow the fluid oscillation almost exactly as the viscous force terms dominate the inertial force terms. Also, no phase angle can be visually observed. The calculations showed a decoupling $A_p/A_f \approx 0.99$ and a phase angle $\varphi \approx -0.01\ rad$, which is negligible.

Increasing the weight of the particle by either increasing its size (d) or its density (ρ_p) should result in higher inertial difference between the fluid and the particle and therefore a higher decoupling.

Setting the particle size to a diameter of $2\ mm$ results in the following particle response behavior:

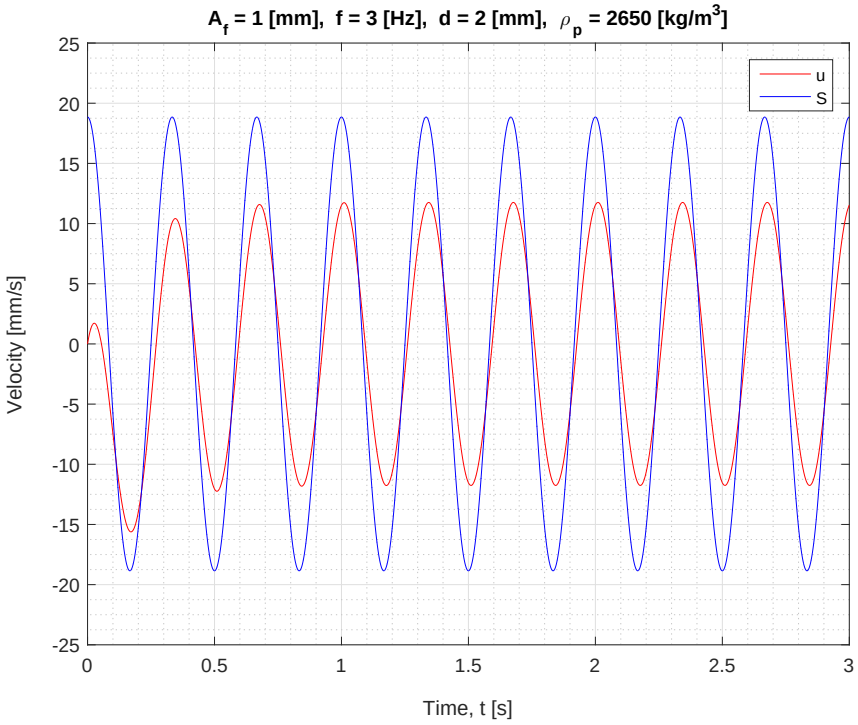

Figure 6.2: Horizontal particle response velocity u, uniform oscillations $\gamma > 1$, $d = 2\,mm$

Now the decoupling was found to be $A_p/A_f \approx 0.61$ and the phase difference $\varphi \approx -0.17\,rad$. If the particle density is lowered again, such that the density ratio $\gamma < 1$, the following is found:

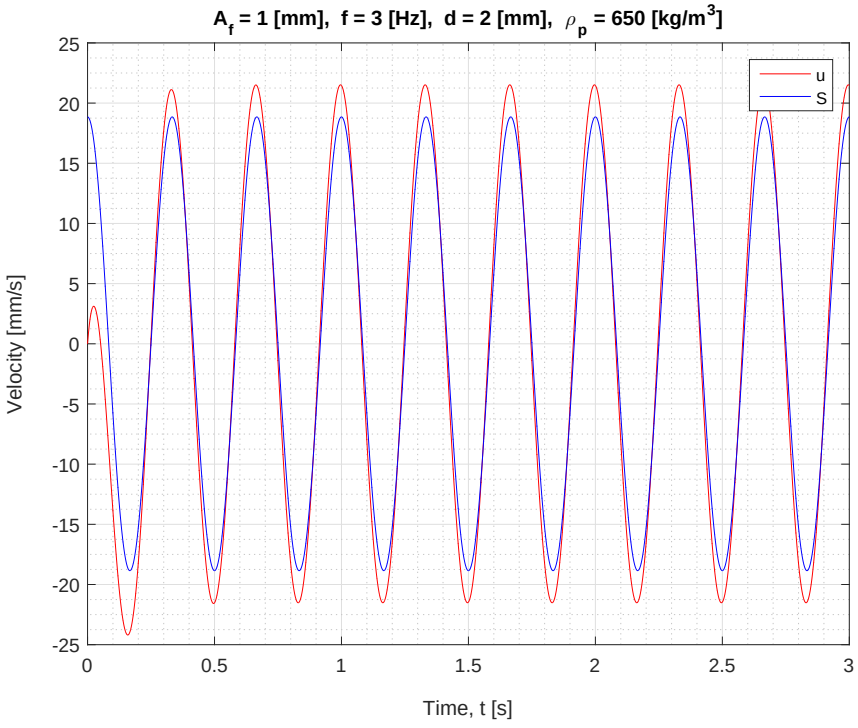

Figure 6.3: Horizontal particle response velocity u, uniform oscillations $\gamma < 1$, $d = 2\,mm$

As expected, it is shown that the decoupled motion between the particle and fluid is larger than unity when the density ratio is smaller than unity ($\gamma < 1$). Running the calculation showed that the decoupling turned out to be $A_p/A_f \approx 1.13$ and the phase difference $\varphi \approx 0.10\ rad$. The phase angle has shifted from lagging behind (negative value) to leading (positive value) with respect to the fluid motion. These observations are experimentally validated for dense solid particles (Van Oeveren and Houghton, 1971; Herringe, 1976) as well as for particles with a very low density (Weinstein, 2008).

In the limit of low viscosity (inertial forces dominate) using potential theory, no phase differences will occur between the fluid and the particle and the amplitude ratio is at maximum $A_p/A_f = 3$. In cases that the drag forces dominate the inertial forces, no decoupling or phase angle will be found (Figure 6.1). Non-zero values for the phase angle are only found when the drag and inertial forces compete.

6.1.2 Non-uniform oscillations

Using non-uniform fluid oscillations, the exact same particle response behavior is found as for the uniform oscillations. Using the same settings as at Figure 5.4 but now using the viscous model, yields:

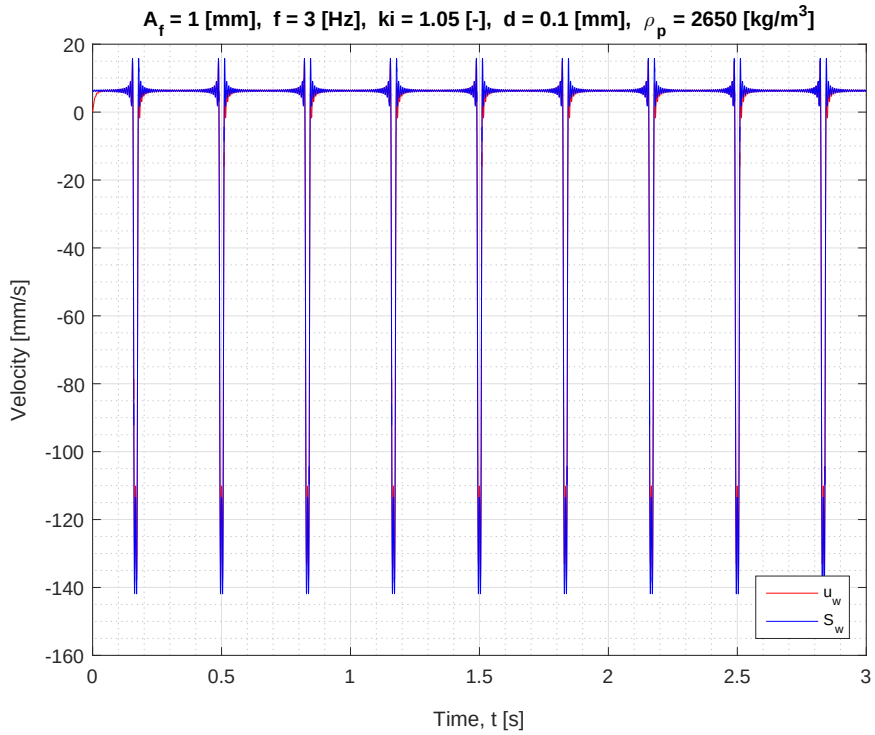

Figure 6.4: Horizontal particle response velocity u_w, $\gamma > 1$, $d = 0.1\ mm$

It may be difficult to distinguish directly, but it is again shown that the Stokes drag force (F_d) and the history force (F_h) cause the particle to follow the fluid oscillations more closely.

To clarify Figure 6.4, again an enlarged single wave is added:

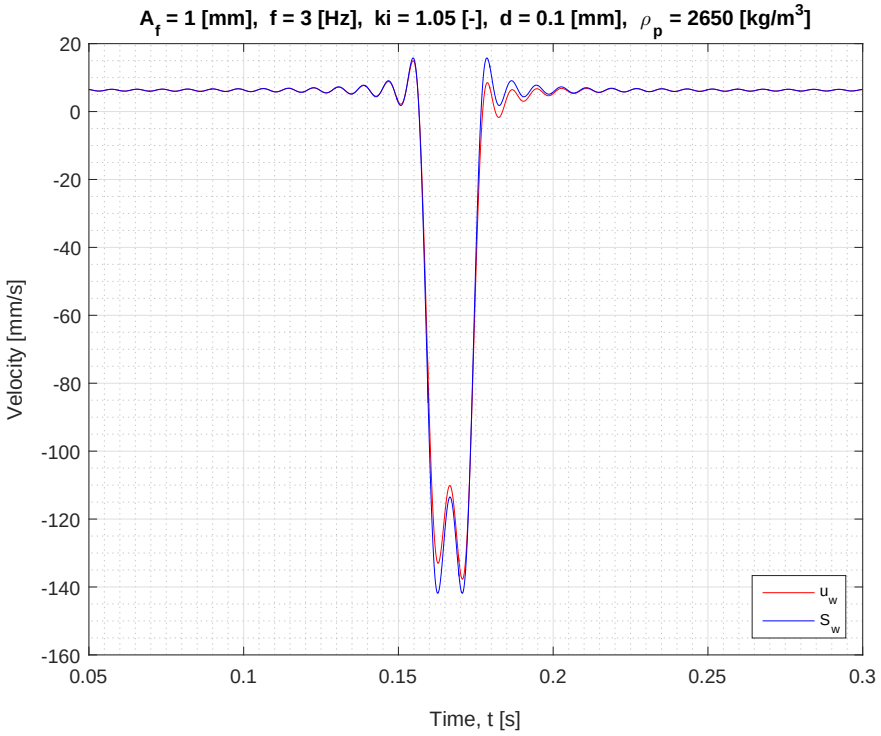

Figure 6.5: Horizontal particle response velocity u_w, $\gamma > 1$, $d = 0.1\ mm$

Despite higher fluid velocities, viscous forces are still dominant in Figure 6.5, causing the fluid and particle motion to be almost one to one. Using the same method to calculate the amplitude ratio and phase angle showed that the results were similar, compared with the uniform fluid oscillations. Hence, the larger fluid accelerations (using these settings) did not influence the particle response motion (amplitude ratio or phase angle).

Again, the case of a particle being less dense than the fluid $(\gamma < 1)$ has been examined. Similar results were found, compared with the uniform oscillations (Figure 6.3). This also holds for changing the shape factor of the non-uniform fluid oscillations $(ki = 21)$. Similar behavior (mirrored over the x-axis) is found compared with Figure 6.5. These calculations are therefore not adopted in the thesis.

The analysis between the uniform and non-uniform fluid oscillations has not shown any significant difference, besides that the fluid and particle velocities are both one order of magnitude larger. Currently, the used amplitudes (A_f) and frequencies (f) are low, to qualitatively indicate the particle response behavior. Later, both are enlarged to determine whether an average relative velocity (migration) will occur between the particle and fluid.

6.1.3 Decoupling dependency on frequency

Performing calculations using the inviscid and viscous model, showed that the amplitude ratio is influenced by the inertial difference between fluid and particle. The addition of viscous forces caused the particle to follow the fluid motion more closely. To determine whether the amplitude ratio is sensitive on frequency, an analysis is performed where the above mentioned parameters were kept constant except for the particle diameter (d) and oscillation frequency (f).

If the relative motion is not sensitive to small changes in frequency, then it is not important to always be on the exact frequency to describe the particle response behavior. Figure 6.6 shows the decoupling or amplitude ratio for the particle sizes of interest using uniform (red dotted lines) and non-uniform (black dotted lines) fluid oscillations. The shape factor was set to be $ki = 1.05$.

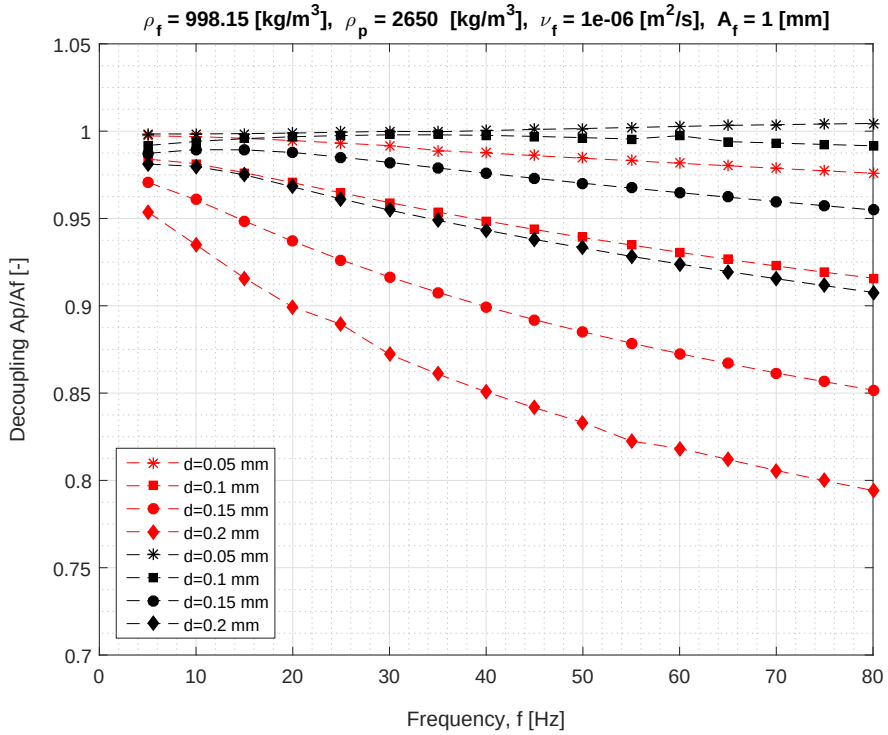

Figure 6.6: Decoupling (A_p/A_f) as function of frequency (f)

It is nicely shown that the amplitude ratio is smaller than unity for the chosen range of frequencies when the particle is more dense than the fluid $(\gamma > 1)$. A wide range of frequencies was chosen in order to achieve higher accuracy in theoretically predicting the dependency between the amplitude ratio and oscillation frequency.

Considering the y-axis, Figure 6.6 shows that the amplitude ratio is not particularly sensitive to small changes in oscillation frequency. The maximum decrease in amplitude ratio of approximately 2% is found when the frequency is increased with $5\ Hz$ using $d = 0.2\ mm$. However, the dependency increases with increasing particle size. Because only the very small fractions are of interest, it can be assumed that decoupling does not depend on frequency. Is is remarkable though, that the non-uniform fluid oscillations show even more constant behavior. Using the other limit of the shape factor $(ki = 21)$ resulted in similar magnitudes, so this figure will not be adopted in the thesis.

To study the shown behavioral difference between the uniform and non-uniform oscillations, the particle response velocities are plotted in a single figure for $f = 5\ Hz$ and $f = 80\ Hz$.

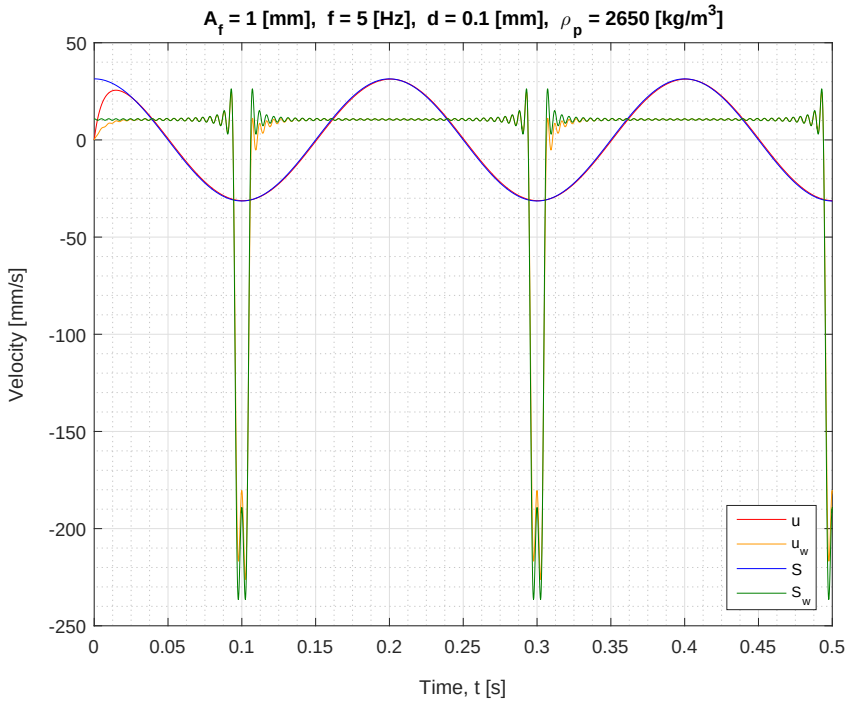

Figure 6.7: Decoupled motion for uniform and non-uniform oscillations, $f = 5\ Hz$

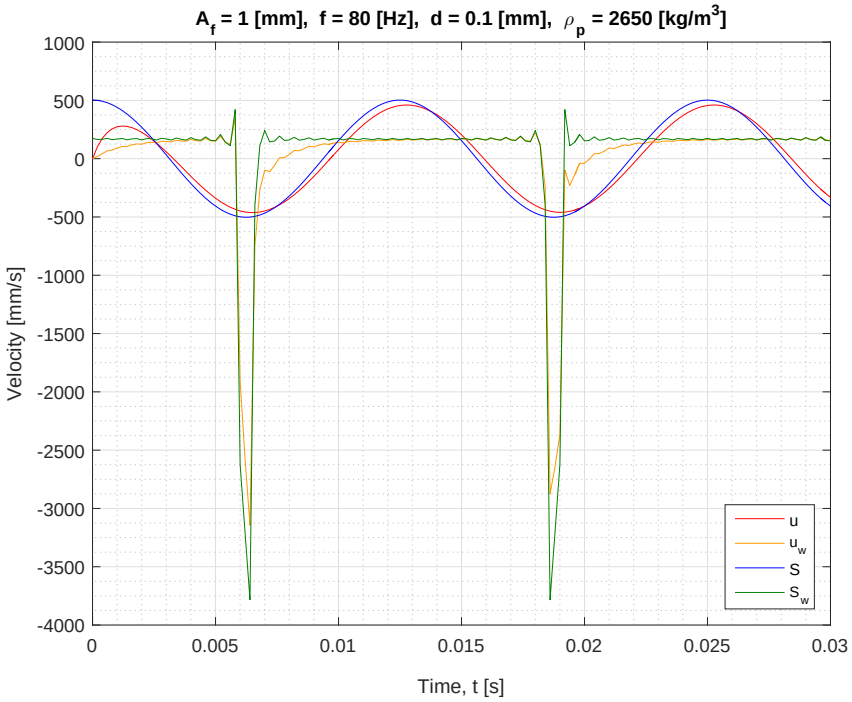

Figure 6.8: Decoupled motion for uniform and non-uniform oscillations, $f = 80\ Hz$

It is indeed shown that an increase in fluid oscillation frequency of 75 Hz, causes the decoupled motion to increase for both the uniform and non-uniform oscillations. Analyzing Figure 6.7 and Figure 6.8, it is questionable whether the non-uniform oscillations are indeed less dependent on frequency. It is also clearly shown that the increase in oscillations frequency causes a phase angle (φ) increase to occur. A similar analysis is therefor performed, studying the dependency of the phase angle on oscillation frequency.

6.1.4 Phase angle dependency on frequency

Calculating the phase angle dependency on frequency, resulted in Figure 6.9. Again, the red dotted lines indicate uniform fluid oscillations whereas the black dotted lines indicate non-uniform fluid oscillations $(ki = 1.05)$.

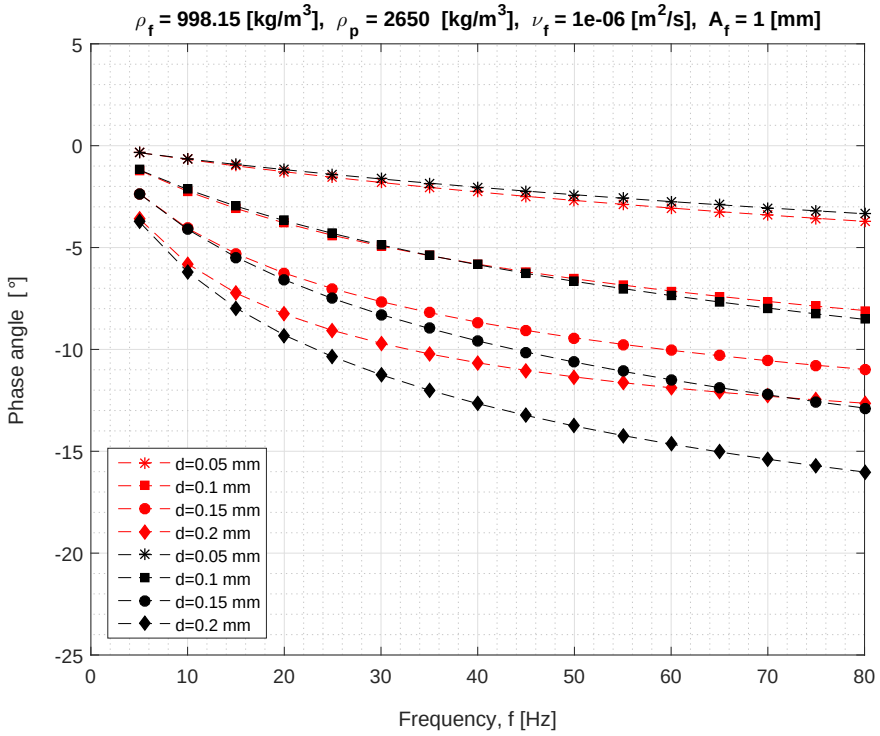

Figure 6.9: Phase angle (φ) as function of frequency (f)

Figure 6.9 shows that the phase angle (φ), just like the amplitude ratio, does not significantly change over small changes in frequency for the smallest particle sizes. Again, increasing the particle size causes the dependency of phase angle with frequency to increase as well. Unlike the amplitude ratio however, the non-uniform show a larger dependency on frequency than the uniform oscillations. Analyzing Figure 6.7 and Figure 6.8 is it again questionable whether is is truly the case.

The dependency must be considered when large differences in oscillation frequency are analyzed. Then, both the decoupling and phase angle are not just dependent on the ratio between viscous and inertial forces.

6.1.5 Decoupling dependency on viscosity

During the inviscid modelling of the particle response behavior, decoupling was shown to occur because of inertial differences between the fluid and particle. When the viscosity terms $(F_d \ \& \ F_h)$ were added to the model, the decoupling decreased. This shows that the amplitude ratio (A_p/A_f) is dependent on the balance between the inertial forces $(F_a \ \& \ F_p)$ and the viscosity forces $(F_d \ \& \ F_h)$. To determine the decoupling behavior as function of viscosity and particle size (using a fixed particle density of quartz sand), Figure 6.10 was created. Note that *uniform* fluid oscillations at a fixed frequency of $f = 15 \ Hz$ were used.

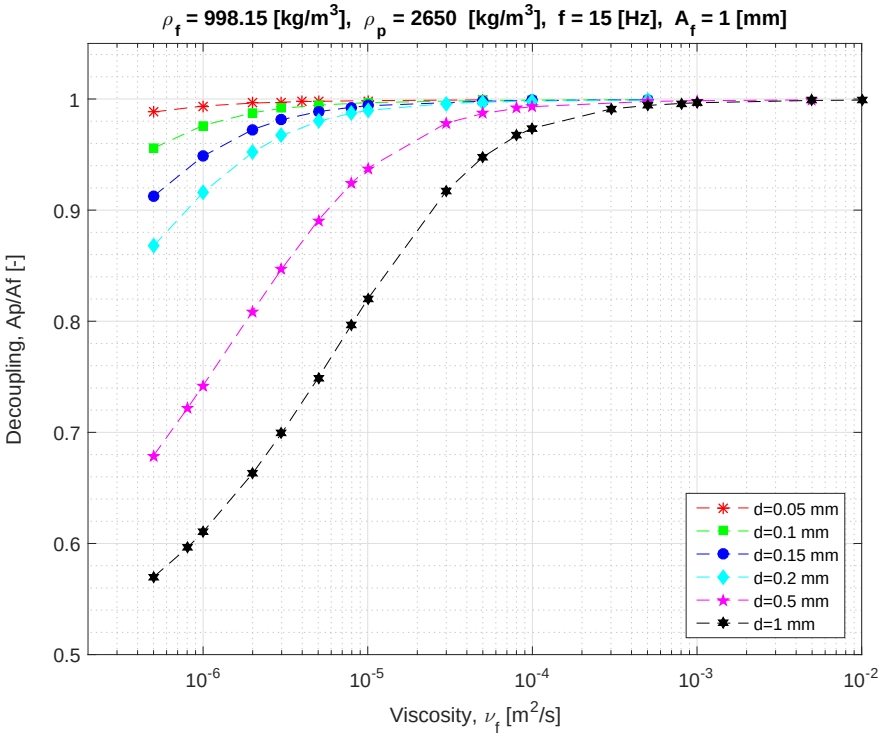

Figure 6.10: Decoupling (A_p/A_f) as function of viscosity (ν_f), uniform oscillations

As the particle size (d) increases at fixed viscosity, the viscous drag on the particle is overwhelmed by the inertial forces due to the decreased particle surface to volume ratio. It is nicely shown that in the limit of low viscosity, the same decoupling is found as predicted by the inviscid model (Figure 5.3). The lowest viscosity used is $5 \times 10^{-7} \ m^2/s$, which is equivalent to the viscosity of fresh water of approximately 50 degrees. It is not possible to run the model at viscosities less than this value because the particle Reynolds number (Re_p) becomes too large for the model to remain valid. The kinematic viscosity of water (using a temperature of 20 degrees) is approximately $1 \times 10^{-6} m^2/s$.

The particle density was kept constant during the analysis, but if it would be preferable to study a certain higher or lower particle density, the same behavior would be found as long as $\gamma > 1$. The lower viscosity limit would shift to another value which can be determined using Figure 5.3, but the shape of the dependency will remain similar.

Besides the uniform fluid oscillations, the same figure for the amplitude ratio was created using non-uniform fluid oscillations. A shape factor $ki = 1.05$ was used.

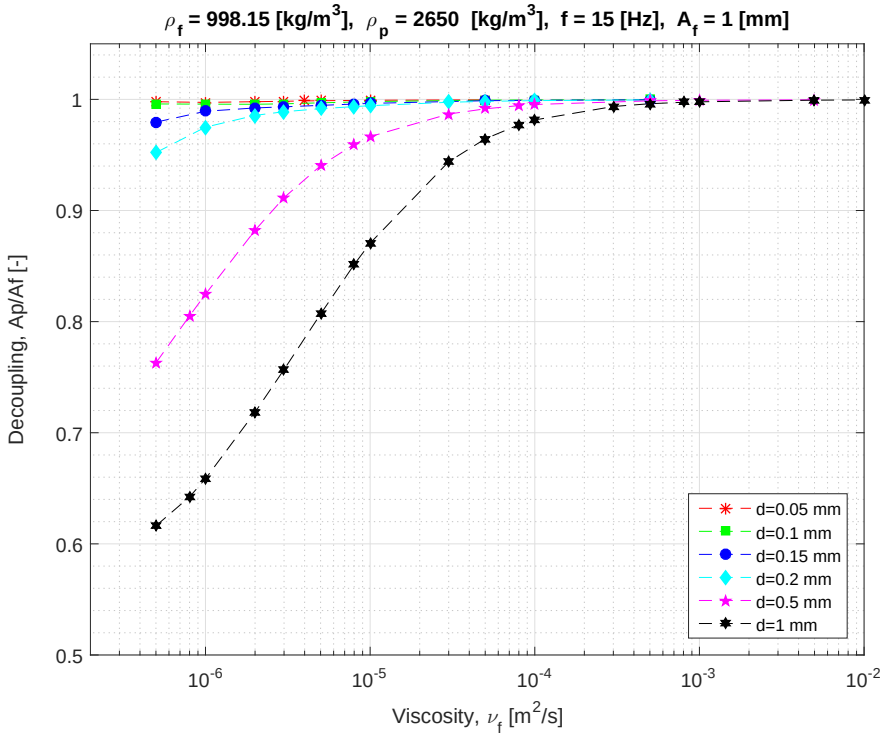

Figure 6.11: Decoupling (A_p/A_f) as function of viscosity (ν_f), non-uniform oscillations

Considering the amplitude ratio between the particle and fluid using non-uniform fluid oscillations, it was found that the average decoupling is lower compared to the uniform fluid oscillations. This observation is expected to be caused by the higher dependency on the fluid acceleration for the uniform oscillations (Figure 6.6). Considering the amplitude ratio at the used frequency of $15\ Hz$, it is shown that (especially for the particles larger than $d = 0.1mm$) the found difference in dependency is in the order of 10%.

6.1.6 Phase angle dependency on viscosity

Unlike the amplitude ratio (A_p/A_f), the phase angle (φ) reaches a maximum at intermediate values of particle size and fluid viscosity and will go to zero for the inviscid and infinite viscosity limits (Figure 6.12). This balance between the viscous and inertial forces is especially well shown for the larger particle sizes $d = 0.5\ mm$ and $d = 1\ mm$. When the viscous forces dominate, the relative motion is reduced, eventually to the extent that no relative motion and no phase angle are possible.

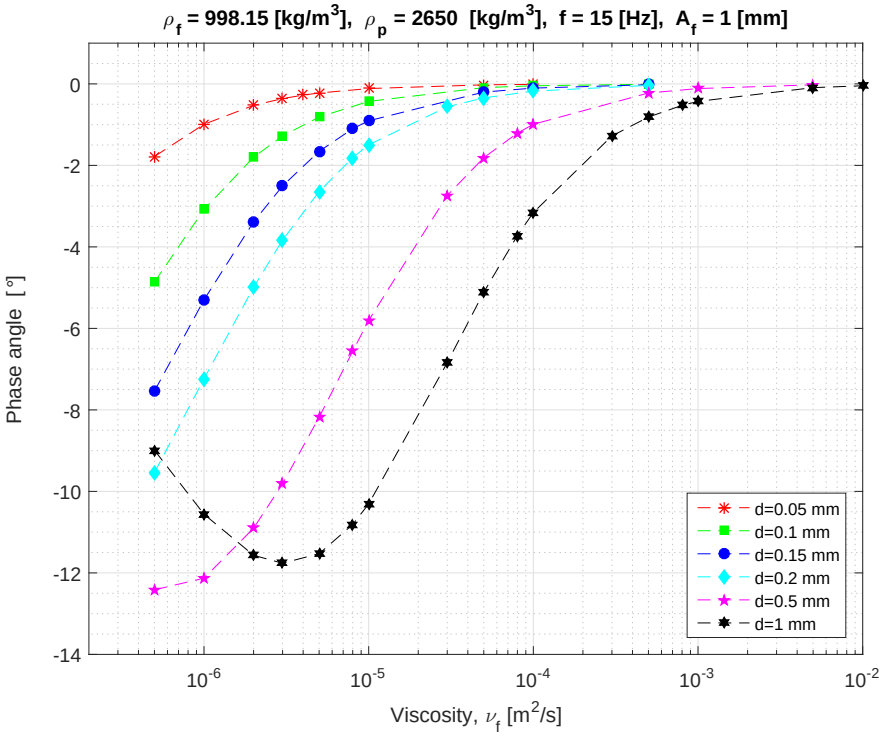

Figure 6.12: Phase angle (φ) as function of viscosity (ν_f), uniform oscillations

As viscosity decreases (especially for the larger particles, having larger inertial forces) the inviscid model is approached where there is no phase angle but maximum decoupling. In summary, when the ratio inertial to viscous forces is either extremely large or extremely small, there is no phase angle:

$$1 \ll \frac{F_{inertial}}{F_{viscous}} \ll 1, \qquad \varphi = 0, \tag{6.2}$$

but when these forces roughly balance, the phase angle will be maximum:

$$\frac{F_{inertial}}{F_{viscous}} \approx 1, \qquad \varphi = \text{maximum}. \tag{6.3}$$

This causes the nicely shown parabola, using a particle size $d = 1\,mm$. Again performing the similar analysis but applying non-uniform fluid oscillations resulted in Figure 6.13:

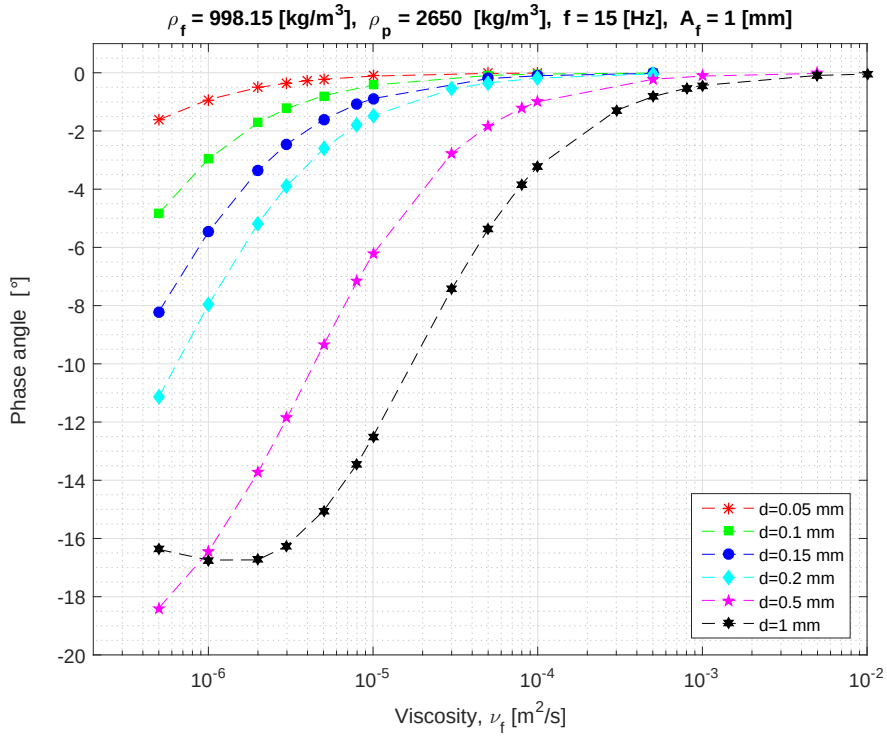

Figure 6.13: Phase angle (φ) as function of viscosity (ν_f), non-uniform oscillations

Analyzing Figure 6.13, it is observed that the maximum phase angles found before inertial forces dominate, are somewhat larger compared to the uniform oscillations. Considering Figure 6.9 at again an oscillation frequency of 15 Hz, it does not directly show this discrepancy. It is however expected that this found difference has the same cause as found with the decoupling dependency on frequency.

As mentioned, this study is mostly interested in the behavior of the smallest fractions, up to approximately 170 μm. For these particle sizes, the particle response behavior is more or less similar for both uniform and non-uniform fluid oscillations. The performed analysis of the particle response behavior dependency on viscosity showed that the response behavior will always be dominated by the viscous forces.

6.1.7 Particle migration

Now that the influence of the inertial and viscous force terms in the BBO-equation on the decoupling and phase angle is quantified, it is interesting to study the particle response velocity as function of frequency and amplitude. Doing so, it can be determined whether the first hypothesis can be numerically proven for a single particle.
Figure 6.14 shows the particle response velocity for uniform (red dotted lines) and non-uniform fluid oscillations (black and blue dotted lines), as function of the inverse Stokes number (δ). A variety of fluid amplitudes (A_f) are applied in combination with the limiting shape factors $ki = 1.05$ (black dotted lines) and $ki = 21$ (blue dotted lines).

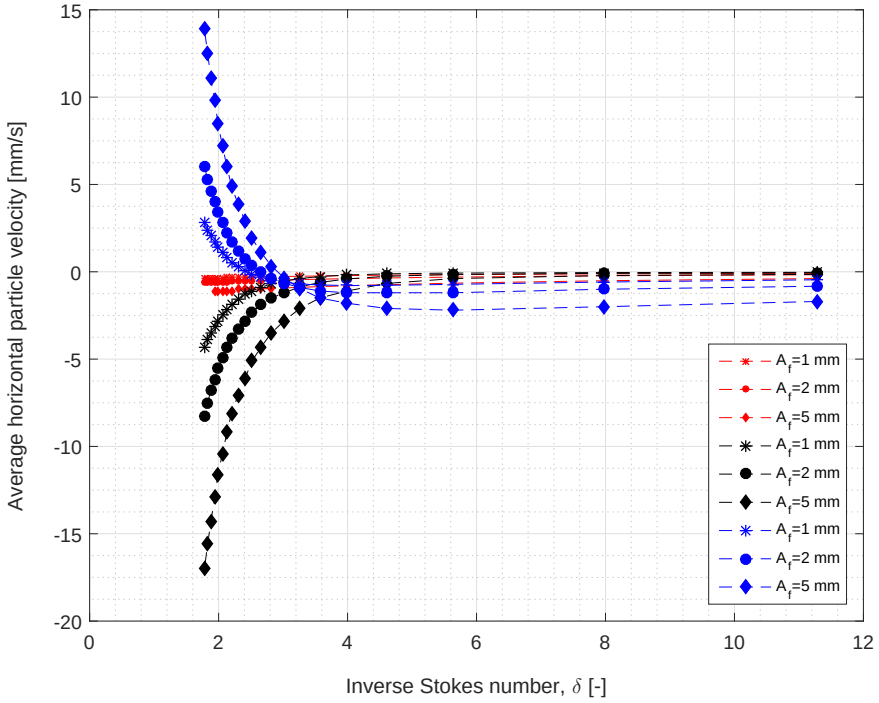

Figure 6.14: Average migration velocities $(\bar{u}$ & $\bar{u_w})$ as function of the inverse Stokes number (δ)

Clearly, the non-uniform fluid oscillations are capable of producing an average relative particle velocity in a certain direction. Note that the sign convention indicates the direction of motion. A negative value describes an average velocity to the left, whereas a positive value indicates an average velocity to the right. This difference is caused by the shape factor (ki). It must be emphasized that the results are highly theoretical. The wave shapes used for the fluid as excitation input will not be the wave shapes found in practice because of friction and inertia of the system. For this reason Van Oeveren and Houghton (1971) also defined an output shape factor ko:

$$ko = \frac{\text{downstroke duration}}{\text{upstroke duration}}, \tag{6.4}$$

where the ratio of ki over ko describes the transfer function between theory and practice. The magnitude of the average particle migration velocities shown in Figure 6.14 will therefore always be within the extremes. As expected, the uniform oscillations cause almost no relative particle velocity. But at very low inverse Stokes numbers, still an average velocity of $1\,mm/s$ is found. By integrating the relative particle response velocity, the relative particle displacement is found.

Let's consider the oscillating and average relative particle displacement at $\delta \approx 3.57$ and $\delta \approx 2.52$ for $ki = 1.05$:

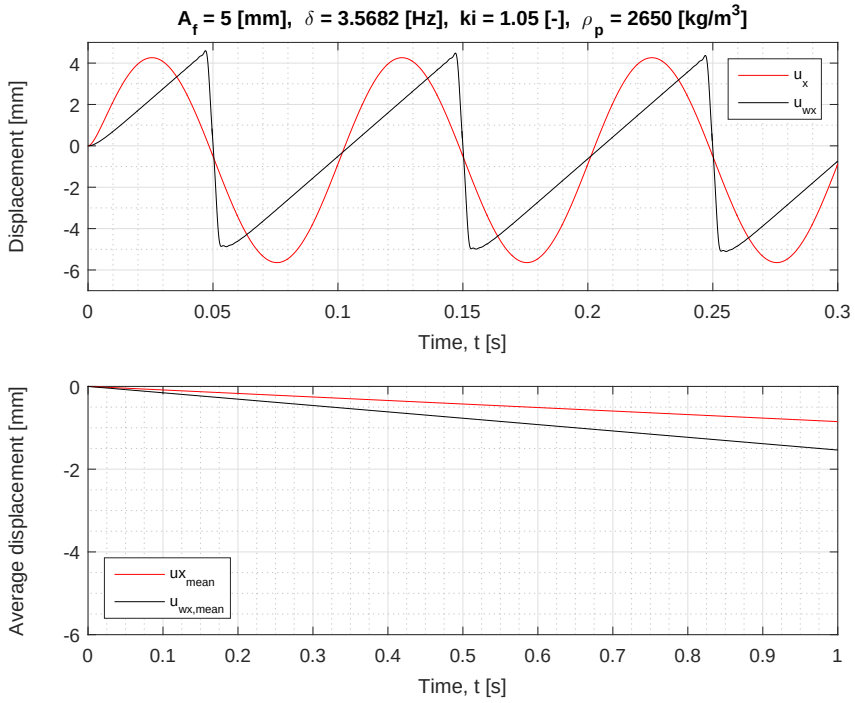

Figure 6.15: Relative particle displacement $(u_x \ \& \ u_{wx})$ at $\delta \approx 3.57$, $A_f = 1\ mm$

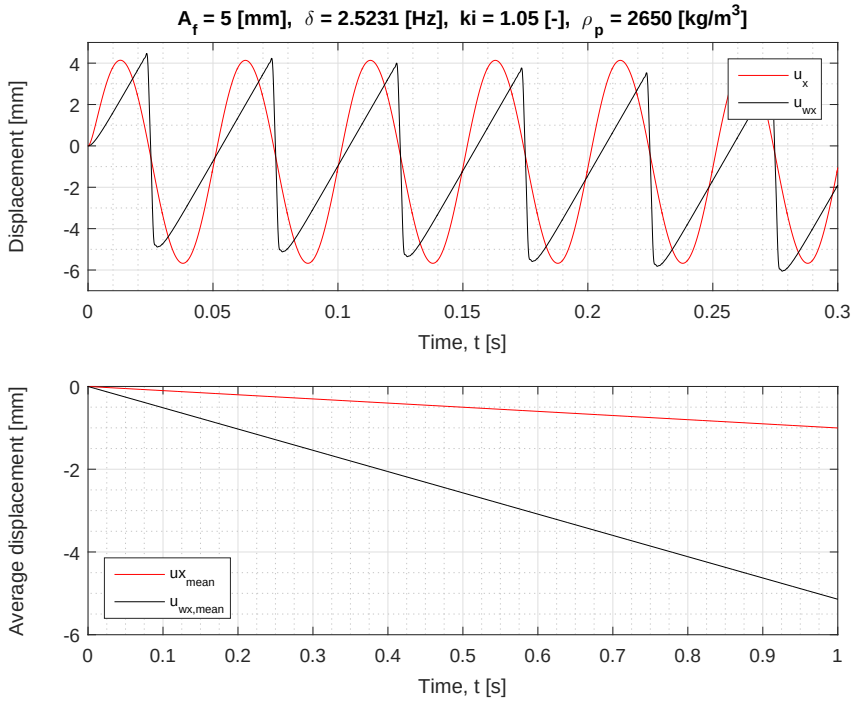

Figure 6.16: Relative particle displacement $u_x \ \& \ u_{wx}$ at $\delta \approx 2.52$, $A_f = 5\ mm$

The colors used, correspond with Figure 6.14. It is nicely shown that the average relative particle displacements for the uniform and non-uniform are almost equal at $\delta \approx 3.57$ and $A_f = 1mm$. However, when the inverse Stokes number decreases, with an increased fluid amplitude $A_f = 5\,mm$ the average relative particle displacement for the uniform oscillations stays more or less constant, while the displacement for the non-uniform oscillations increases rapidly.

Considering the oscillating and average relative displacement using $\delta \approx 2.52$, $A_f = 5\,mm$ and the shape factor $ki = 21$, resulted in:

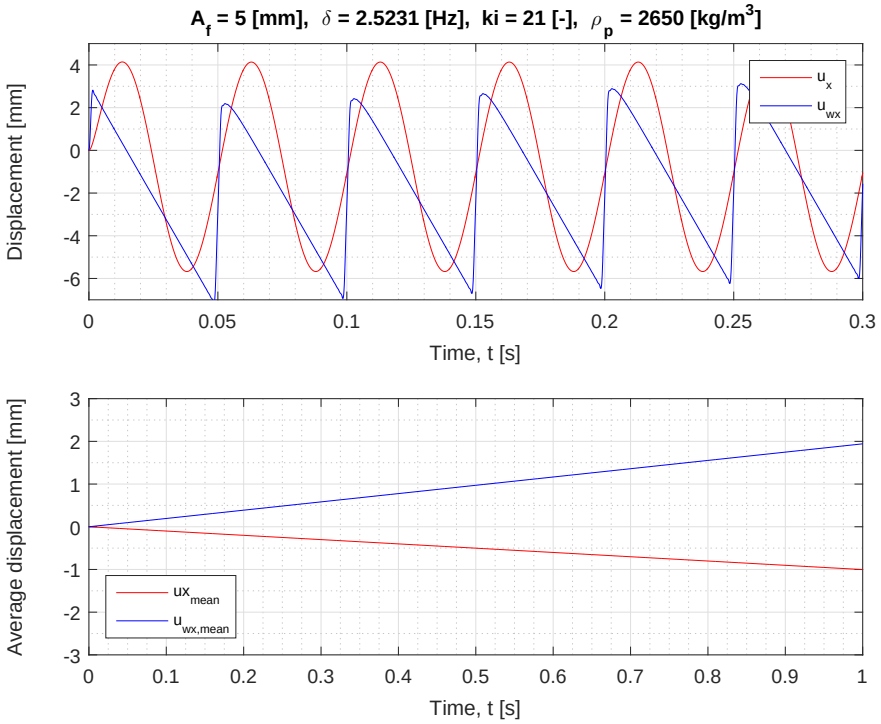

Figure 6.17: Relative particle displacement u_x & u_{wx} at $\delta \approx 2.52$, $A_f = 5\,mm$

Using the other limit of the shape factor $(ki = 21)$ shows the expected migration in opposite direction (right). This displacement however, is shown to be less pronounced compared with a shape factor $ki = 1.05$. It is expected that this difference is caused by the initial difference between the two wave types.

6.1.8 Force analysis

To determine the origin of the relative velocities, a force analysis has been performed.

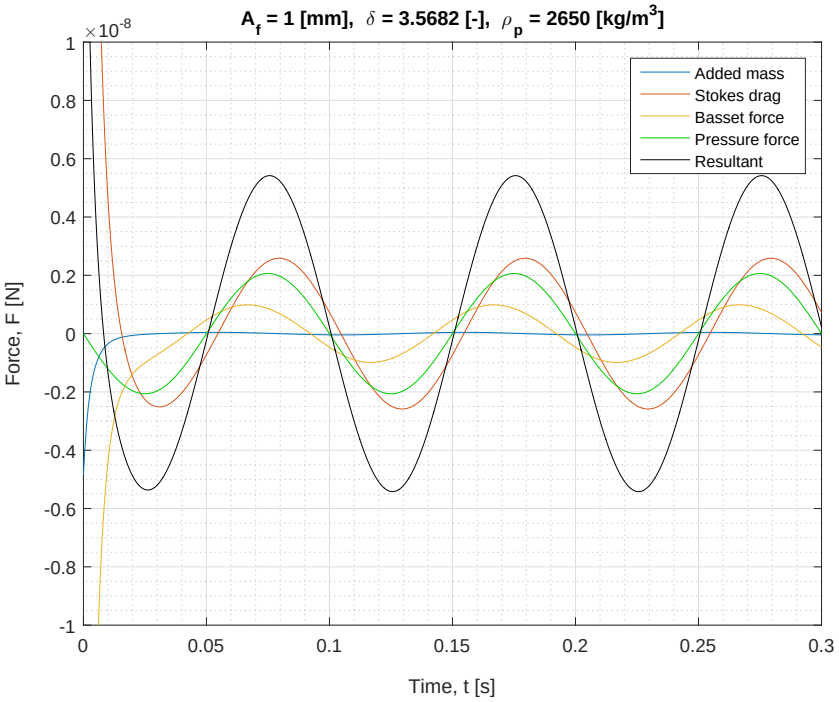

Figure 6.18: Forces due to uniform fluid oscillations at inverse Stokes number, $\delta \approx 3.57$

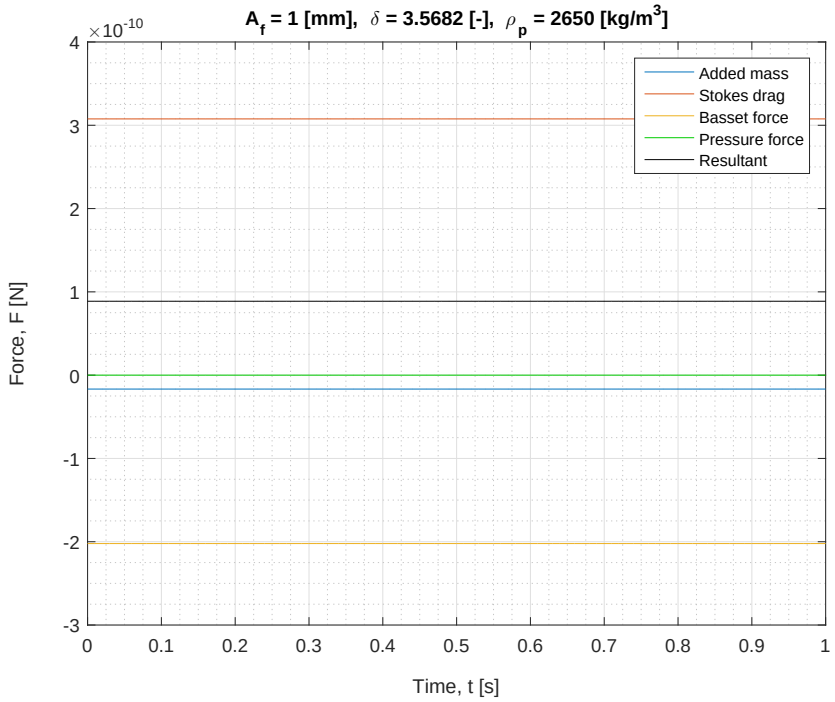

Figure 6.19: Average forces due to uniform fluid oscillations at inverse Stokes number, $\delta \approx 3.57$

In Figure 6.18 the different uniformly oscillating forces are visualized together with a resultant force (F_{res}). The colors used, correspond to the colors in Figure 3.3(a), whereas the resultant (summation) force is indicated by the black line. At a relatively high inverse Stokes number (equal to the displacement figures), the added mass force (F_a) is approximately zero. Furthermore, the Stokes drag force (F_d), the history or Basset force (F_h) and the pressure force (F_p), all oscillate with different amplitudes and phase angles with respect to each other.

To determine which force has the largest influence, the average of each oscillating force is shown in Figure 6.19. Here, the average pressure force (F_p) is shown to be zero, because of its dependency on the particle volume (V_p) and the fluid acceleration (dS/dt). Figure 6.19 also proves that the conclusion of the viscous forces ($F_d \& F_h$) being dominant, is correct. As expected and shown at Figure 6.14, decreasing the inverse Stokes number to ≈ 2.52 did not show significant difference for the average forces (not adopted in the thesis).

Still Figure 6.19 does not instantly show why a migration velocity occurs when the fluid is oscillating uniformly. Therefore, each of the force terms from the BBO-equation was suppressed one by one to study the individual influence on the particle velocity. Doing so, it was found that a relative velocity is only achieved if the history or Basset force (F_h) is included:

$$F_h = 6\pi\mu_f \, r \left[\frac{S - v}{\delta} + \frac{\delta\tau_v}{2} \left(\frac{dS}{dt} - \frac{du}{dt} \right) \right]. \tag{6.5}$$

The history force shows a dependency on both the viscosity as well as the relative acceleration between the fluid and particle, causing it to contribute both to the viscous forces and the inertial forces. For now, a physical explanation cannot be given for this phenomenon.

The behavioral difference between shape factors and inverse Stokes numbers should translate in a difference between specific forces as well. Considering the oscillating forces for the uniform and non-uniform fluid oscillations using $ki = 1.05$ and two different inverse Stokes numbers are given in Figure 6.18, Figure 6.20 and Figure 6.22. It is shown that the forces increase linearly with increasing fluid acceleration. This is expected behavior, taking into account Newton's second law of motion.

More interesting are the average forces, shown at Figure 6.19, Figure 6.21 and Figure 6.23, respectively. All three figures show that the pressure force (F_p) is again zero. A surprising difference between Figure 6.19 and Figure 6.21 is that the uniform oscillations show a resultant force (F_{res}) which is one order of magnitude larger compared with the non-uniform oscillations. Taking into account Figure 6.14, it is suspected that the uniform oscillations have a slightly higher acceleration at $\delta \approx 3.57$.

Comparing Figure 6.21 and Figure 6.23 it is found that the history force (F_h) and Stokes drag force (F_d) have a changed sign. The combination of the two is expected to be the driving force for the horizontal particle migration in left direction, as they are dominant and therefore mainly determine the magnitude of the resultant force.

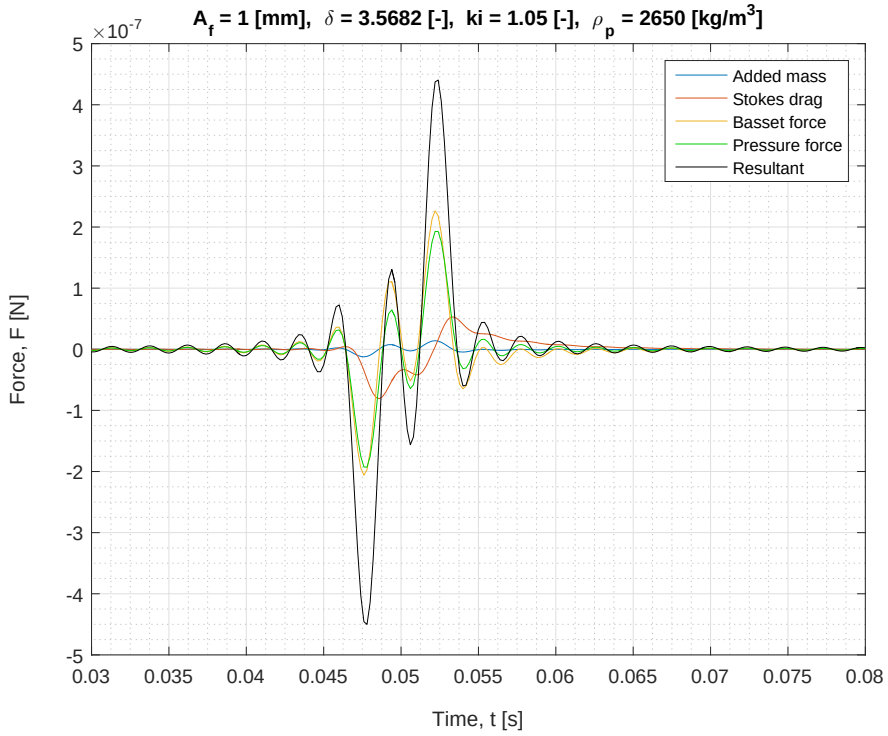

Figure 6.20: Forces due to non-uniform fluid oscillations, $ki = 1.05$, $\delta \approx 3.57$

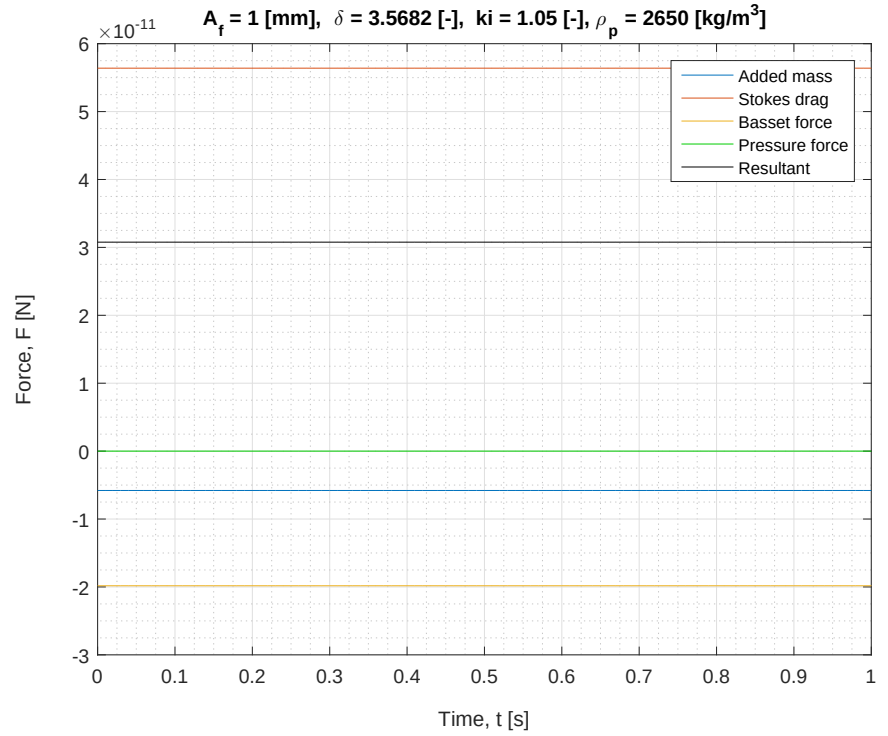

Figure 6.21: Average forces due to non-uniform fluid oscillations, $ki = 1.05$, $\delta \approx 3.57$

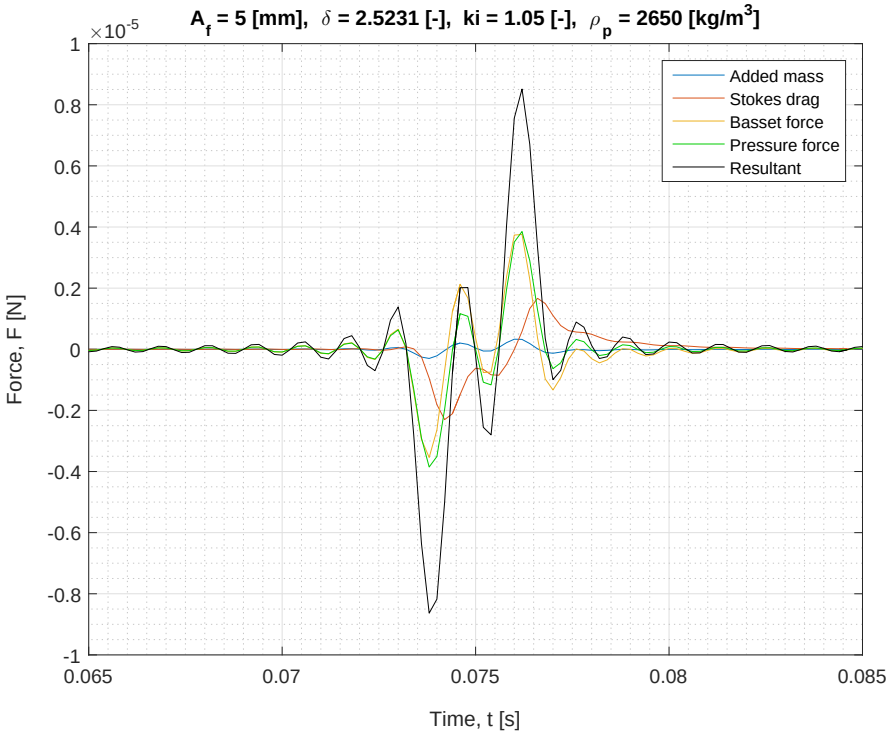

Figure 6.22: Forces due to non-uniform fluid oscillations, $ki = 1.05$, $\delta \approx 2.52$

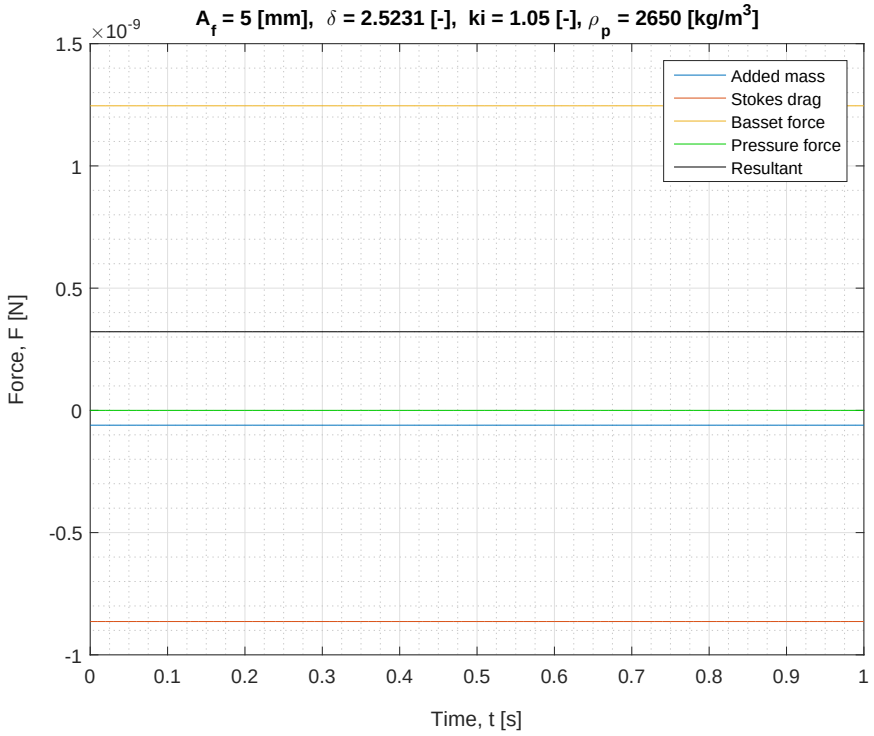

Figure 6.23: Average forces due to non-uniform fluid oscillations, $ki = 1.05$, $\delta \approx 2.52$

Besides the horizontal particle migration in left (negative) direction using $ki = 1.05$, a migration velocity in right (positive) direction is found at $ki = 21$. To determine the influence of both limiting shape factors, Figure 6.20, Figure 6.21, Figure 6.22 and Figure 6.23 have been reproduced using the shape factor $ki = 21$. Analyzing the oscillating forces (Figure 6.20 and Figure 6.24) it is found that both magnitudes are exactly equal. As expected, they are again mirrored over the x-axis. The pressure force (F_p) always shows a significant influence in the oscillating force plots, but when averaged it loses its contribution to the resultant force (F_{res}) because:

$$\bar{F_p} = 0. \tag{6.6}$$

Comparing their average magnitudes (Figure 6.21 and Figure 6.25), there is not much of a difference other than that they differ one order of magnitude. This difference could explain why both shape factor do not show equal particle migration behavior at $\delta \approx 3.57$. The physical origin however is not yet known. The Stokes drag force (F_d) and history force (F_h) show the exact same behavior despite different shape factors.

The inverse Stokes number has again been lowered to $\delta \approx 2.52$. Analyzing the oscillating forces (Figure 6.22 and Figure 6.26), again results in an equal magnitude and mirrored appearance with respect to the x-axis. Their average magnitudes shown at Figure 6.23 and Figure 6.27 predict opposite behavior between the Stokes drag force and history force. It is expected that this causes the difference in either a positive average relative velocity or a negative average relative velocity between particle and fluid. It is also shown that the resulting average forces for $ki = 21$ are generally one order of magnitude larger, despite the migration velocities not begin as high as using $ki = 1.05$. Currently, there is no physical explanation why this occurs.

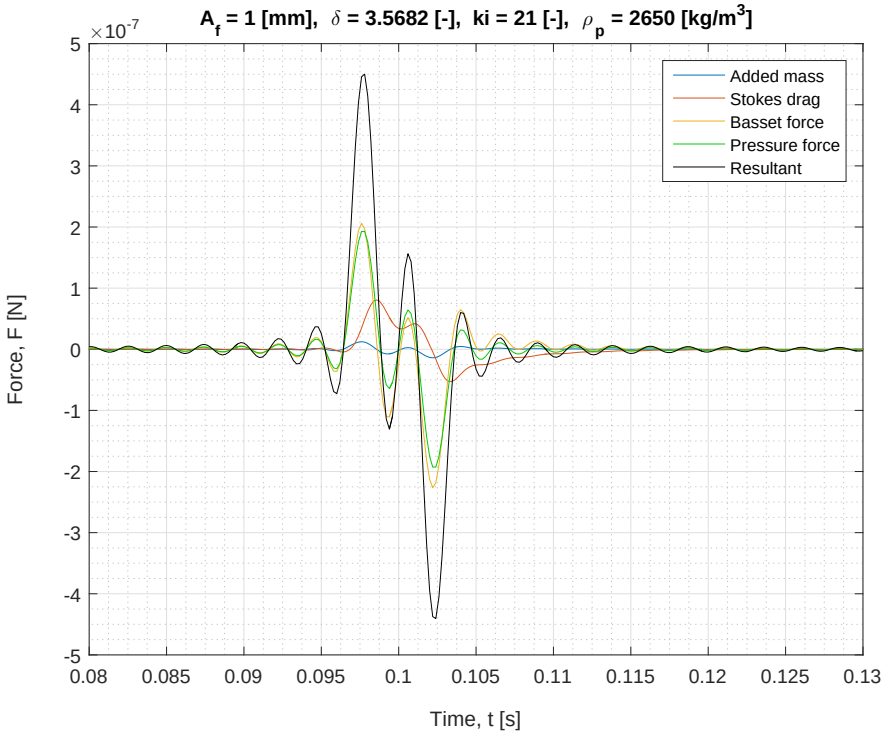

Figure 6.24: Forces due to non-uniform fluid oscillations, $ki = 21$, $\delta \approx 3.57$

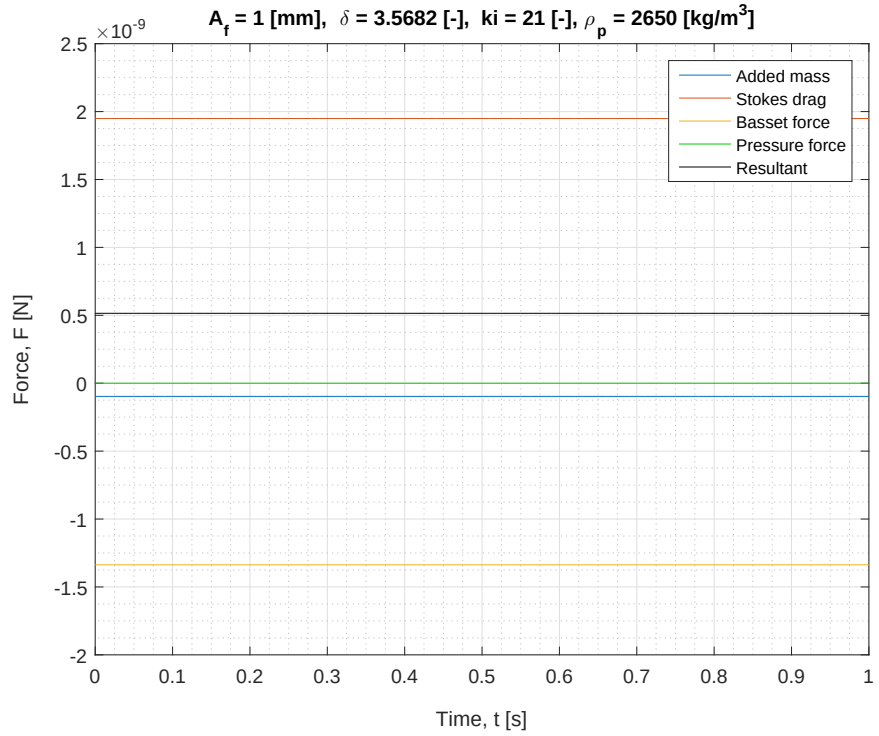

Figure 6.25: Average forces due to non-uniform fluid oscillations, $ki = 21$, $\delta \approx 3.57$

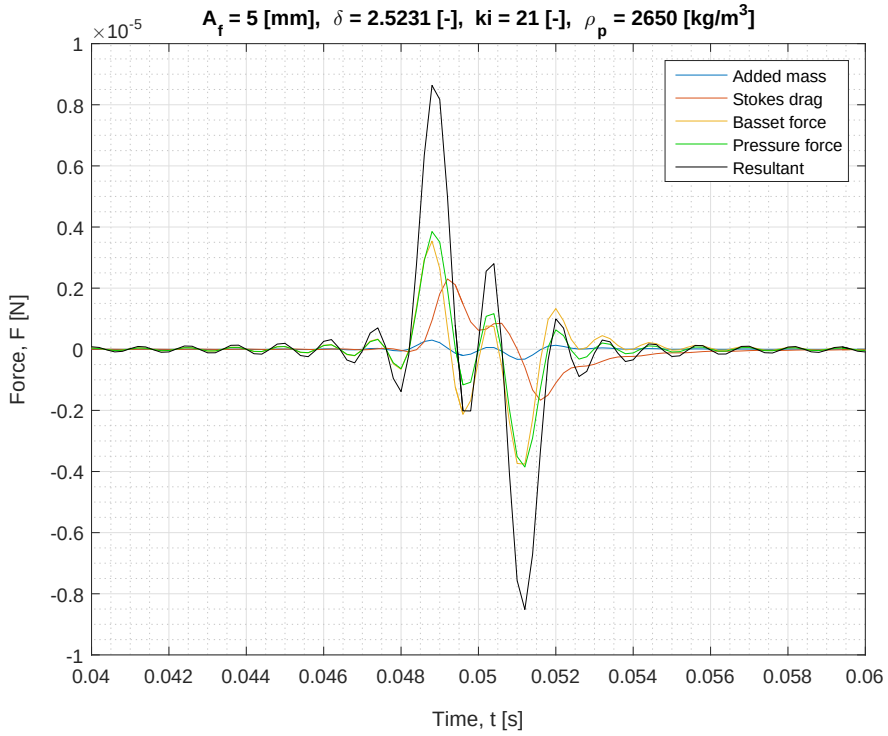

Figure 6.26: Forces due to non-uniform fluid oscillations, $ki = 21$, $\delta \approx 2.52$

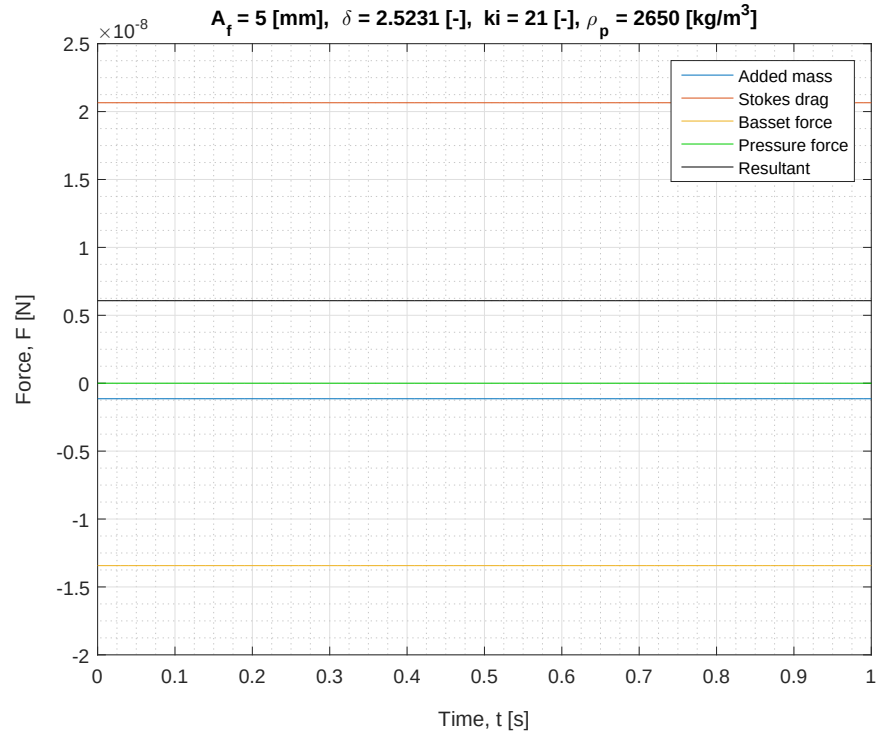

Figure 6.27: Average forces due to non-uniform fluid oscillations, $ki = 21$, $\delta \approx 2.52$

6.2 Vertical oscillations

6.2.1 Uniform oscillations

Let's now consider a vertically oscillating settling tube using uniform oscillations. Because of the orientation, gravity and buoyancy are included in the BBO-equation using a single force term (F_g):

$$F_g = V_p\, g\, (\rho_p - \rho_f). \tag{6.7}$$

This term is also known as the *submerged weight*. Using the same settings as Figure 6.1 yields:

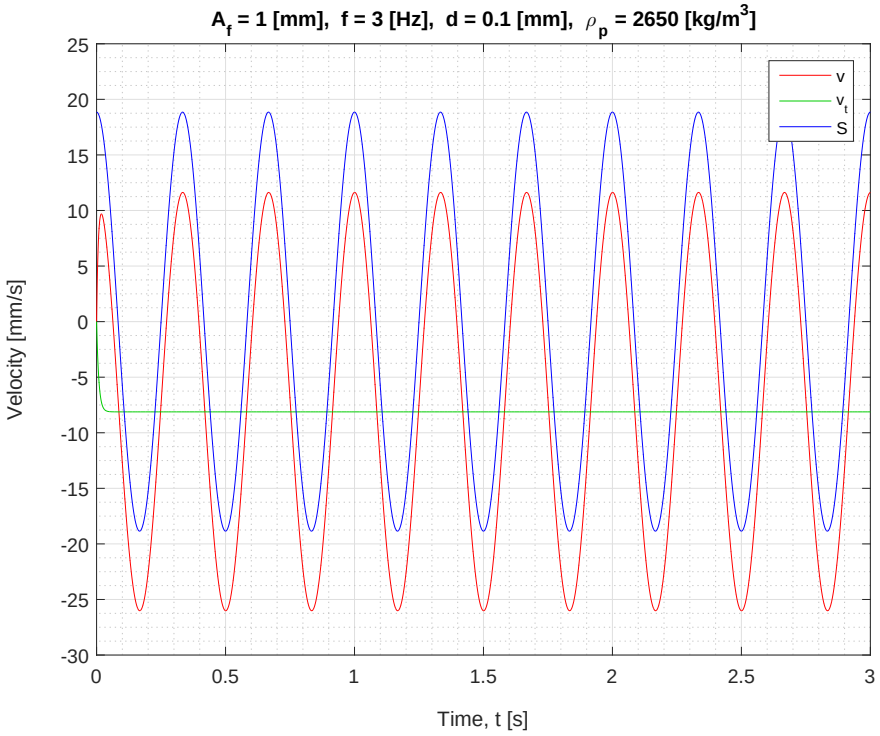

Figure 6.28: Vertical particle response velocity v, uniform oscillations $\gamma > 1$, $d = 0.1\ mm$

Besides the vertically oscillating response velocity of the particle (v) and the fluid velocity (S) the terminal settling velocity in stagnant water (v_t) is shown by the green line for comparison. It is shown that the submerged weight of the particle causes an average negative velocity. The particle velocity oscillates slightly above the terminal settling velocity whereas the fluid oscillation velocity logically oscillates around zero. Because of the relatively small particle size chosen, hardly any decoupling $A_p/A_f \approx 0.99$ or phase difference $\varphi \approx -0.012\ rad$ is found.
Again, increasing the weight of the particle by increasing either its size (d) or its density (ρ_p) should result in a higher inertial difference, which will translate in a larger decoupling and phase angle. Considering Figure 6.29, the particle size was increased to $d = 2\ mm$. It is now clearly shown that retardation $(b0 = \bar{v}/|v_t| < 1)$ occurs, because the average oscillating settling velocity of the particle $(\bar{v})$ is well above the terminal settling velocity. As expected, the phase difference increased to $\varphi \approx -0.346\ rad$. The amplitude ratio however, shows different behavior compared to the case of the horizontally oscillating settling tube. Because of the gravity term being 20 times larger, the fluid oscillations are no longer capable of fully controlling the particle and a decoupling $A_p/A_f \approx 1.15$ is found. This indicates that a downward overshoot exists due to the higher inertial forces.

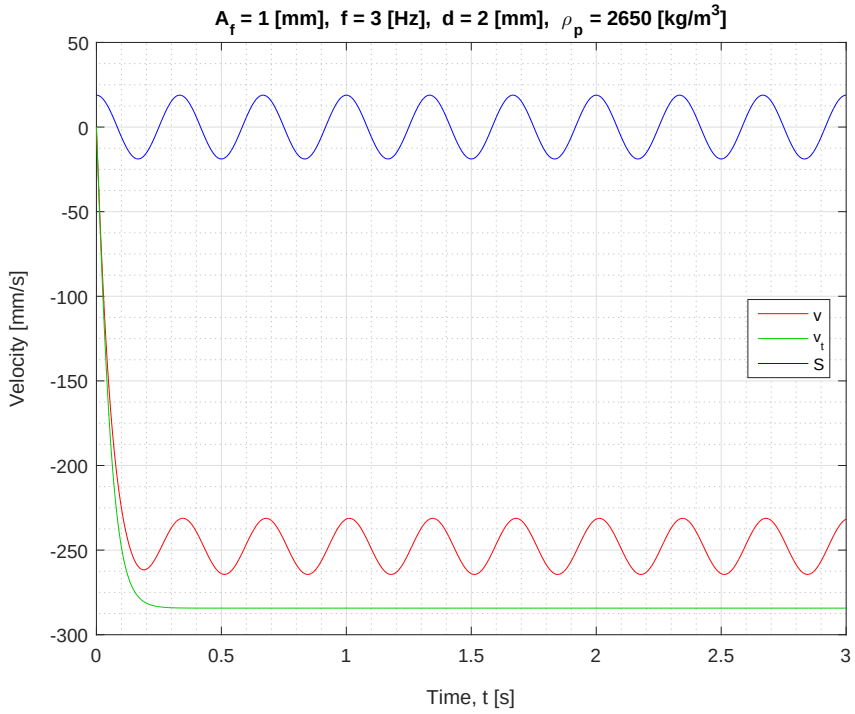

Figure 6.29: Vertical particle response velocity v, uniform oscillations $\gamma > 1$, $d = 2\,mm$

Integrating the velocity yields the displacement. Using a frequency $f = 5\,Hz$ and an amplitude $A_f = 5\,mm$ resulted in the following oscillating and average relative particle displacement:

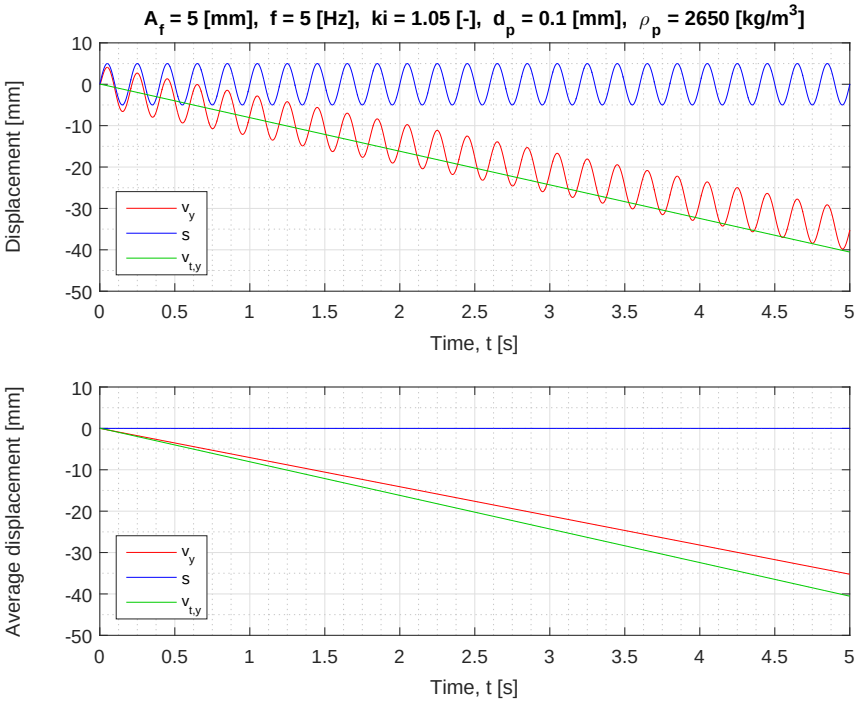

Figure 6.30: Vertical particle displacement v_y & $v_{t,y}$, uniform oscillations $\gamma > 1$

Analyzing Figure 6.30, it is shown that at $t = 0$, the oscillating displacement of the particle is approximately equal to the terminal displacement. The oscillating displacement oscillates nicely around the terminal displacement. Using the average displacements, it is clearly shown that these two lines separate after some time due to the retardation effect. Obviously, the average displacement of the fluid (blue line) is shown to be zero.

Now considering a density ratio $\gamma < 1$ yields a positive phase angle $\varphi \approx 0.004\,rad$ and an amplitude ratio $A_p/A_f \approx 0.99$:

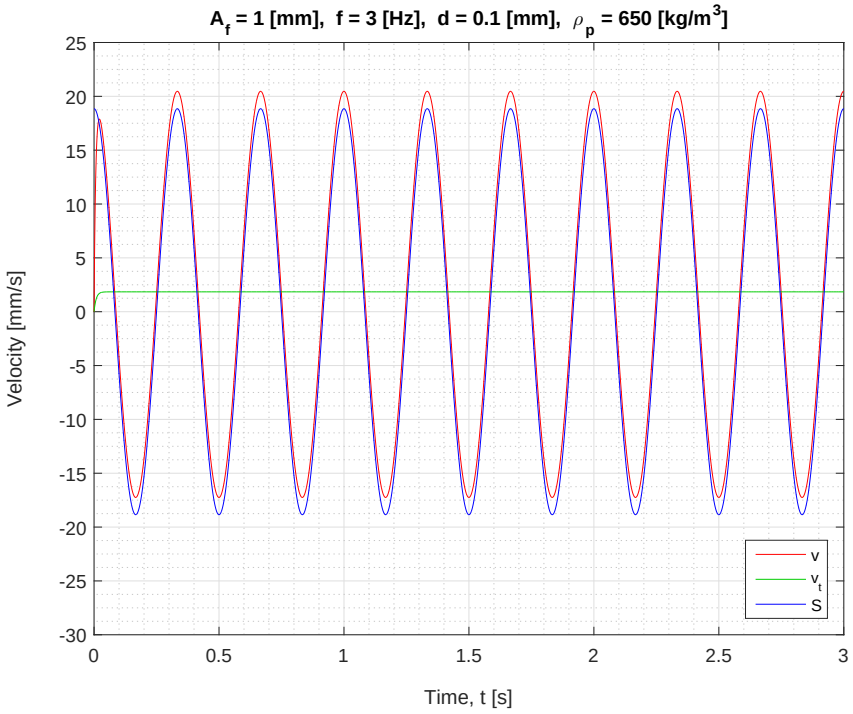

Figure 6.31: Vertical particle response velocity v, uniform oscillations $\gamma < 1$, $d = 0.1\ mm$

The density ratio being less than unity, results in an average upward velocity due to the change in sign of the gravity term. The decoupling between particle and fluid proved to be minimum. It was expected that, using for instance a bubble (having very small particle density) an amplitude ratio greater than unity would be found. This however, is not the case. The amplitude ratio remained smaller than unity $A_p/A_f \approx 0.99$. Equation 6.7 shows why this does not occur. Because the difference between fluid and particle density is taken, the resultant density will never be as high for a bubble as for a solid particle. Even when the particle size was increased twenty times, no amplitude ratio larger than unity was found.

6.2.2 Non-uniform oscillations

In case of non-uniform fluid oscillations (using a shape factor $ki = 1.05$), again particle response behavior similar to Figure 6.28 was found. Because the peak velocity is one order of magnitude larger than the uniform oscillations it may be difficult to see, but the average settling velocity is exactly the same as in case of the uniform oscillations.

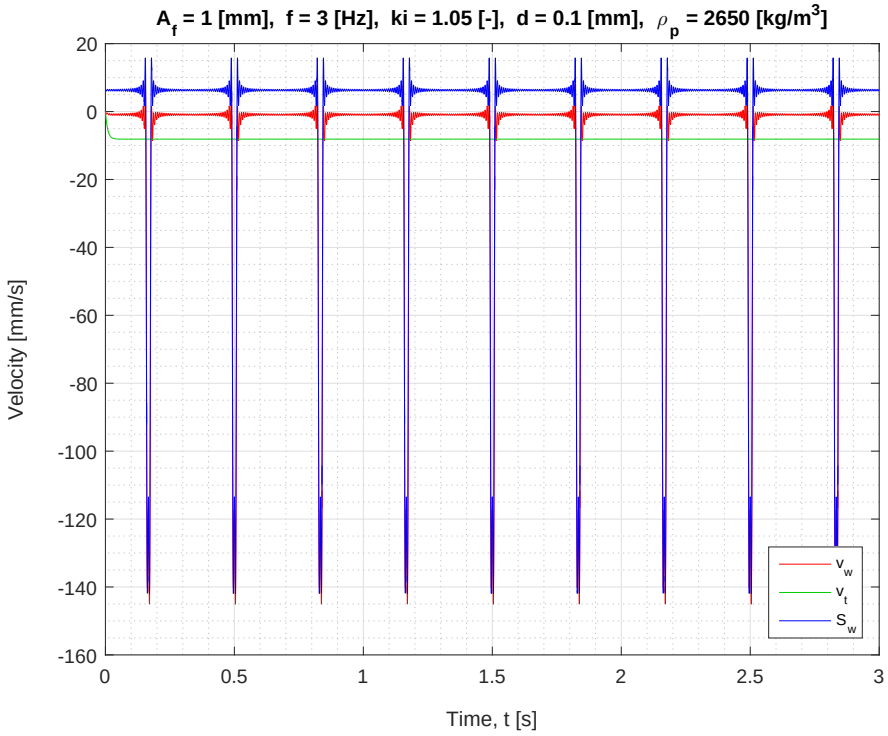

Figure 6.32: Vertical particle response velocity v_w, $\gamma > 1$, $d = 0.1\ mm$, $ki = 1.05$

The amplitude ratio (A_p/A_f) and phase angle (φ) were also found to be exactly similar to these of the uniform fluid oscillations (Figure 6.28). Because the fluid and particle motion are shown to be almost one to one, it can be concluded that viscous forces are dominant using these oscillation settings. Following the mentioned similarities, no difference in retardation $(\bar{v_w}/|v_t|)$ was found.

Because the gravity force term (F_g) is static (only dependent on the particle volume (V_p), particle density (ρ_p) and fluid density (ρ_f)) it has no influence on the overall particle response behavior described by the amplitude ratio (A_p/A_f) and phase angle (φ). As described in the previous subsection, the particle response behavior only depends on the ratio between the inertial forces $(F_{interial})$ and viscous forces $(F_{viscous})$.

It is therefore concluded that the figures describing the decoupling dependency on frequency (Figure 6.6) and phase angle dependency on frequency (Figure 6.9) are also valid for the vertically oscillating settling tube. This also holds for the dependency of decoupling on viscosity (Figure 6.10) and the phase angle dependency on viscosity (Figure 6.12).

To clarify the vertical particle response velocity for the limiting shape factors $ki = 1.05$ and $ki = 21$, Figure 6.33 and Figure 6.34 are added. The influence of gravity is visible in the regions with the largest discontinuities. When the largest fluid velocity is pointed in downward direction $(ki = 1.05)$, a slight overshoot is found, whereas the largest velocity pointed upwards, shows that gravity impedes the particle from fully following the fluid.

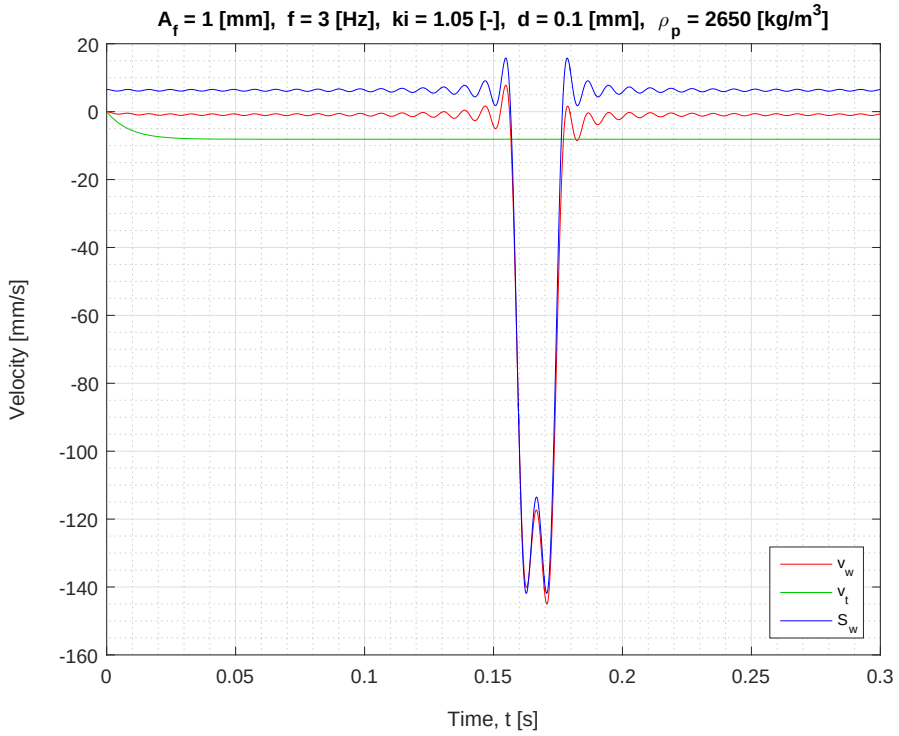

Figure 6.33: Vertical particle response velocity v_w, $\gamma > 1$, $d = 0.1\ mm$, $ki = 1.05$

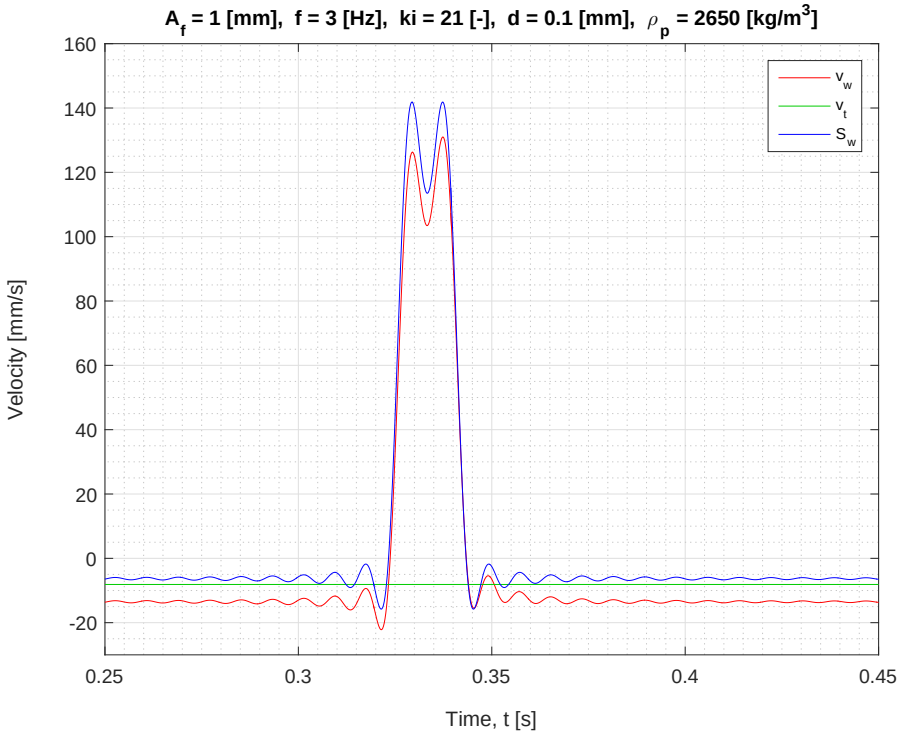

Figure 6.34: Vertical particle response velocity v_w, $\gamma > 1$, $d = 0.1\ mm$, $ki = 21$

6.2.3 Particle retardation and levitation

It only rests to prove the second hypothesis, mentioned in Chapter 2. The inverse Stokes number again has been used in combination with different amplitudes to describe the vertical particle response behavior. This is done by the retardation coefficients for uniform oscillations $b0$ (indicated by the red dotted lines) and $b1$ for the non-uniform oscillations. The blue dotted lines use a shape factor $ki = 21$ and the black dotted lines a shape factor $ki = 1.05$. The retardation coefficients describe the mean oscillating velocity $\bar{v}$ or $\bar{v_w}$, normalized by the absolute terminal settling velocity $|v_t|$:

$$b0 = \frac{\bar{v}}{|v_t|} \qquad \text{and} \qquad b1 = \frac{\bar{v_w}}{|v_t|}. \tag{6.8}$$

The coefficient $b0$ or $b1$ being between zero and minus one, describes a retarded settling velocity of the particle. When the coefficient is found to be zero, particle hovering is predicted, as experimentally found by Van Oeveren and Houghton (1971). Hovering means that the particle will not settle nor rise against gravity. When the coefficient becomes larger than zero, the particle will rise against gravity due to the present combination of fluid amplitude, oscillation frequency and shape factor. As shown on Figure 6.35, this is only possible using $ki = 21$ (blue dotted lines).

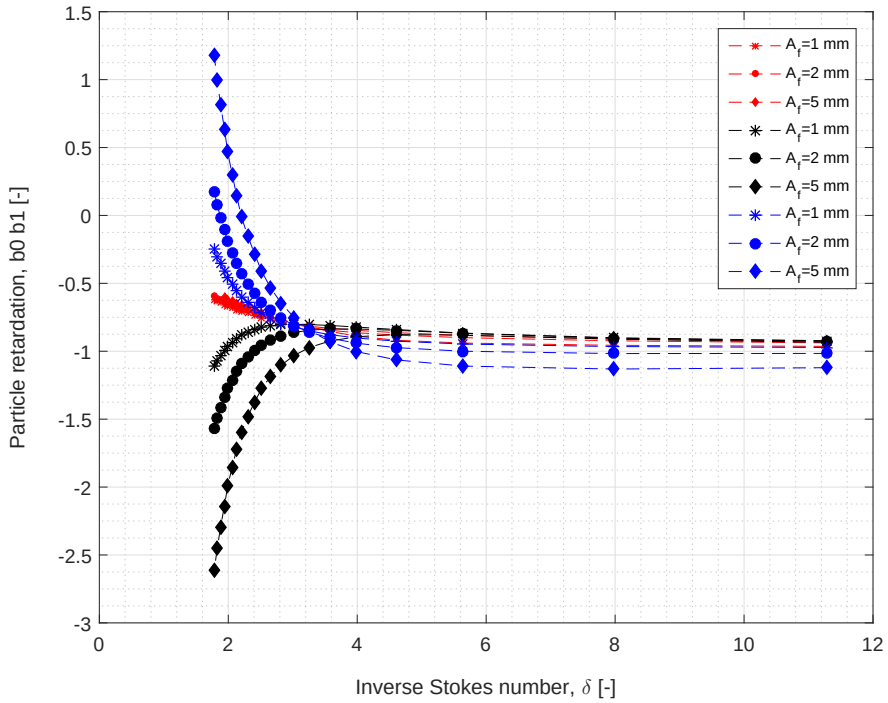

Figure 6.35: Particle retardation $b0$ & $b1$ as function of the inverse Stokes number (δ)

The other extreme is found when the retardation coefficient predicts a value smaller than minus one. If this is the case (which is only possible using a shape factor $ki = 1.05$) an increasing settling velocity is found. Considering Figure 6.35, using these settings a theoretical increase of 2.5 times the terminal settling velocity is found. Again it must be mentioned that these retardation results (using the non-uniform oscillations) are highly theoretical. The wave shapes used as input (k_i) to excite the settling tube will be different from the wave shapes found in practice due to the specific system properties such as inertia and friction.

6.2.4 Force analysis

A force analysis has again been performed to determine which force is causing the increase in settling velocity or the possibility of particle levitation.

The uniformly oscillating forces are given at Figure 6.36 for the specific case of the inverse Stokes number $\delta \approx 3.57$. In contrast with Figure 6.18, the history force (F_h) and Stokes drag force (F_d) are both positive. Due the presence of the gravity term (F_g) the average response velocity of the particle will be negative (settling), this is expected to cause the history force and Stokes drag force to be positive.

Considering the average oscillating forces (Figure 6.37), the pressure force is again found to be exactly zero, whereas the added mass force is two orders of magnitude smaller compared to the gravity, history and drag terms and therefore not clearly visible. As expected, the balance of forces is dominated by the gravity term and the Stokes drag term, similar to a particle settling in stagnant water. The retardation $(b0)$ found using Figure 6.35 has a magnitude of approximately 20%. It is again expected to be caused by the presence of the history force, as will be shown by further analyzing the particle response behavior.

Considering the retardation plot (Figure 6.35) using again $\delta \approx 3.57$ but for the non-uniform waves having an equal fluid amplitude of $1\ mm$ and a shape factor $ki = 1.05$, shows that the found retardation is almost exactly equal. This finding is clearly if Figure 6.37 is compared with Figure 6.39. Despite the higher fluid accelerations the force balance is dominated by the Stokes drag force and the gravity force. The pressure force is again exactly zero, whereas the added mass force and the resultant force are two orders of magnitude smaller than the Stokes drag force and gravity force. This leads to the conclusion that at this inverse Stokes number, not much difference is found between the uniform and non-uniform fluid oscillations.

Increasing both the fluid amplitude and frequency such that the inverse Stokes number decreases to $\delta \approx 2.52$ in combination with a shape factor $ki = 1.05$ shows an increased history force. Taking into account Figure 6.35, the increased history force causes the relative motion of the particle to increase in negative direction. An increase in settling velocity of approximately 30% is found.

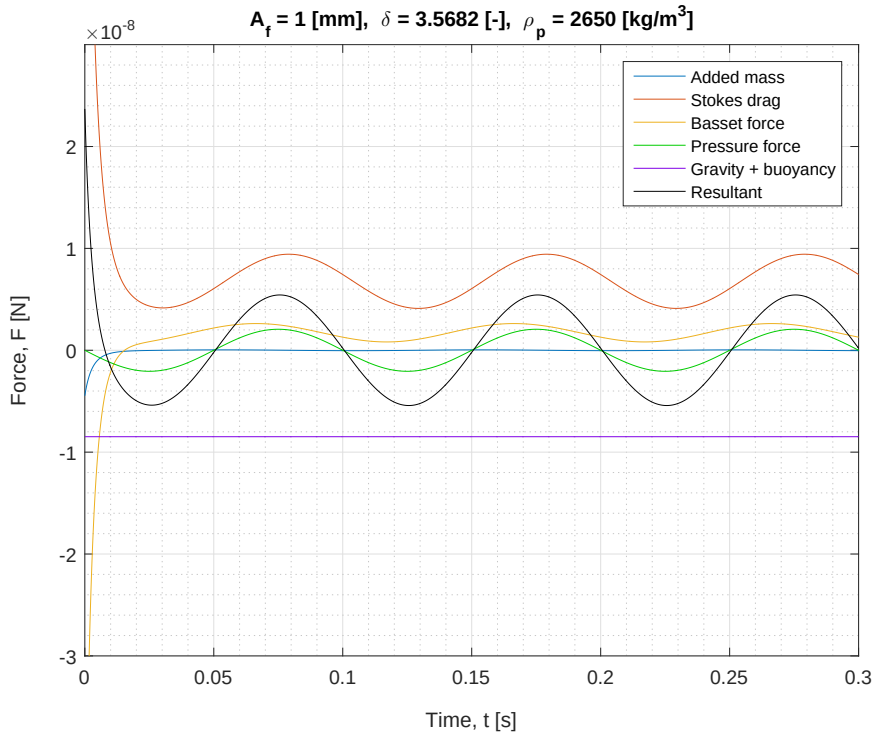

Figure 6.36: Forces due to uniform fluid oscillations at inverse Stokes number $\delta \approx 3.57$

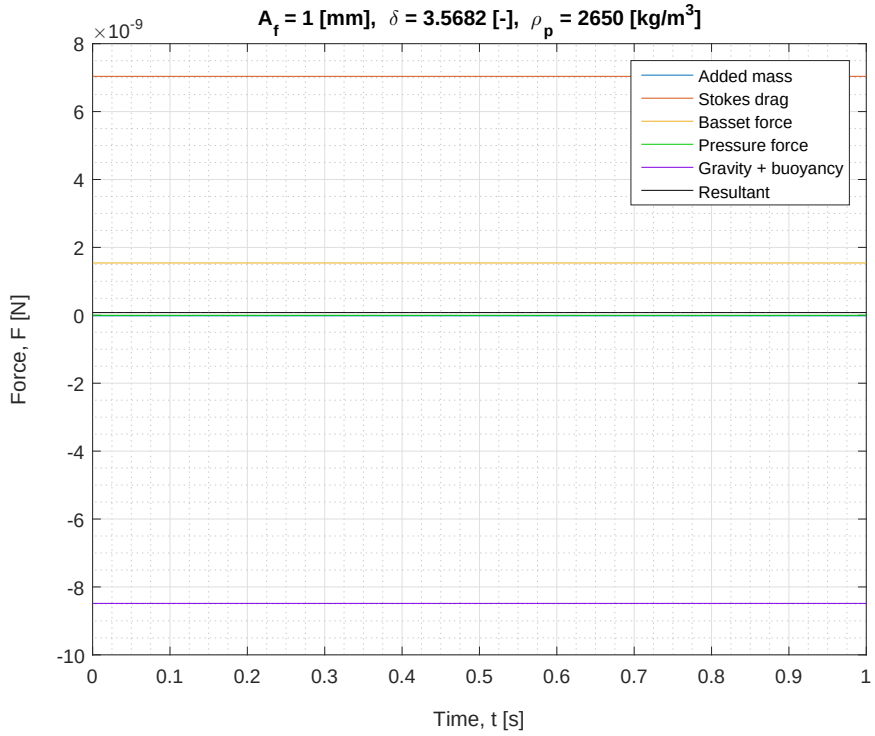

Figure 6.37: Average forces due to uniform fluid oscillations at inverse Stokes number $\delta \approx 3.57$

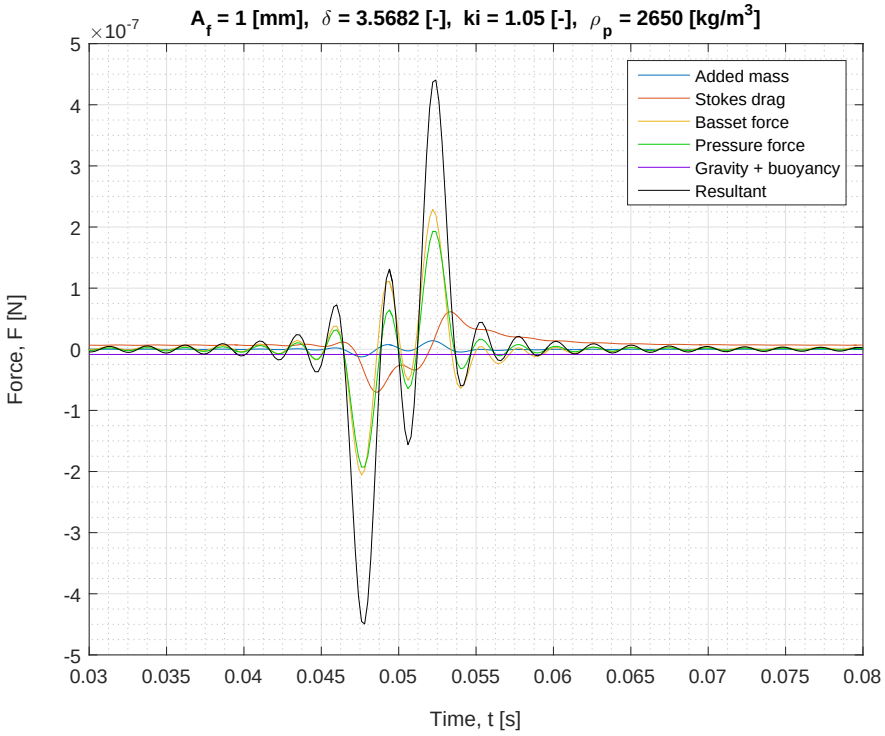

Figure 6.38: Forces due to non-uniform fluid oscillations, shape factor $ki = 1.05$, $\delta \approx 3.57$

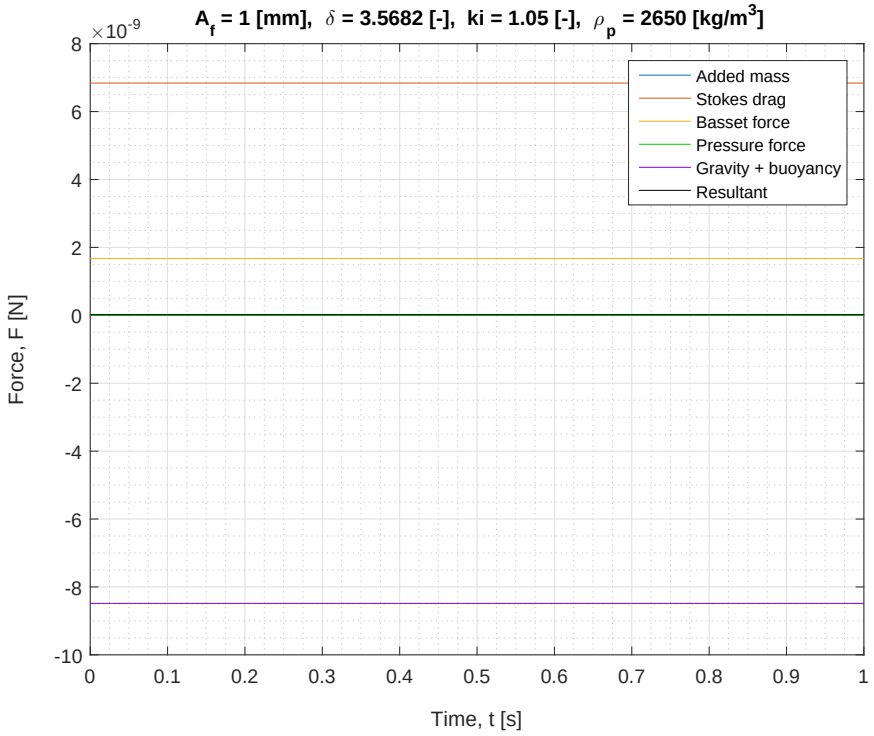

Figure 6.39: Average forces due to non-uniform oscillations, shape factor $ki = 1.05$, $\delta \approx 3.57$

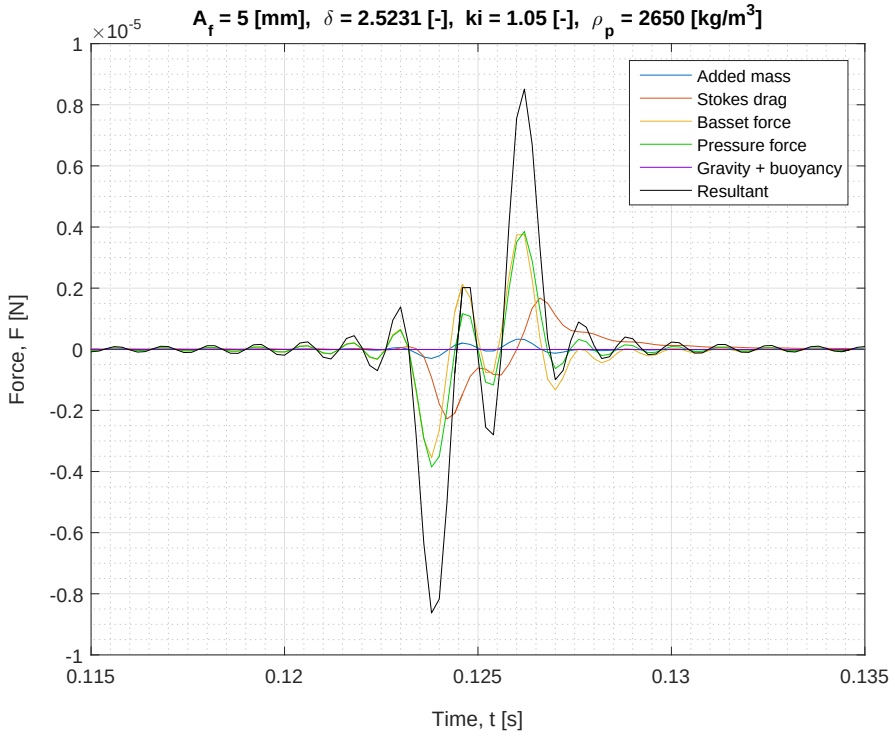

Figure 6.40: Forces due to non-uniform fluid oscillations, shape factor $ki = 1.05$, $\delta \approx 2.52$

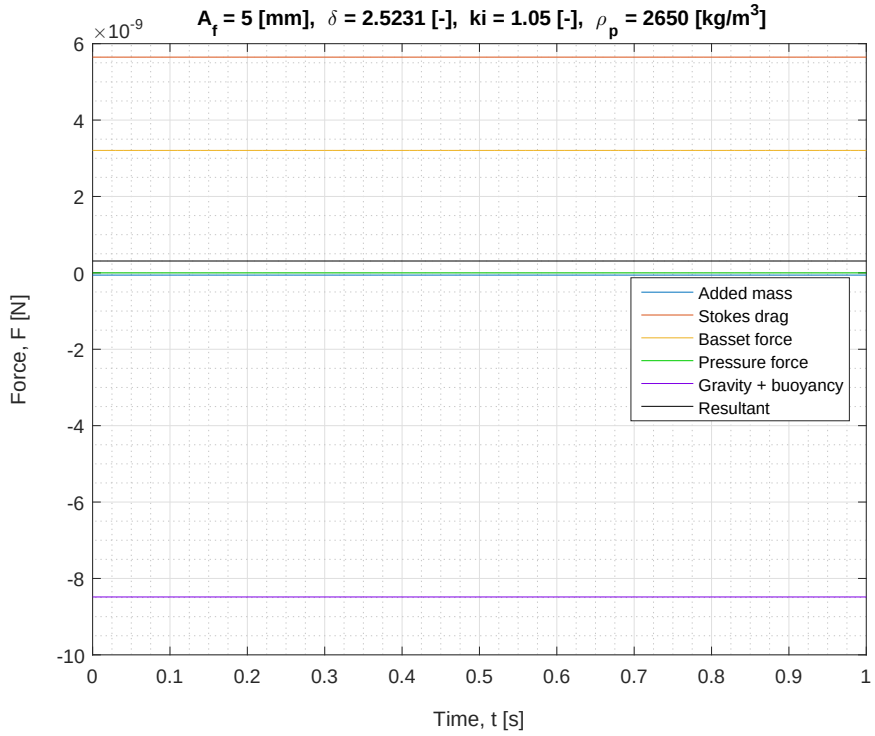

Figure 6.41: Average forces due to non-uniform oscillations, shape factor $ki = 1.05$, $\delta \approx 2.52$

Changing the shape factor to $ki = 21$, resulted in the four figures presented from this point onward. Figure 6.42 uses exactly the same settings as used at Figure 6.38. Both magnitudes were found to be equal, as expected. Again, the forces are mirrored around the x-axis due to the mentioned change in shape factor. Their averages (Figure 6.25 and Figure 6.21) also show similar magnitudes. Considering the particle retardation behavior presented at Figure 6.35, this proves to be a logical conclusion, as the predicted retardation is shown to be approximately equal.

Again increasing both the fluid amplitude and frequency such that the inverse Stokes number decreases to $\delta \approx 2.52$, in combination with a shape factor $ki = 21$ shows a significant decreased average history force (Figure 6.27). The sign change as found during the horizontal analysis is again found. This decrease instantly causes the history force to be more dominant than the gravity force, causing the particle to rise against gravity. This however, still raises some questions, because the history force obtained the same sign as the gravity force, but levitation is found.

The ratio between forces is found to be similar to the horizontal particle migration analysis at Figure 6.27. It is thus concluded that the history force is the driving force for the relative motion between fluid and particle.

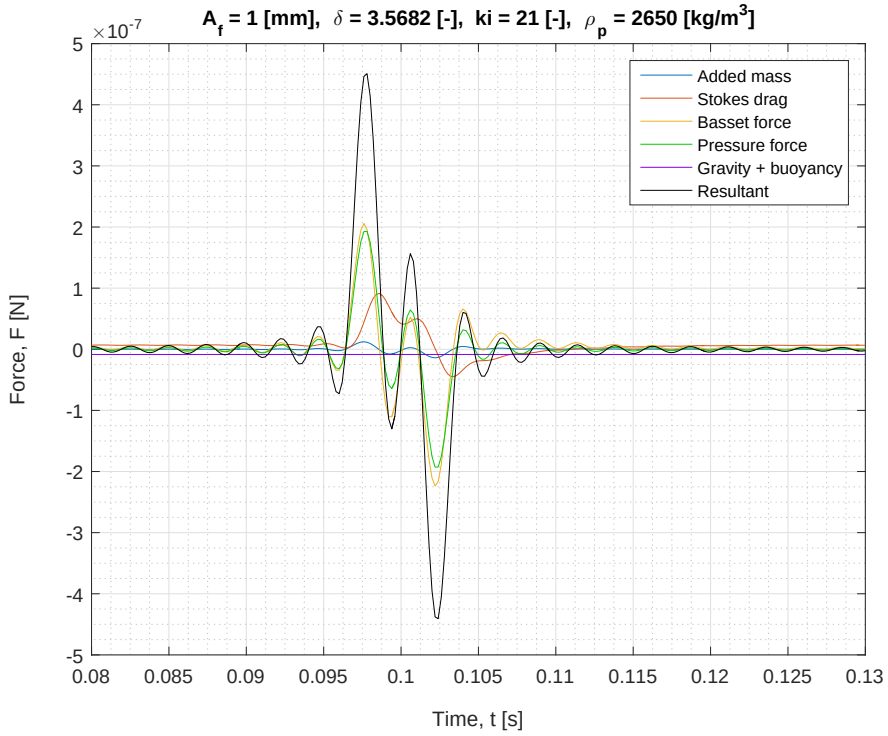

Figure 6.42: Forces due to non-uniform fluid oscillations, shape factor $ki = 21$, $\delta \approx 3.57$

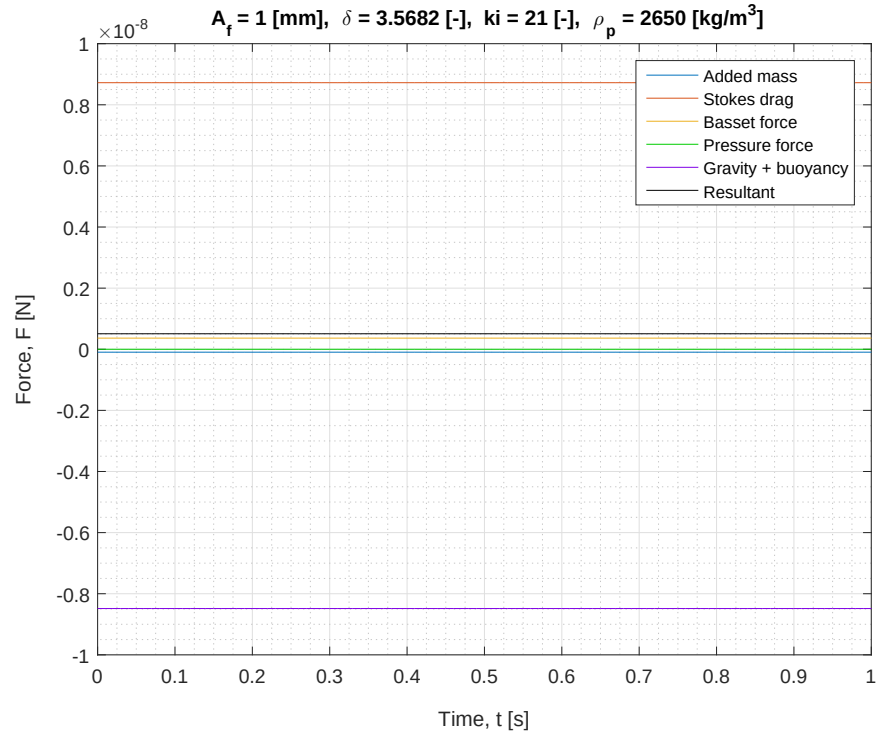

Figure 6.43: Average forces due to non-uniform oscillations, shape factor $ki = 21$, $\delta \approx 3.57$

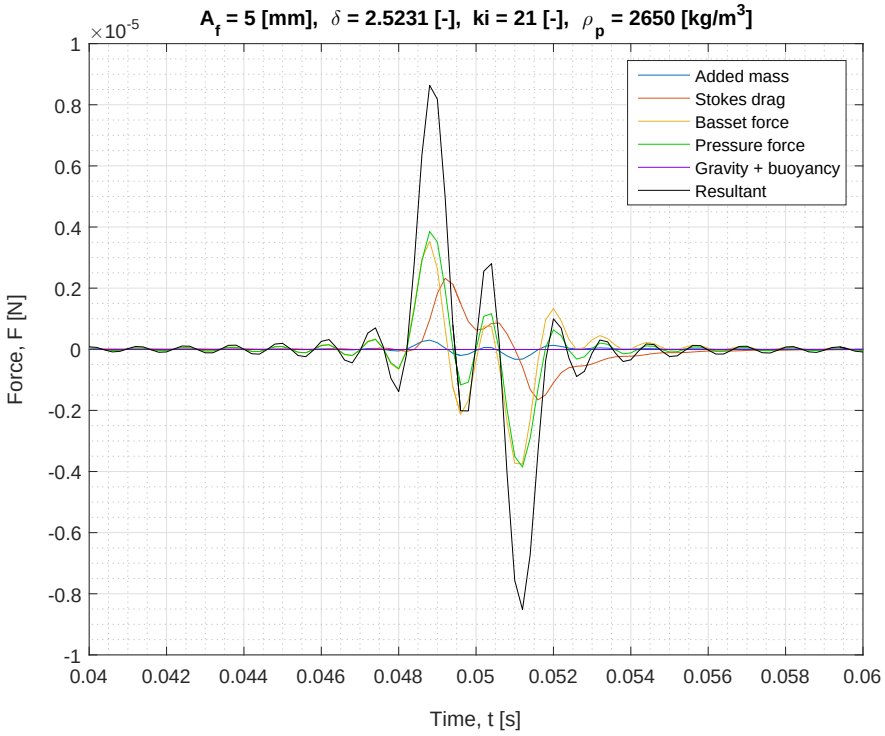

Figure 6.44: Forces due to non-uniform oscillations, shape factor $ki = 21$, $\delta \approx 2.52$

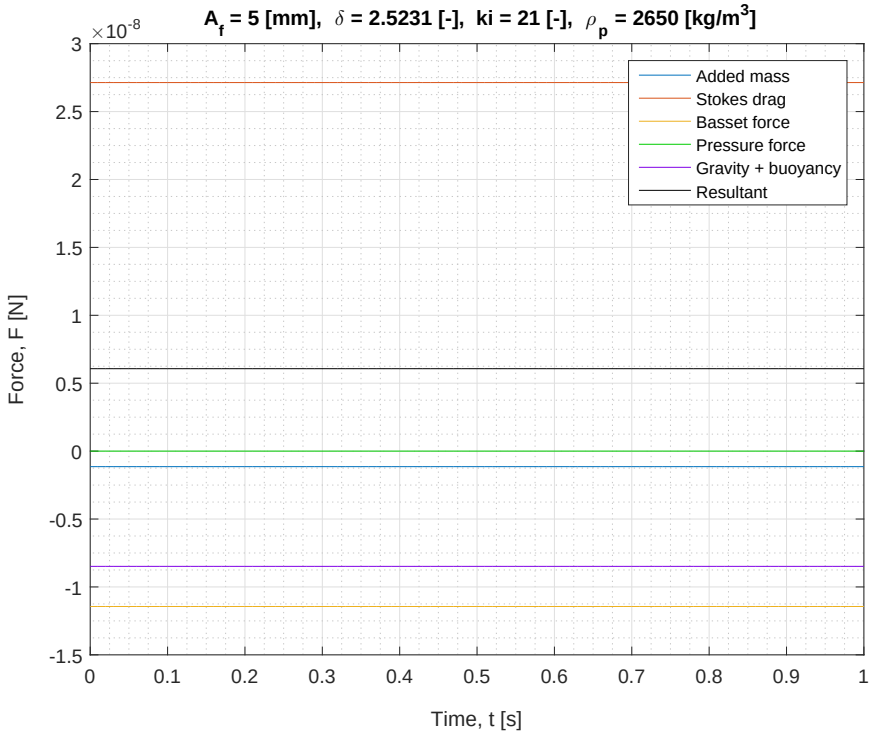

Figure 6.45: Average forces due to non-uniform oscillations, shape factor $ki = 21$, $\delta \approx 2.52$

CHAPTER 7

Conclusions & Recommendations

The main goal of this research was to theoretically and numerically investigate whether it would be possible to increase the hindered settling velocity using fluid oscillations. The idea of increasing the hindered settling velocity using fluid oscillations (shock wave) was first suggested by Stam (2007).

A literature study was performed to theoretically examine his hypothesis (Van de Wetering, 2015b). It was concluded that horizontal fluid oscillations (in the form of a shock wave) perpendicular to the settling direction will increase the drag coefficient and elongate the total distance to be covered by the particle. However, an interesting technique was found which uses non-uniform fluid oscillations to manipulate particle motion. That the response particle motion to these non-uniform fluid oscillations could be described by a differential equation, suggested by Boussinesq (1885), Basset (1888) and Oseen (1927) (*BBO-equation*). The BBO-equation was adjusted to account for both uniform (sinusoidal) and non-uniform (sawtooth) fluid oscillations and its validity range was extended by an empirical factor to the Stokes drag force, suggested by Clift et al. (1978).

Two hypotheses were created to increase the hindered settling velocity by applying the mentioned non-uniform fluid oscillations in either horizontal or vertical direction. In horizontal direction it is numerically examined whether particles could migrate in order to create a vein-like system (Kuenen, 1968), introducing a density driven convection flow. This convection flow would increase the settling velocity. In vertical direction it is numerically examined whether reversed sawtooth fluid oscillations (largest velocity in downward direction) could accelerate the particle in gravitational direction with an increased settling velocity.

This chapter presents the conclusions of the research towards the hypotheses, together with some general conclusions and discusses the possible improvements in the form of recommendations.

7.1 Conclusions

7.1.1 Increased settling velocity using horizontal fluid oscillations

The first hypothesis this thesis has studied, is repeated here for convenience:

"Using non-uniform fluid oscillations in horizontal direction causes solid spherical particles to migrate in the direction of oscillation, creating a horizontal density gradient which introduces a convection flow and therefore increases the average settling velocity".

The numerical model has shown that non-uniform fluid oscillations cause an average relative motion between the particle and fluid. The shape factor (ki) used to change the wave shape of the non-uniform oscillations determines the direction of migration. The migration velocity was calculated as function of the inverse Stokes number and fluid amplitude. Migration velocities in the order of two times the terminal settling velocity were found, which showed that the hypothesis is qualitatively feasible.

However, the limiting shape factors $ki = 1.05$ and $ki = 21$, produce wave shapes which in practice will not occur due to system properties such as friction and inertia. The predicted migration velocities are therefore highly theoretical. Furthermore, the model is only capable of predicting the migration velocity for a single particle. Because the hypothesis suggests a mixture to be present, migration velocities will be lower than theoretically predicted (as known from hindered settling theory).

7.1.2 Increased settling velocity using vertical fluid oscillations

The second hypothesis this thesis has studied, is also repeated here for convenience:

"Using non-uniform fluid oscillations in vertical direction with the highest velocity faced downwards, causes solid spherical particles to settle with increased average settling velocity".

Applying the numerical model in vertical direction, using the same limiting shape factors $ki = 1.05$ and $ki = 21$ has shown that the settling velocity of a single particle can be increased. Using non-uniform oscillations with the largest velocity pointed downwards $(ki = 1.05)$, resulted in predicted settling velocities being approximately two and a half times larger than the terminal settling velocity. It is therefore concluded that the second hypothesis is predicted to be qualitatively correct.

To prove this conclusion, the direction of highest velocity was reversed $(ki = 21)$, resulting in the experimentally found particle hovering and levitation (Van Oeveren and Houghton, 1971). This gave confidence in the usability and accuracy of the model.

7.1.3 General

1. *Neglecting viscosity results in a decoupled motion between particle and fluid without a phase angle.*

   Using the inviscid model, it is concluded that the decoupled motion (A_p/A_f) between the particle and fluid is caused by inertial differences. It is also shown that the lack of viscosity causes the particle and fluid to oscillate at the driving frequency of the settling tube without a phase difference $(\varphi = 0)$.

2. *The model has proven to be accurate within certain ranges, using datasets from literature.*

   From the validation study it can be concluded that the phase angle (φ) and decoupling (A_p/A_f) are reasonably well predicted by the numerical model, having a accuracy of 17.6% and 10%, respectively. The retardation coefficient $(b0)$ however, proved to be significantly overestimated at the higher inverse Stokes numbers $(0.2 < \delta < 1.6)$ in combination with particle Reynolds numbers within the validity range. When the particle Reynolds numbers went well outside the validity range, but the inverse Stokes number were low $\delta < 0.16$, it was found that the retardation coefficient could be estimated within 6.4% accuracy. However, the retardation behavior at higher frequencies was underestimated.

3. *The addition of the gravity term did not influence the amplitude ratio or the phase angle for both the inviscid and viscous model.*

   Because the gravity force term is not dependent on the fluid or particle acceleration and therefore static, it did not contribute to the particle response behavior described by the amplitude ratio and phase angle.

4. *The addition of viscosity decreased the decoupled motion between fluid and particle and causes a phase difference.*

   As mentioned, using the inviscid model showed that the decoupled motion between fluid and particle is causes by the inertial differences. The addition of viscosity showed a reduced decoupled motion, as the viscous forces impede the particle from acceleration and deceleration. This causes the particle to follow the fluid motions more closely.

5. *The amplitude ratio and phase angle were found to be not particularly sensitive for small changes in oscillation frequency, especially for the smallest fractions $d < 100\ \mu m$.*

   The oscillation frequency (f) was varied over a wide range of frequencies using constant oscillation amplitude (A_f), particle density (ρ_p) and fluid density (ρ_f). It was concluded that, especially for the smallest fractions, the amplitude ratio and phase angle were not particularly sensitive for small changes in frequency. However, the dependency on frequency tends to increase with increasing particle size for both the amplitude ratio and phase angle. When large frequency differences are compared, this dependency should be taken into account.

6. *The dependency of the amplitude ratio on viscosity is accurately predicted by the viscous model.*

   The dependency of the amplitude ratio on fluid viscosity was examined for a variety of particle sizes. The viscous model nicely showed that equal values were found in the limit of low viscosity, compared with the inviscid model. This shows that the decoupled motion between particle and fluid is correctly predicted by the viscous model, using the BBO-equation.

7. *The phase angle is maximum when the ratio of the inertial forces over the viscous forces is approximately unity.*

   The inviscid model showed that no phase angle occurred between the particle and fluid. The viscous model showed that in the limit of high viscosity also no phase angle would occur, as the particle would follow the fluid motion one to one. When the particle size was increased (increasing the inertial forces), it was found that the maximum phase angle occurs when the ratio between the inertial and viscous forces is approximately unity.

8. *The average relative velocity between the particle and the oscillating fluid is caused by a combination of the Stokes drag force and the history force.*

   By performing a force analysis, it is shown that the Stokes drag force and the history force change consistently with changing shape factor ki. Neglecting every term of the BBO-equation one by one, showed that no average relative velocity would occur if the history force was not included in the numerical model. It is therefore concluded that the combination of these forces is responsible for the relative motion between particle and fluid. A physical explanation for this phenomenon can not yet be given.

9. *Particle hovering and rising against gravity is predicted by the model using a shape factor* $ki = 21$.

   Van Oeveren and Houghton (1971) experimentally demonstrated that it would be possible to cause solid particles to hover (no relative vertical displacement) or even rise against gravity using vertical non-uniform fluid oscillations. The model predicts the same behavior using the retardation coefficient $(b1)$ as function of the inverse Stokes number (δ). Unfortunately, it is not possible to use the data from Van Oeveren and Houghton (1971) to validate the model because of the mentioned difference between theoretical input and practical output of the fluid oscillations.

10. *The fluid amplitude is the most dominant fluid variable in particle migration or settling behavior.*

    Examining the average particle response velocities in both horizontal and vertical direction using the inverse Stokes number (δ) and a variety of oscillations frequencies (f) and amplitudes (A_f), proved that the increase in fluid amplitude is more effective than the increase of oscillation frequency.

7.2 Recommendations

1. *Extend the numerical model by wave shape inputs which are more feasible in practice.*

   The used wave shapes for the non-uniform fluid oscillations (sawtooth) are highly theoretical. System properties such as friction and inertia cause the sawtooth wave to be much more continuous, especially at sharp transitions between upward and downward motion or vice versa. To create more accurate predictions, it is therefore recommended to extend the numerical model by implementing wave shapes which are more feasible in practice. This limits the transfer function between the input shape factor ki and output shape factor ko (Van Oeveren and Houghton, 1971).

2. *Physical experiments (single particle) should be conducted to validate the numerical model.*

   To extend the already performed validation, physical experiments using a single particle should be conducted to validate the numerical model and found average relative particle velocities in Chapter 6.

3. *The numerical model should be extended to calculate the particle response motion for multiple particles (concentration).*

   Both hypotheses suggest multiple particles (concentration) to be present in the settling tube, whereas the model is only capable of predicting the behavior of a single solid spherical particle. The influences of a concentration instead of a single particle are thoroughly described in Van de Wetering (2015b). If the model could be extended with the option to add a concentration, even greater accuracy in predicting migration and settling velocities could be achieved.

4. *Phyiscal experiments (multiple particles) should be conducted to entirely prove the hypotheses.*

   If the physical experiments using a single particle are in good agreement with the numerical model and average relative particle velocities are found, then the hypotheses should be proven entirely by adding a concentration.

5. *Investigate whether the assumption of the history force being valid over the entire range of particle Reynolds numbers can be justified.*

   The history force (F_h) suggested by Abbad and Souhar (2004a) is used in the numerical model, to account for the particle oscillating back and forth in its own wake. This term however, was not proven to be accurate for large particle Reynolds numbers. It should therefore be studied whether the used form of the history force is still valid in the current calculations.

6. *The numerical model could be extended to take both the horizontal oscillations and the vertical settling behavior into account.*

   Currently, both the horizontal and vertical particle motions are completely separated. Because a solid particle tends to settle vertically during the horizontal migration, the rectilinear model looses its validity. Weinstein (2008) experimentally validated that the model still predicts the horizontal particle response behavior accurately when the settling velocity is small compared to the horizontal fluid oscillations $\Theta \leq 0.4$. To increase accuracy in determining the necessary migration time during horizontal oscillations, the settling motion of the particle should be added to the horizontal particle response motion.

7. *The numerical model should be improved by additional function handles.*

   Currently, the model calculates the particle response velocities in every direction during each calculation. Calculation times are acceptable, but the efficiency could be improved by the addition of function handles in the model. This enables the user to specify the desired direction of the particle response velocity, therefore reducing the calculation time.

APPENDIX A

MATLAB CODE

```
%%%%%%%%%%%%%%%%%%%%%%%%%%%%%%%%%%%%%%%%%%%%%%%%%%%%%%%%%%%%%%%%%%%%%%%%%%%%%%%%
%%%%%%%%%%%%%%%%%%%%%%%%%%%%%%%%%%%%%%%%%%%%%%%%%%%%%%%%%%%%%%%%%%%%%%%%%%%%%%%%
% Solving the nonlinear Boussinesq (1885), Basset (1888) & Oseen (1927) equation  %
%                  Copyright R.G. van de Wetering 2015 - 2016 ©                   %
%                In achievement of the Master of Science degree                   %
%%%%%%%%%%%%%%%%%%%%%%%%%%%%%%%%%%%%%%%%%%%%%%%%%%%%%%%%%%%%%%%%%%%%%%%%%%%%%%%%
%%%%%%%%%%%%%%%%%%%%%%%%%%%%%%%%%%%%%%%%%%%%%%%%%%%%%%%%%%%%%%%%%%%%%%%%%%%%%%%%

tic
clc
clear all
close all

h = waitbar(0,'Please wait...   0%','Name','Nonlinear BBO-equation');

disp('Copyright R.G. van de Wetering, 2015 - 2016 ©')
disp('All rights reserved')
disp('This program is valid for particle Reynolds numbers in the range 0 - 1500')
disp('This program is valid for terminal settling velocities v_t of max. 0.08 m/s')
disp('_____________________________________________________________________________')

%% Oscillatory properties
A_f     = 0.001;                        % Amplitude                                 [m]
f       = 20;                           % Temporal frequency                        [1/s]
P       = 1/f;                          % Period                                    [s]
w       = f*2*pi;                       % Angular frequency                         [rad/s]
ki      = 1.05;                         % Shape factor 1.05-21                      [-]
c       = 1:1:40;                       % Harmonics in Fourier series (n)           [-]

%% Physical properties
T       = 20;                           % Temperature                               [Celcius]
g       = 9.81;                         % Gravitational acceleration                [m/s^2]

%% Particle geometry and properties
r       = 50E-6;                        % Particle radius                           [m]
d       = 2*r;                          % Particle diameter                         [m]
Vp      = 4/3*pi*r^3;                   % Particle volume                           [m^3]
rho_p   = 2650;                         % Partical density                          [kg/m^3]
mp      = Vp*rho_p;                     % Particle mass                             [kg]
c1      = 18;                           % Coefficient Ferguson & Church (2004)      [-]
c2      = 0.44;                         % Ferguson & Church (spherical)             [-]

waitbar(10/100,h,'Please wait...   10%') % Update waitbar
%% Calculating theoretical terminal settling velocity in stagnant water

% Density as function of temperature (Matousek, 2004)                               [kg/m^3]
rho_f   = 999.7-0.10512*(T-10)-0.005121*(T-10)^2+0.00001329*(T-10)^3;

% Viscosity as function of temperature (van Rhee, 2002)
nu_f    = (40E-6)/(20+T);               % Kinematic viscosity                       [m^2/s]
mu_f    = nu_f*rho_f;                   % Dynamic viscosity                         [Pa s]

% Relative density                                                                  [-]
Delta   = (rho_p-rho_f)/rho_f;

% Terminal settling velocity vt         [m/s]
vp      = Delta*g*d^2/(c1*nu_f+sqrt(0.75*c2*Delta*g*d^3)); % F&G     (2004)
vs      = (g*d^2*(rho_p-rho_f/rho_f))/(nu_f*18);           % Stokes (1851)

```

```
% Inverse Stokes number or the penetration depth of vorticity
delta    = sqrt((2*nu_f)/(r^2*w));

% Timescales
tau_v    = (r^2)/nu_f;          % Diffusive or viscous timescale          [-]
f_v      = 9/w;                 % Flow time scale (Coimbra (2004) 9=sphere [-]

%% Intial conditions for the ODE45 solver

% Initial time conditions      [s]
t0       = 0;                   % Starting time solver
dt       = 1/5000;              % Time step RK solver
tmax     = 1;                   % Total time
t        = t0:dt:tmax;          % Timespan

% Initial velocity conditions  [m/s]
v0       = 0;                   % Vertical sinusoidal oscillating velocity
vt0      = 0;                   % Vertical stagnant settling velocity
vw0      = 0;                   % Vertical sawtooth oscillating velocity
u0       = 0;                   % Horizontal sinusoidal oscillating velocity
uw0      = 0;                   % Horizontal sawtooth oscillating velocity

% Fluid displacements, velocities and accelerations at t=0 [m],[m/s] or [m/s2]
swf(c,1) = 0;                   % First column sawtooth displacement Fourier
Sw(1) = (-2*A_f*w/pi)*(-1)*(cos(w*t(1))); % First entry sawtooth velocity Fourier
dSw(1)   = 0;                   % First entry sawtooth acceleration Fourier
dSwv(c,1)= 0;                   % First column acceleration Fourier series

%% Fluid displacement, velocity and acceleration for sinusoidal and sawtooth

% Sinusoidal oscillations
s        = A_f.*sin(w.*t);                  % Fluid displacement      [m]
S        = A_f*w.*cos(w.*t);                % Fluid velocity          [m/s]
dS       = -A_f*w^2.*sin(w.*t);             % Fluid acceleration      [m/s^2]

%%%%%%%%%%%%%%%%%%%%%%%%%%%%%%%%%%%%%%%%%%%%%%%%%%%%%%%%%%%%%%%%%%%%%%%%%%%%%%%
% Sawtooth displacement using Fourier Series
if ki == 1;
    for n = c;
        for j=1:ceil(tmax/dt);
            % Update timestep
            t(j+1) = t(j)+dt;
            % Fourier series sawtooth wave if ki = 1
            swf(n,j+1) = ((-2*A_f)/(pi*n))*((-1)^n)*(sin(n*w*t(j+1)));
        end
    end
else
    for n = c;
        for j=1:ceil(tmax/dt)
            % Update timestep
            t(j+1) = t(j)+dt;
            % Fourier series triangle wave if ki =/= 1
            swf(n,j+1) = (A_f)*(((-2*((-1)^n)*(ki^2))/...
                ((n^2)*(ki-1)*(pi^2)))*sin((n*(ki-1)*pi)/ki)*sin(n*w*t(j+1)));
        end
    end
end

% Summation of all rows to find the Fourier curve
```

```
swx = sum(swf,1);

% Standard sawtooth wave in MATLAB
sw     = A_f*sawtooth(w.*t+(pi/ki),1/ki);

%%%%%%%%%%%%%%%%%%%%%%%%%%%%%%%%%%%%%%%%%%%%%%%%%%%%%%%%%%%%%%%%%%%%%%%%%%%%%%%%
% First derivative to find the velocity wave from previous Fourier series
if ki == 1;
    % Create a non-zero first column with calculated values
    for n = c
        Swv(n,1) = (-2*A_f*w/pi)*(((-1)^n)*(cos(w*t(1)*n)));
    end
    % Fill the rest of the matrix
    for n = c;
        for j=1:ceil(tmax/dt)
            % Update timestep
            t(j+1) = t(j)+dt;
            % Fourier series wave if ki == 1
            Swv(n,j+1) = (-2*A_f*w/pi)*(((-1)^n)*(cos(w*t(j+1)*n)));
        end
    end
else
    % Create a non-zero first column with calculated values
    for n = c;
        Swv(n,1) = (A_f*n*w)*(((-2*((-1)^n)*(ki^2))/...
            ((n^2)*(ki-1)*(pi^2)))*sin((n*(ki-1)*pi)/ki)*cos(n*w*t(1)));
    end
    for n = c;
        for j=1:ceil(tmax/dt)
            % Update timestep
            t(j+1) = t(j)+dt;
            % Fourier series wave if ki =/= 1
            Swv(n,j+1) = (A_f*n*w)*(((-2*((-1)^n)*(ki^2))/...
                ((n^2)*(ki-1)*(pi^2)))*sin((n*(ki-1)*pi)/ki)*cos(n*w*t(j+1)));
        end
    end
end

% Summation of all rows to find the Fourier curve
Sw = sum(Swv,1);

% Using standard MATLAB command to find the derivative
Sw_mat = diff(swx)./dt;

%%%%%%%%%%%%%%%%%%%%%%%%%%%%%%%%%%%%%%%%%%%%%%%%%%%%%%%%%%%%%%%%%%%%%%%%%%%%%%%%
% Second derivative to find acceleration from previous Fourier series
if ki == 1;
    for n = c;
        for j=1:ceil(tmax/dt)
            % Update timestep
            t(j+1) = t(j)+dt;
            % Fourier series wave if ki == 1
            dSwv(n,j+1) = (-2*A_f*n*w^2/pi)*(((-1)^n)*(sin(w*t(j+1)*n)));
        end
    end
else
    for n = c;
       for j=1:ceil(tmax/dt)
           % Update timestep
```

```
            t(j+1) = t(j)+dt;
            % Fourier series wave if ki =/= 1
            dSwv(n,j+1) = (-A_f*n^2*w^2)*(((-2*((-1)^n)*(ki^2))/...
                ((n^2)*(ki-1)*(pi^2)))*sin((n*(ki-1)*pi)/ki)*sin(n*w*t(j+1)));
        end
    end
end
% Summation of all rows to find the Fourier curve
dSw= sum(dSwv,1);

% Using standard MATLAB command to find the derivative
dSw_mat = diff(Sw_mat)./dt;

waitbar(20/100,h,'Please wait...   20%')            % Update waitbar
%% Oscillating particle velocity using potential flow theory (inviscid, irrotational):

% Vertical direction sinusoidal and sawtooth
v_pot  = (3.*S)./(1+2*(rho_p/rho_f))  + (2*g*(rho_f-rho_p)/(rho_f+2*rho_p));
vw_pot = (3.*Sw)./(1+2*(rho_p/rho_f)) + (2*g*(rho_f-rho_p)/(rho_f+2*rho_p));

% Horizontal direction sinusoidal and sawtooth
u_pot  = (3.*S)./(1+2*(rho_p/rho_f));
uw_pot = (3.*Sw)./(1+2*(rho_p/rho_f));

% Inviscid decoupling behavior as function of density ratio
decoup = xlsread('Decoupling_beta.xlsx','Decoupling','B4:E48');

%% Use the built-in ODE45 solver to solve the nonlinear BBO equation

% Tolerance settings
reltol = 1E-7;
abstol = 1E-9;
options = odeset('RelTol',reltol,'AbsTol',abstol);

%%%%%%%%%%%%%%%%%%%%%%%%%%%%%%%%%%%%%%%%%%%%%%%%%%%%%%%%%%%%%%%%%%%%%%%%%%%%%%%%%%%%%%%%%%
% Solve bbo-equation for vertical direction (terminal)
[t,vt_ode45] = ode45(@(t,vt_ode45) bboequation_vt(t,vt_ode45,mu_f,rho_f,nu_f,rho_p,Vp...
    ,r,d,delta,tau_v,g),[t0:dt:tmax],vt0,options);
Re_vt_ode45  = (abs(vt_ode45').*d)./nu_f;           % Calculate particle Reynolds number

% Calculating the correction factor for the Stokes Drag Force (Clift et al., (1978))
for k = 1:1:length(Re_vt_ode45);
    for i = Re_vt_ode45(k);
        if i == 0;                                   %Re=0
            phi_vt_ode45(k) = 1;
        elseif (i>0) && (i<=0.01);                   %0<Re<=0.01
            phi_vt_ode45(k) = 1+(3/16)*i;
        elseif (i>0.01) && (i<=20);                  %0.01<Re<20
            phi_vt_ode45(k) = 1+0.1315*i^(0.82-0.05*(log10(i)));
        elseif (i>20) && (i<=260);                   %20<Re<260
            phi_vt_ode45(k) = 1+0.1935*i^(0.6305);
        elseif (i>260) && (i<=1500);                 %260<Re<1500
            phi_vt_ode45(k) = 1.8335*(i)*10^(-1.1242*(log10(i))+0.1558*(log10(i))^2);
        else
            phi_vt_ode45(k) = 1.8335*(i)*10^(-1.1242*(log10(i))+0.1558*(log10(i))^2);
            (disp('WARNING Re_vt_ode45 is too high, equation no longer valid'));
        end
    end
end
```

```
% Calculating particle acceleration using the BBO-equation
dvt_ode45dt = ...
    +   (Vp*g*(rho_f-rho_p))/(Vp*rho_p+3*pi*mu_f*r*delta*tau_v+(2/3)*pi*r^3*rho_f)...
    -   (6*pi*r*mu_f.*phi_vt_ode45.*vt_ode45')./...
        (Vp*rho_p+3*pi*mu_f*r*delta*tau_v+(2/3)*pi*r^3*rho_f);

% Validate dvt_ode45dt using built-in Matlab diff() function
dvtdt_mat = diff(vt_ode45)./dt;

waitbar(30/100,h,'Please wait...   30%')             % Update waitbar

%%%%%%%%%%%%%%%%%%%%%%%%%%%%%%%%%%%%%%%%%%%%%%%%%%%%%%%%%%%%%%%%%%%%%%%%%%%%%%%%%%%%%%%%%%
% Solve bbo-equation for vertical direction (sinusoidal)
[t,v_ode45]  = ode45(@(t,v_ode45) bboequation_v(t,v_ode45,A_f,f,mu_f,rho_f,nu_f,rho_p,...
    Vp,r,d,delta,tau_v,g),[t0:dt:tmax],v0,options);
vm_ode45      = mean(v_ode45').*ones(1,length(t));     % Calculate mean oscillating velocity
Re_v_ode45    = (abs(S-v_ode45').*d)./nu_f;            % Calculate particle Reynolds number

% Calculating the correction factor for the Stokes Drag Force (Clift et al., (1978))
for k = 1:1:length(Re_v_ode45);
    for i = Re_v_ode45(k);
        if i == 0;                                    %Re=0
            phi_v_ode45(k) = 1;
        elseif (i>0) && (i<=0.01);                    %0<Re<=0.01
            phi_v_ode45(k) = 1+(3/16)*i;
        elseif (i>0.01) && (i<=20);                   %0.01<Re<20
            phi_v_ode45(k) = 1+0.1315*i^(0.82-0.05*(log10(i)));
        elseif (i>20) && (i<=260);                    %20<Re<260
            phi_v_ode45(k) = 1+0.1935*i^(0.6305);
        elseif (i>260) && (i<=1500);                  %260<Re<1500
            phi_v_ode45(k) = 1.8335*(i)*10^(-1.1242*(log10(i))+0.1558*(log10(i))^2);
        else
            phi_v_ode45(k) = 1.8335*(i)*10^(-1.1242*(log10(i))+0.1558*(log10(i))^2);
            (disp('WARNING Re_v_ode45 is too high, equation no longer valid'));
        end
    end
end

% Calculating particle acceleration using the BBO-equation
dv_ode45dt = ...
    +   (Vp*g*(rho_f-rho_p))/(Vp*rho_p+3*pi*mu_f*r*delta*tau_v+(2/3)*pi*r^3*rho_f)...
    +   (6*pi*r*mu_f.*phi_v_ode45.*(S-v_ode45'))./...
        (Vp*rho_p+3*pi*mu_f*r*delta*tau_v+(2/3)*pi*r^3*rho_f)...
    +   (6*pi*r*mu_f.*(((S-v_ode45')./delta)+0.5*delta*tau_v.*dS))./...
        (Vp*rho_p+3*pi*mu_f*r*delta*tau_v+(2/3)*pi*r^3*rho_f)...
    +   (2*pi*r^3*rho_f.*dS)./(Vp*rho_p+3*pi*mu_f*r*delta*tau_v+(2/3)*pi*r^3*rho_f);

% Validate dv_ode45dt using built-in Matlab diff() function
dvdt_mat = diff(v_ode45)./dt;

waitbar(40/100,h,'Please wait...   40%')            % Update waitbar

%%%%%%%%%%%%%%%%%%%%%%%%%%%%%%%%%%%%%%%%%%%%%%%%%%%%%%%%%%%%%%%%%%%%%%%%%%%%%%%%%%%%%%%%%%%%
% Solve bbo-equation for vertical direction (sawtooth)
[t,vw_ode45] = ode45(@(t,vw_ode45) bboequation_vw(t,vw_ode45,A_f,f,mu_f,rho_f,nu_f,rho_p,...
    Vp,r,d,delta,tau_v,g,ki,c,tmax,dt),[t0:dt:tmax],vw0,options);
vwm_ode45     = mean(vw_ode45').*ones(1,length(t));    % Calculate mean oscillating velocity
Re_vw_ode45   = (abs(Sw-vw_ode45').*d)./nu_f;          % Calculate particle Reynolds number
```

```
% Calculating the correction factor for the Stokes Drag Force (Clift et al., (1978))
for k = 1:1:length(Re_vw_ode45);
    for i = Re_vw_ode45(k);
        if i == 0;                                          %Re=0
            phi_vw_ode45(k) = 1;
        elseif (i>0) && (i<=0.01);                          %0<Re<=0.01
            phi_vw_ode45(k) = 1+(3/16)*i;
        elseif (i>0.01) && (i<=20);                         %0.01<Re<20
            phi_vw_ode45(k) = 1+0.1315*i^(0.82-0.05*(log10(i)));
        elseif (i>20) && (i<=260);                          %20<Re<260
            phi_vw_ode45(k) = 1+0.1935*i^(0.6305);
        elseif (i>260) && (i<=1500);                        %260<Re<1500
            phi_vw_ode45(k) = 1.8335*(i)*10^(-1.1242*(log10(i))+0.1558*(log10(i))^2);
        else
            phi_vw_ode45(k) = 1.8335*(i)*10^(-1.1242*(log10(i))+0.1558*(log10(i))^2);
            (disp('WARNING Re_vw_ode45 is too high, equation no longer valid'));
        end
    end
end

% Calculating particle acceleration using the BBO-equation
dvw_ode45dt = ...
    +   (Vp*g*(rho_f-rho_p))/(Vp*rho_p+3*pi*mu_f*r*delta*tau_v+(2/3)*pi*r^3*rho_f)...
    +   (6*pi*r*mu_f.*phi_vw_ode45.*(Sw-vw_ode45'))./...
        (Vp*rho_p+3*pi*mu_f*r*delta*tau_v+(2/3)*pi*r^3*rho_f)...
    +   (6*pi*r*mu_f.*(((Sw-vw_ode45')./delta)+0.5*delta*tau_v.*dSw))./...
        (Vp*rho_p+3*pi*mu_f*r*delta*tau_v+(2/3)*pi*r^3*rho_f)...
    +   (2*pi*r^3*rho_f.*dSw)./(Vp*rho_p+3*pi*mu_f*r*delta*tau_v+(2/3)*pi*r^3*rho_f);

% Validate dvw_ode45dt using built-in Matlab diff() function
dvwdt_mat    = diff(vw_ode45)./dt;

waitbar(50/100,h,'Please wait...   50%')              % Update waitbar

%%%%%%%%%%%%%%%%%%%%%%%%%%%%%%%%%%%%%%%%%%%%%%%%%%%%%%%%%%%%%%%%%%%%%%%%%%%%%%%%%%%%%%%%%%%%%%%%
% Solve bbo-equation for horizontal direction (sinusoidal)
[t,u_ode45]   = ode45(@(t,u_ode45) bboequation_u(t,u_ode45,A_f,f,mu_f,rho_f,nu_f,rho_p,...
    Vp,r,d,delta,tau_v,g),[t0:dt:tmax],u0,options);
um_ode45      = mean(u_ode45').*ones(1,length(t));     % Calculate mean oscillating velocity
Re_u_ode45    = (abs(S-u_ode45').*d)./nu_f;            % Calculate particle Reynolds number

% Calculating the correction factor for the Stokes Drag Force (Clift et al., (1978))
for k = 1:1:length(Re_u_ode45);
    for i = Re_u_ode45(k);
        if i == 0;                                          %Re=0
            phi_u_ode45(k) = 1;
        elseif (i>0) && (i<=0.01);                          %0<Re<=0.01
            phi_u_ode45(k) = 1+(3/16)*i;
        elseif (i>0.01) && (i<=20);                         %0.01<Re<20
            phi_u_ode45(k) = 1+0.1315*i^(0.82-0.05*(log10(i)));
        elseif (i>20) && (i<=260);                          %20<Re<260
            phi_u_ode45(k) = 1+0.1935*i^(0.6305);
        elseif (i>260) && (i<=1500);                        %260<Re<1500
            phi_u_ode45(k) = 1.8335*(i)*10^(-1.1242*(log10(i))+0.1558*(log10(i))^2);
        else
            phi_u_ode45(k) = 1.8335*(i)*10^(-1.1242*(log10(i))+0.1558*(log10(i))^2);
            (disp('WARNING Re_u_ode45 is too high, equation no longer valid'));
        end
```

```
    end
end

% Calculating particle acceleration using the BBO-equation
du_ode45dt = ...
    +   (6*pi*r*mu_f.*phi_u_ode45.*(S-u_ode45'))./...
        (Vp*rho_p+3*pi*mu_f*r*delta*tau_v+(2/3)*pi*r^3*rho_f)...
    +   (6*pi*r*mu_f.*(((S-u_ode45')./delta)+0.5*delta*tau_v.*dS))./...
        (Vp*rho_p+3*pi*mu_f*r*delta*tau_v+(2/3)*pi*r^3*rho_f)...
    +   (2*pi*r^3*rho_f.*dS)./(Vp*rho_p+3*pi*mu_f*r*delta*tau_v+(2/3)*pi*r^3*rho_f);

% Validate du_ode45dt using built-in Matlab diff() function
dudt_mat = diff(u_ode45)./dt;

waitbar(60/100,h,'Please wait...  60%')              % Update waitbar

%%%%%%%%%%%%%%%%%%%%%%%%%%%%%%%%%%%%%%%%%%%%%%%%%%%%%%%%%%%%%%%%%%%%%%%%%%%%%%%%%%%%%%%%%%%%%%%%%%%%
% Solve bbo-equation for horizontal direction (sawtooth)
[t,uw_ode45] = ode45(@(t,uw_ode45) bboequation_uw(t,uw_ode45,A_f,f,mu_f,rho_f,nu_f,rho_p,...
    Vp,r,d,delta,tau_v,g,ki,c,tmax,dt),[t0:dt:tmax],uw0,options);
uwm_ode45    = mean(uw_ode45').*ones(1,length(t));   % Calculate mean oscillating velocity
Re_uw_ode45  = (abs(Sw-uw_ode45').*d)./nu_f;         % Calculate particle Reynolds number

% Calculating the correction factor for the Stokes Drag Force (Clift et al., (1978))
for k = 1:1:length(Re_uw_ode45);
    for i = Re_uw_ode45(k);
        if i == 0;                                   %Re=0
            phi_uw_ode45(k) = 1;
        elseif (i>0) && (i<=0.01);                   %0<Re<=0.01
            phi_uw_ode45(k) = 1+(3/16)*i;
        elseif (i>0.01) && (i<=20);                  %0.01<Re<20
            phi_uw_ode45(k) = 1+0.1315*i^(0.82-0.05*(log10(i)));
        elseif (i>20) && (i<=260);                   %20<Re<260
            phi_uw_ode45(k) = 1+0.1935*i^(0.6305);
        elseif (i>260) && (i<=1500);                 %260<Re<1500
            phi_uw_ode45(k) = 1.8335*(i)*10^(-1.1242*(log10(i))+0.1558*(log10(i))^2);
        else
            phi_uw_ode45(k) = 1.8335*(i)*10^(-1.1242*(log10(i))+0.1558*(log10(i))^2);
            (disp('WARNING Re_uw_ode45 is too high, equation no longer valid'));
        end
    end
end

% Calculating particle acceleration using the BBO-equation
duw_ode45dt = ...
    +   (6*pi*r*mu_f.*phi_uw_ode45.*(Sw-uw_ode45'))./...
        (Vp*rho_p+3*pi*mu_f*r*delta*tau_v+(2/3)*pi*r^3*rho_f)...
    +   (6*pi*r*mu_f.*(((Sw-uw_ode45')./delta)+0.5*delta*tau_v.*dSw))./...
        (Vp*rho_p+3*pi*mu_f*r*delta*tau_v+(2/3)*pi*r^3*rho_f)...
    +   (2*pi*r^3*rho_f.*dSw)./(Vp*rho_p+3*pi*mu_f*r*delta*tau_v+(2/3)*pi*r^3*rho_f);

% Validate duw_ode45dt using Matlab's built in diff() function
duwdt_mat = diff(uw_ode45)./dt;

waitbar(70/100,h,'Please wait...  70%')              % Update waitbar

%% Analyzing the different force terms in the nonlinear BBO equation

% Terminal settling velocity non-oscillating fluid
```

```
Fb_vt_ode45    = Vp*g*(rho_f-rho_p).*ones(1,length(t));
Fd_vt_ode45    = -(6*pi*r*mu_f.*phi_vt_ode45.*vt_ode45');
Fa_vt_ode45    = -(2/3)*pi*r^3*rho_f.*dvt_ode45dt;

Fres_vt_ode45 = Fb_vt_ode45 + Fd_vt_ode45 + Fa_vt_ode45;

% Sinusoidal waveform vertically oscillating
Fb_v_ode45     = Vp*g*(rho_f-rho_p).*ones(1,length(t));
Fd_v_ode45     = (6*pi*r*mu_f.*phi_v_ode45.*(S-v_ode45'));
Fh_v_ode45     = (6*pi*r*mu_f.*(((S-v_ode45')./...
    delta)+0.5*delta*tau_v.*(dS-dv_ode45dt)));
Fa_v_ode45     = (2/3*pi*r^3*rho_f.*(dS-dv_ode45dt));
Fp_v_ode45     = (4/3*pi*r^3*rho_f.*dS);
Fd_vm_ode45    = mean(Fd_v_ode45).*ones(1,length(t));
Fh_vm_ode45    = mean(Fh_v_ode45).*ones(1,length(t));
Fa_vm_ode45    = mean(Fa_v_ode45).*ones(1,length(t));
Fp_vm_ode45    = mean(Fp_v_ode45).*ones(1,length(t));

Fres_v_ode45  = Fb_v_ode45 + Fd_v_ode45 + Fh_v_ode45 + ...
    Fa_v_ode45 + Fp_v_ode45;
Fres_vm_ode45 = Fb_v_ode45 + Fd_vm_ode45 + Fh_vm_ode45 + ...
    Fa_vm_ode45 + Fp_vm_ode45;

% Sawtooth waveform vertically oscillating
Fb_vw_ode45    = Vp*g*(rho_f-rho_p).*ones(1,length(t));
Fd_vw_ode45    = (6*pi*r*mu_f.*phi_vw_ode45.*(Sw-vw_ode45'));
Fh_vw_ode45    = (6*pi*r*mu_f.*(((Sw-vw_ode45')./...
    delta)+0.5*delta*tau_v.*(dSw-dvw_ode45dt)));
Fa_vw_ode45    = (2/3*pi*r^3*rho_f.*(dSw-dvw_ode45dt));
Fp_vw_ode45    = (4/3*pi*r^3*rho_f.*dSw);
Fd_vwm_ode45   = mean(Fd_vw_ode45).*ones(1,length(t));
Fh_vwm_ode45   = mean(Fh_vw_ode45).*ones(1,length(t));
Fa_vwm_ode45   = mean(Fa_vw_ode45).*ones(1,length(t));
Fp_vwm_ode45   = mean(Fp_vw_ode45).*ones(1,length(t));

Fres_vw_ode45 = Fb_vw_ode45 + Fd_vw_ode45 + Fh_vw_ode45 + ...
    Fa_vw_ode45 + Fp_vw_ode45;
Fres_vwm_ode45= Fb_vw_ode45 + Fd_vwm_ode45 + Fh_vwm_ode45 + ...
    Fa_vwm_ode45 + Fp_vwm_ode45;

% Sinusoidal waveform horizontally oscillating
Fd_u_ode45     = (6*pi*r*mu_f.*phi_u_ode45.*(S-u_ode45'));
Fh_u_ode45     = (6*pi*r*mu_f.*(((S-u_ode45')./...
    delta)+0.5*delta*tau_v.*(dS-du_ode45dt)));
Fa_u_ode45     = (2/3*pi*r^3*rho_f.*(dS-du_ode45dt));
Fp_u_ode45     = (4/3*pi*r^3*rho_f.*dS);
Fd_um_ode45    = mean(Fd_u_ode45).*ones(1,length(t));
Fh_um_ode45    = mean(Fh_u_ode45).*ones(1,length(t));
Fa_um_ode45    = mean(Fa_u_ode45).*ones(1,length(t));
Fp_um_ode45    = mean(Fp_u_ode45).*ones(1,length(t));

Fres_u_ode45  = Fd_u_ode45 + Fh_u_ode45 + Fa_u_ode45 + Fp_u_ode45;
Fres_um_ode45 = Fd_um_ode45 + Fh_um_ode45 + Fa_um_ode45 + Fp_um_ode45;

% Sawtooth waveform horizontally oscillating
Fd_uw_ode45    = (6*pi*r*mu_f.*phi_uw_ode45.*(Sw-uw_ode45'));
Fh_uw_ode45    = (6*pi*r*mu_f.*(((Sw-uw_ode45')./...
    delta)+0.5*delta*tau_v.*(dSw-duw_ode45dt)));
Fa_uw_ode45    = (2/3*pi*r^3*rho_f.*(dSw-duw_ode45dt));
```

```
473 Fp_uw_ode45    = (4/3*pi*r^3*rho_f.*dSw);
474 Fd_uwm_ode45   = mean(Fd_uw_ode45).*ones(1,length(t));
475 Fh_uwm_ode45   = mean(Fh_uw_ode45).*ones(1,length(t));
476 Fa_uwm_ode45   = mean(Fa_uw_ode45).*ones(1,length(t));
477 Fp_uwm_ode45   = mean(Fp_uw_ode45).*ones(1,length(t));
478
479 Fres_uw_ode45 = Fd_uw_ode45 + Fh_uw_ode45 + Fa_uw_ode45 + Fp_uw_ode45;
480 Fres_uwm_ode45= Fd_uwm_ode45 + Fh_uwm_ode45 + Fa_uwm_ode45 + Fp_uwm_ode45;
481
482 waitbar(80/100,h,'Please wait...   80%')  % Update waitbar
483 %% Calculated velocity integrated to find particle displacement as function of time
484
485 % Vertical
486 vy     = cumtrapz(t,v_ode45.*1000);   % Particle displacement sinusoidal       [mm]
487 vty    = cumtrapz(t,vt_ode45.*1000);  % Particle displacement terminal          [mm]
488 vwy    = cumtrapz(t,vw_ode45.*1000);  % Particle displacement sawtooth          [mm]
489 vmy    = cumtrapz(t,vm_ode45.*1000);  % Particle displacement sinusoidal mean [mm]
490 vwmy   = cumtrapz(t,vwm_ode45.*1000); % Particle displacement sawtooth mean    [mm]
491
492 % Horizontal
493 ux     = cumtrapz(t,u_ode45.*1000);   % Particle displacement sinusoidal       [mm]
494 umx    = cumtrapz(t,um_ode45.*1000);  % Particle displacement sinusoidal mean [mm]
495 uwx    = cumtrapz(t,uw_ode45.*1000);  % Particle displacement sawtooth          [mm]
496 uwmx   = cumtrapz(t,uwm_ode45.*1000); % Particle displacement sawtooth mean    [mm]
497
498 % Fluid sinusoidal
499 S_int = cumtrapz(t,S.*1000);          % Integrate to find fluid displacement   [mm]
500
501 waitbar(90/100,h,'Please wait...   90%')        % Update waitbar
502 %% Calculate Dimensionless numbers
503
504 % Stokes number (Herringe, 1974)
505 Sto      = sqrt((nu_f)/(w*d^2));
506
507 % Inverse Stokes number (Weinstein et al., 2008)
508 Sto_inv = sqrt((2*nu_f)/(w*r^2));
509
510 % Strouhal number vertical sinus osc. (Weinstein et al., 2008)
511 Str_v    = w*r./abs(S-v_ode45');
512
513 % Strouhal number vertical sawtooth osc. (Weinstein et al., 2008)
514 Str_vw   = w*r./abs(Sw-vw_ode45');
515
516 % Strouhal number horizontal sinus osc. (Weinstein et al., 2008)
517 Str_u    = w*r./abs(S-u_ode45');
518
519 % Strouhal number horizontal sawtooth osc. (Weinstein et al., 2008)
520 Str_uw   = w*r./abs(Sw-uw_ode45');
521
522 % Velocity ratio oscillated sinusoidal wave to stagnant
523 b0       = mean(v_ode45')/abs(vt_ode45(end));
524
525 % Velocity ratio oscillated sawtooth wave to stagnant
526 b1       = mean(vw_ode45')/abs(vt_ode45(end));
527
528 % Ratio of fluid acceleration over gravitational acceleration (Herringe, 1975)
529 Ra       = (A_f*w^2)/g;
530
531 % Density ratio (Weinstein et al., 2008)
```

```
Rd       = rho_p/rho_f;

% Ratio between distance travelled and particle diameter (Weinstein, 2008)
Rf       = abs(vt_ode45(end))/(2*r*w);

% Dimensionless frequency (Coimbra et al., 2004)
Om       = (r^2*w)/(9*nu_f);

%% Calculate phase difference and amplitude ratio Ap/Af (decoupling)

% Horizontal
[amp_u_pot, ph_u_pot] = response_u_pot(S,u_pot,dt,t);
[amp_u, ph_u]         = response_u(S,u_ode45,dt,t);
[amp_uw, ph_uw]       = response_uw(Sw,uw_ode45,dt,t);

% Vertical
[amp_v, ph_v]         = response_v(S,v_ode45,dt,t);
[amp_v_pot, ph_v_pot] = response_v_pot(S,v_pot,dt,t);
[amp_vw, ph_vw]       = response_vw(Sw,vw_ode45,dt,t);

%% Load experimental validation data

% Data Herringe (1976) [-]
herringe1976  = xlsread('Validation.xlsx','Herringe (1976)','B3:X31');

% Data  Herringe (1977) [-]
herringe1977  = xlsread('Aquaeous_glycerol.xlsx','Herringe (1977)','B4:F34');

% Data Takahashi (1992) [-]
takahashi1992 = xlsread('Validation.xlsx','Takahashi (1992)','B3:Z74');

%% Check Stokes drag correction factor phi(Re)

% Arbitrary particle Reynolds numbers to check phi(Re)
Re = 1:1/10:1500;

% Calculating the correction factor for the Stokes Drag Force (Clift et al., (1978))
for z = 1:1:length(Re);
    for i = Re(z);
        if i == 0;                                  %Re=0
            phi(z) = 1;
        elseif (i>0) && (i<=0.01);                  %0<Re<=0.01
            phi(z) = 1+(3/16)*i;
        elseif (i>0.01) && (i<=20);                 %0.01<Re<20
            phi(z) = 1+0.1315*i^(0.82-0.05*(log10(i)));
        elseif (i>20) && (i<=260);                  %20<Re<260
            phi(z) = 1+0.1935*i^(0.6305);
        elseif (i>260) && (i<=1500);                %260<Re<1500
            phi(z) = 1.8335*(i)*10^(-1.1242*(log10(i)) + 0.1558*(log10(i))^2);
        end
    end
end

waitbar(100/100,h,'Please wait...    100%')       % Update waitbar
close(h)                                          % Close waitbar
%% Load Decoupling Ap/Af and Phase Angle as function of frequency

% Amplitude ratio as function of frequency
decoup_freq = xlsread('Decoupling_frequency.xlsx','diameter','B3:M70');
```

```
591
592 % Phase angle as function of frequency
593 phase_freq  = xlsread('Phase_angle_frequency.xlsx','diameter','B3:Q70');
594
595 %% Load Decoupling Ap/Af and Phase Angle as function of viscosity
596
597 % Phase angle as function of viscosity
598 phase_visc = xlsread('Phase_angle_viscosity.xlsx','viscosity','B3:H72');
599
600 % Decoupling as function of viscosity
601 decoup_visc  = xlsread('Decoupling_viscosity.xlsx','viscosity','B3:F73');
602
603 %% Load migration velocity (u & uw) as function of inverse Stokes number
604
605 % Horizontal migration velocities as function of the inverse Stokes number
606 horvel_stokes = xlsread('Partvel_invStokes_hor','amplitude','B3:L128');
607
608 toc
```

APPENDIX B

Dataset Herringe (1976)

rho_s (kg/m3)	rho_f (kg/m3)	d (m)	r (m)	St (-)	St.inverse (-)	Nu (m^2/s)	Ra (-)	beta (-)	Af (m)	w (rad/s)	f (Hz)	b0 (-)	Ap/Af (-)	phase lag phi (rad)	F&G (2004) Vt (m/s)	Model Vt (m/s)	Model V (m/s)	Model b0 (-)	Model Ap/Af (-)	Model phase lag (rad)	Model valid
2960	1222	1,85E-03	9,25E-04	0,256	0,724	9,87E-05	62,10	1,70	3,15E-03	440,12	70	-0,94	0,77	-0,24	-0,0245	-0,0251	-0,0097	-0,40	0,81	-0,19	Y
2960	1138	1,64E-03	8,20E-04	0,122	0,345	7,10E-06	10,10	1,92	3,15E-03	177,39	28	-0,95	0,61	-0,23	-0,1514	-0,1261	-0,0518	-0,34	0,66	-0,22	Y
2960	1145	1,70E-03	8,50E-04	0,129	0,365	8,23E-06	9,38	1,85	3,15E-03	171,05	27	-0,91	-	-	-0,1464	-0,1222	-0,0508	-0,35	-	-	Y
2960	1141	1,74E-03	8,70E-04	0,075	0,212	7,49E-06	62,10	1,81	3,15E-03	439,81	70	-0,89	0,56	-0,13	-0,158	-0,1315	-0,0343	-0,22	0,60	-0,19	Y
2960	1148	5,40E-04	2,70E-04	0,419	1,185	8,72E-06	9,38	5,87	3,17E-03	170,38	27	-0,89	0,88	-0,13	-0,0244	-0,0243	-0,0123	-0,50	0,90	-0,15	Y
2960	998	5,00E-04	2,50E-04	0,149	0,421	9,35E-07	9,11	6,30	3,15E-03	168,44	27	-0,85	0,66	-0,29	-0,1071	-0,0892	-0,0378	-0,35	0,70	-0,28	Y
2960	997	5,30E-04	2,65E-04	0,087	0,246	9,17E-07	21,10	2,10	1,11E-03	431,25	69	-0,94	-	-	-0,1147	-0,0958	-0,0334	-0,29	-	-	Y
2960	997	5,30E-04	2,65E-04	0,137	0,387	8,73E-07	3,11	2,10	1,11E-03	165,56	26	-0,95	0,62	-0,27	-0,1166	-0,0976	-0,0562	-0,48	0,66	-0,28	Y
2960	997	4,60E-04	2,30E-04	0,078	0,221	8,11E-07	44,30	2,38	1,09E-03	630,04	100	-0,89	0,61	-0,25	-0,1035	-0,0862	-0,0245	-0,24	0,56	-0,24	Y
2960	1138	5,10E-04	2,55E-04	0,214	0,605	7,18E-06	40,80	2,16	1,10E-03	602,77	96	-0,91	0,77	-0,26	-0,0263	-0,026	-0,0086	-0,33	0,77	-0,22	Y
2960	1153	5,20E-04	2,60E-04	0,453	1,281	9,77E-06	3,47	2,11	1,10E-03	176,14	28	-0,89	-	-	-0,0205	-0,0207	-0,0119	-0,58	-	-	Y
2960	1142	5,60E-04	2,80E-04	0,242	0,684	7,88E-06	20,50	1,95	1,09E-03	429,14	68	-0,89	0,78	-0,22	-0,0285	-0,0281	-0,0107	-0,38	0,79	-0,21	Y
2960	998	1,77E-03	8,85E-04	0,022	0,062	9,53E-07	129,00	1,81	3,20E-03	628,50	100	-0,86	0,48	-0,11	-0,2947	-0,2893	-0,0609	-0,21	0,47	-0,13	N
2960	998	2,44E-03	1,22E-03	0,016	0,045	9,59E-07	129,00	1,31	3,20E-03	629,21	100	-0,79	0,45	-0,02	-0,3573	-0,362	-0,0836	-0,23	0,46	-0,10	N
2960	1224	1,60E-03	8,00E-04	0,500	1,414	1,14E-04	9,94	1,93	3,09E-03	177,70	28	-0,92	0,91	-0,08	-0,0163	-0,0167	-0,0099	-0,61	0,92	-0,12	Y
7800	1223	1,59E-03	7,95E-04	0,509	1,440	1,03E-04	7,92	1,99	3,16E-03	156,70	25	-1,00	0,69	-0,25	-0,063	-0,0637	-0,0353	-0,56	0,76	-0,36	Y
7800	1222	1,59E-03	7,95E-04	0,299	0,846	9,92E-05	62,10	1,99	3,16E-03	438,79	70	-1,00	0,58	-0,51	-0,0651	-0,0657	-0,0239	-0,37	0,59	-0,45	Y
7800	1223	1,59E-03	7,95E-04	0,494	1,397	1,04E-04	9,24	1,99	3,16E-03	169,26	27	-1,00	0,71	-	-0,0624	-0,0632	-0,0341	-0,55	0,75	-	Y
7800	1136	1,59E-03	7,95E-04	0,123	0,348	6,77E-06	10,10	1,99	3,16E-03	176,96	28	-1,00	-	-	-0,3654	-0,3079	-0,1526	-0,42	-	-	Y
7800	1143	1,56E-03	7,80E-04	0,138	0,390	7,92E-06	9,24	1,99	3,10E-03	170,88	27	-1,00	0,33	-0,57	-0,339	-0,2833	-0,1409	-0,42	0,38	-0,48	Y
7800	1141	1,59E-03	7,95E-04	0,083	0,235	7,54E-06	60,40	1,99	3,16E-03	432,74	69	-0,92	0,31	-0,39	-0,3519	-0,2949	-0,0905	-0,26	0,30	-0,40	Y
7800	997	1,59E-03	7,95E-04	0,024	0,068	9,21E-07	129,00	1,99	3,16E-03	632,42	101	-0,44	0,23	-0,43	-0,538	-0,5457	-0,1367	-0,25	0,21	-0,27	N
11400	998	4,90E-04	2,45E-04	0,153	0,433	9,56E-07	9,38	6,49	3,18E-03	170,10	27	-0,61	0,27	-0,77	-0,3061	-0,2684	-0,1412	-0,46	0,34	-0,70	Y
11400	997	4,90E-04	2,45E-04	0,094	0,266	9,15E-07	21,10	2,27	1,11E-03	431,38	69	-0,77	0,17	-0,35	-0,3091	-0,2724	-0,1291	-0,42	0,21	-0,53	Y
11400	997	5,10E-04	2,55E-04	0,140	0,396	8,69E-07	3,28	2,17	1,11E-03	170,51	27	-0,91	0,24	-0,71	-0,3224	-0,2879	-0,2095	-0,65	0,33	-0,71	Y
11400	997	4,00E-04	2,00E-04	0,091	0,257	8,07E-07	40,80	2,70	1,08E-03	608,77	97	-0,71	0,11	-0,07	-0,2684	-0,2322	-0,0881	-0,33	0,21	-0,54	Y
11400	1136	4,10E-04	2,05E-04	0,251	0,710	6,85E-06	45,40	2,60	1,07E-03	646,37	103	-0,72	0,34	-0,54	-0,0886	-0,0827	-0,0282	-0,32	0,42	-0,61	Y
11400	1153	4,90E-04	2,45E-04	0,317	0,897	9,84E-06	18,70	2,25	1,10E-03	407,91	65	-0,95	0,58	-0,62	-0,089	-0,084	-0,0357	-0,40	0,48	-0,58	Y
11400	1138	5,20E-04	2,60E-04	0,248	0,701	7,14E-06	20,50	2,10	1,09E-03	429,14	68	-0,82	0,45	-0,55	-0,1242	-0,1117	-0,0454	-0,37	0,40	-0,60	Y

APPENDIX C

Dataset Takahashi (1992)

rho_s (kg/m3)	d (m)	r (m)	St (-)	St.inverse (-)	nu (m2/s)	Ra (-)	beta (-)	Af (m)	w (rad/s)	f (Hz)	Vt (m/s)	V (m/s)	b0 (-)	Sigma/V (-)	Std. Dev. (m/s)	F&G (2004) Vt (m/s)	Model Vt (m/s)	Model V (m/s)	Model b0 (-)	Model valid
1380	8,00E-03	4,00E-03	0,0558	0,1578	1,001E-06	0,04	1,70	1,36E-02	5,03	0,8	-0,292	-0,286	-0,979	0,018	-0,0051	-0,295	-0,3089	-0,281	-0,953	N
1380	8,00E-03	4,00E-03	0,0499	0,1411	1,001E-06	0,05	1,70	1,36E-02	6,28	1,0	-0,292	-0,284	-0,973	0,021	-0,0060	-0,295	-0,3089	-0,279	-0,947	N
1380	8,00E-03	4,00E-03	0,0455	0,1288	1,001E-06	0,08	1,70	1,36E-02	7,54	1,2	-0,292	-0,286	-0,979	0,018	-0,0051	-0,295	-0,3089	-0,277	-0,940	N
1380	8,00E-03	4,00E-03	0,0422	0,1193	1,001E-06	0,11	1,70	1,36E-02	8,80	1,4	-0,292	-0,287	-0,983	0,019	-0,0055	-0,295	-0,3089	-0,276	-0,935	N
1380	8,00E-03	4,00E-03	0,0394	0,1116	1,001E-06	0,14	1,70	1,36E-02	10,05	1,6	-0,292	-0,288	-0,986	0,024	-0,0069	-0,295	-0,3089	-0,274	-0,929	N
1380	8,00E-03	4,00E-03	0,0372	0,1052	1,001E-06	0,18	1,70	1,36E-02	11,31	1,8	-0,292	-0,283	-0,969	0,022	-0,0062	-0,295	-0,3089	-0,273	-0,924	N
1380	8,00E-03	4,00E-03	0,0353	0,0998	1,001E-06	0,22	1,70	1,36E-02	12,57	2,0	-0,292	-0,269	-0,921	0,031	-0,0083	-0,295	-0,3089	-0,271	-0,919	N
1380	8,00E-03	4,00E-03	0,0336	0,0951	1,001E-06	0,26	1,70	1,36E-02	13,82	2,2	-0,292	-0,257	-0,880	0,026	-0,0067	-0,295	-0,3089	-0,270	-0,915	N
1350	1,27E-02	6,35E-03	0,035	0,0994	1,001E-06	0,04	1,07	1,36E-02	5,03	0,8	-0,353	-0,349	-0,989	0,029	-0,0101	-0,361	-0,3764	-0,346	-0,960	N
1350	1,27E-02	6,35E-03	0,031	0,0889	1,001E-06	0,05	1,07	1,36E-02	6,28	1,0	-0,353	-0,353	-1,000	0,021	-0,0074	-0,361	-0,3764	-0,344	-0,954	N
1350	1,27E-02	6,35E-03	0,029	0,0811	1,001E-06	0,08	1,07	1,36E-02	7,54	1,2	-0,353	-0,347	-0,983	0,021	-0,0073	-0,361	-0,3764	-0,343	-0,950	N
1350	1,27E-02	6,35E-03	0,027	0,0751	1,001E-06	0,11	1,07	1,36E-02	8,80	1,4	-0,353	-0,347	-0,983	0,026	-0,0090	-0,361	-0,3764	-0,341	-0,945	N
1350	1,27E-02	6,35E-03	0,025	0,0703	1,001E-06	0,14	1,07	1,36E-02	10,05	1,6	-0,353	-0,343	-0,972	0,021	-0,0072	-0,361	-0,3764	-0,340	-0,941	N
1350	1,27E-02	6,35E-03	0,023	0,0663	1,001E-06	0,18	1,07	1,36E-02	11,31	1,8	-0,353	-0,346	-0,980	0,025	-0,0087	-0,361	-0,3764	-0,338	-0,938	N
1350	1,27E-02	6,35E-03	0,022	0,0629	1,001E-06	0,22	1,07	1,36E-02	12,57	2,0	-0,353	-0,333	-0,943	0,027	-0,0090	-0,361	-0,3764	-0,337	-0,934	N
1350	1,27E-02	6,35E-03	0,021	0,0599	1,001E-06	0,26	1,07	1,36E-02	13,82	2,2	-0,353	-0,319	-0,904	0,033	-0,0105	-0,361	-0,3764	-0,336	-0,930	N
1250	1,59E-02	7,95E-03	0,028	0,0794	1,001E-06	0,04	0,86	1,36E-02	5,03	0,8	-0,328	-0,321	-0,979	0,04	-0,0128	-0,342	-0,3553	-0,324	-0,948	N
1250	1,59E-02	7,95E-03	0,025	0,0710	1,001E-06	0,05	0,86	1,36E-02	6,28	1,0	-0,328	-0,329	-1,003	0,038	-0,0125	-0,342	-0,3553	-0,323	-0,944	N
1250	1,59E-02	7,95E-03	0,023	0,0648	1,001E-06	0,08	0,86	1,36E-02	7,54	1,2	-0,328	-0,331	-1,009	0,023	-0,0076	-0,342	-0,3553	-0,321	-0,939	N
1250	1,59E-02	7,95E-03	0,021	0,0600	1,001E-06	0,11	0,86	1,36E-02	8,80	1,4	-0,328	-0,318	-0,970	0,03	-0,0095	-0,342	-0,3553	-0,320	-0,935	N
1250	1,59E-02	7,95E-03	0,020	0,0561	1,001E-06	0,14	0,86	1,36E-02	10,05	1,6	-0,328	-0,316	-0,963	0,031	-0,0098	-0,342	-0,3553	-0,319	-0,932	N
1250	1,59E-02	7,95E-03	0,019	0,0529	1,001E-06	0,18	0,86	1,36E-02	11,31	1,8	-0,328	-0,305	-0,930	0,042	-0,0128	-0,342	-0,3553	-0,317	-0,928	N
1250	1,59E-02	7,95E-03	0,018	0,0502	1,001E-06	0,22	0,86	1,36E-02	12,57	2,0	-0,328	-0,297	-0,905	0,04	-0,0119	-0,342	-0,3553	-0,316	-0,925	N
1250	1,59E-02	7,95E-03	0,017	0,0479	1,001E-06	0,26	0,86	1,36E-02	13,82	2,2	-0,328	-0,285	-0,869	0,026	-0,0074	-0,342	-0,3553	-0,315	-0,921	N
1380	8,00E-03	4,00E-03	0,056	0,1578	1,001E-06	0,06	2,95	2,36E-02	5,03	0,8	-0,292	-0,289	-0,990	0,033	-0,0095	-0,295	-0,3089	-0,283	-0,958	N
1380	8,00E-03	4,00E-03	0,050	0,1411	1,001E-06	0,09	2,95	2,36E-02	6,28	1,0	-0,292	-0,287	-0,983	0,019	-0,0055	-0,295	-0,3089	-0,281	-0,951	N
1380	8,00E-03	4,00E-03	0,046	0,1288	1,001E-06	0,14	2,95	2,36E-02	7,54	1,2	-0,292	-0,286	-0,979	0,022	-0,0063	-0,295	-0,3089	-0,279	-0,945	N
1380	8,00E-03	4,00E-03	0,042	0,1193	1,001E-06	0,19	2,95	2,36E-02	8,80	1,4	-0,292	-0,281	-0,962	0,025	-0,0070	-0,295	-0,3089	-0,277	-0,940	N
1380	8,00E-03	4,00E-03	0,039	0,1116	1,001E-06	0,24	2,95	2,36E-02	10,05	1,6	-0,292	-0,275	-0,942	0,022	-0,0061	-0,295	-0,3089	-0,276	-0,935	N
1380	8,00E-03	4,00E-03	0,037	0,1052	1,001E-06	0,31	2,95	2,36E-02	11,31	1,8	-0,292	-0,264	-0,904	0,035	-0,0092	-0,295	-0,3089	-0,274	-0,929	N
1380	8,00E-03	4,00E-03	0,035	0,0998	1,001E-06	0,38	2,95	2,36E-02	12,57	2,0	-0,292	-0,257	-0,880	0,024	-0,0062	-0,295	-0,3089	-0,273	-0,924	N
1380	8,00E-03	4,00E-03	0,034	0,0951	1,001E-06	0,46	2,95	2,36E-02	13,82	2,2	-0,292	-0,247	-0,846	0,035	-0,0086	-0,295	-0,3089	-0,271	-0,919	N
1350	1,27E-02	6,35E-03	0,035	0,0994	1,001E-06	0,06	1,86	2,36E-02	5,03	0,8	-0,353	-0,359	-1,017	0,049	-0,0176	-0,361	-0,3764	-0,348	-0,963	N
1350	1,27E-02	6,35E-03	0,031	0,0889	1,001E-06	0,09	1,86	2,36E-02	6,28	1,0	-0,353	-0,356	-1,008	0,034	-0,0121	-0,361	-0,3764	-0,346	-0,958	N
1350	1,27E-02	6,35E-03	0,029	0,0811	1,001E-06	0,14	1,86	2,36E-02	7,54	1,2	-0,353	-0,351	-0,994	0,037	-0,0130	-0,361	-0,3764	-0,345	-0,954	N
1350	1,27E-02	6,35E-03	0,027	0,0751	1,001E-06	0,19	1,86	2,36E-02	8,80	1,4	-0,353	-0,335	-0,949	0,065	-0,0218	-0,361	-0,3764	-0,343	-0,950	N
1350	1,27E-02	6,35E-03	0,025	0,0703	1,001E-06	0,24	1,86	2,36E-02	10,05	1,6	-0,353	-0,313	-0,887	0,034	-0,0106	-0,361	-0,3764	-0,342	-0,947	N
1350	1,27E-02	6,35E-03	0,023	0,0663	1,001E-06	0,31	1,86	2,36E-02	11,31	1,8	-0,353	-0,301	-0,853	0,051	-0,0154	-0,361	-0,3764	-0,340	-0,943	N
1350	1,27E-02	6,35E-03	0,022	0,0629	1,001E-06	0,38	1,86	2,36E-02	12,57	2,0	-0,353	-0,289	-0,819	0,027	-0,0078	-0,361	-0,3764	-0,339	-0,939	N
1350	1,27E-02	6,35E-03	0,021	0,0599	1,001E-06	0,46	1,86	2,36E-02	13,82	2,2	-0,353	-0,283	-0,802	0,032	-0,0091	-0,361	-0,3764	-0,338	-0,935	N
1250	1,59E-02	7,95E-03	0,028	0,0794	1,001E-06	0,06	1,48	2,36E-02	5,03	0,8	-0,328	-0,325	-0,991	0,031	-0,0101	-0,342	-0,3553	-0,326	-0,954	N
1250	1,59E-02	7,95E-03	0,025	0,0710	1,001E-06	0,09	1,48	2,36E-02	6,28	1,0	-0,328	-0,324	-0,988	0,028	-0,0091	-0,342	-0,3553	-0,325	-0,950	N
1250	1,59E-02	7,95E-03	0,023	0,0648	1,001E-06	0,14	1,48	2,36E-02	7,54	1,2	-0,328	-0,314	-0,957	0,035	-0,0110	-0,342	-0,3553	-0,324	-0,946	N
1250	1,59E-02	7,95E-03	0,021	0,0600	1,001E-06	0,19	1,48	2,36E-02	8,80	1,4	-0,328	-0,304	-0,927	0,049	-0,0149	-0,342	-0,3553	-0,322	-0,943	N
1250	1,59E-02	7,95E-03	0,020	0,0561	1,001E-06	0,24	1,48	2,36E-02	10,05	1,6	-0,328	-0,297	-0,905	0,044	-0,0131	-0,342	-0,3553	-0,321	-0,939	N
1250	1,59E-02	7,95E-03	0,019	0,0529	1,001E-06	0,31	1,48	2,36E-02	11,31	1,8	-0,328	-0,279	-0,851	0,043	-0,0120	-0,342	-0,3553	-0,320	-0,936	N
1250	1,59E-02	7,95E-03	0,018	0,0502	1,001E-06	0,38	1,48	2,36E-02	12,57	2,0	-0,328	-0,273	-0,832	0,041	-0,0112	-0,342	-0,3553	-0,319	-0,933	N
1250	1,59E-02	7,95E-03	0,017	0,0479	1,001E-06	0,46	1,48	2,36E-02	13,82	2,2	-0,328	-0,254	-0,774	0,033	-0,0084	-0,342	-0,3553	-0,318	-0,930	N

1380	8,00E-03	4,00E-03	0,056	0,1578	1,001E-06	0,11	5,10	4,08E-02	5,03	0,8	-0,292	-0,289	-0,990	0,041	-0,0118	-0,295	-0,3089	-0,284	-0,964	N
1380	8,00E-03	4,00E-03	0,050	0,1411	1,001E-06	0,16	5,10	4,08E-02	6,28	1,0	-0,292	-0,293	-1,003	0,046	-0,0135	-0,295	-0,3089	-0,283	-0,958	N
1380	8,00E-03	4,00E-03	0,046	0,1288	1,001E-06	0,24	5,10	4,08E-02	7,54	1,2	-0,292	-0,285	-0,976	0,082	-0,0234	-0,295	-0,3089	-0,281	-0,952	N
1380	8,00E-03	4,00E-03	0,042	0,1193	1,001E-06	0,32	5,10	4,08E-02	8,80	1,4	-0,292	-0,277	-0,949	0,034	-0,0094	-0,295	-0,3089	-0,279	-0,946	N
1380	8,00E-03	4,00E-03	0,039	0,1116	1,001E-06	0,42	5,10	4,08E-02	10,05	1,6	-0,292	-0,271	-0,928	0,026	-0,0070	-0,295	-0,3089	-0,277	-0,940	N
1380	8,00E-03	4,00E-03	0,037	0,1052	1,001E-06	0,53	5,10	4,08E-02	11,31	1,8	-0,292	-0,246	-0,842	0,062	-0,0153	-0,295	-0,3089	-0,275	-0,933	N
1380	8,00E-03	4,00E-03	0,035	0,0998	1,001E-06	0,66	5,10	4,08E-02	12,57	2,0	-0,292	-0,237	-0,812	0,058	-0,0137	-0,295	-0,3089	-0,273	-0,926	N
1380	8,00E-03	4,00E-03	0,034	0,0951	1,001E-06	0,79	5,10	4,08E-02	13,82	2,2	-0,292	-0,226	-0,774	0,055	-0,0124	-0,295	-0,3089	-0,271	-0,918	N
1350	1,27E-02	6,35E-03	0,035	0,0994	1,001E-06	0,11	3,21	4,08E-02	5,03	0,8	-0,353	-0,358	-1,014	0,044	-0,0158	-0,361	-0,3764	-0,350	-0,970	N
1350	1,27E-02	6,35E-03	0,031	0,0889	1,001E-06	0,16	3,21	4,08E-02	6,28	1,0	-0,353	-0,351	-0,994	0,054	-0,0190	-0,361	-0,3764	-0,349	-0,966	N
1350	1,27E-02	6,35E-03	0,029	0,0811	1,001E-06	0,24	3,21	4,08E-02	7,54	1,2	-0,353	-0,340	-0,963	0,037	-0,0126	-0,361	-0,3764	-0,347	-0,962	N
1350	1,27E-02	6,35E-03	0,027	0,0751	1,001E-06	0,32	3,21	4,08E-02	8,80	1,4	-0,353	-0,331	-0,938	0,069	-0,0228	-0,361	-0,3764	-0,346	-0,957	N
1350	1,27E-02	6,35E-03	0,025	0,0703	1,001E-06	0,42	3,21	4,08E-02	10,05	1,6	-0,353	-0,296	-0,839	0,044	-0,0130	-0,361	-0,3764	-0,344	-0,953	N
1350	1,27E-02	6,35E-03	0,023	0,0663	1,001E-06	0,53	3,21	4,08E-02	11,31	1,8	-0,353	-0,289	-0,819	0,018	-0,0052	-0,361	-0,3764	-0,342	-0,948	N
1350	1,27E-02	6,35E-03	0,022	0,0629	1,001E-06	0,66	3,21	4,08E-02	12,57	2,0	-0,353	-0,275	-0,779	0,049	-0,0135	-0,361	-0,3764	-0,341	-0,943	N
1350	1,27E-02	6,35E-03	0,021	0,0599	1,001E-06	0,79	3,21	4,08E-02	13,82	2,2	-0,353	-0,262	-0,742	0,051	-0,0134	-0,361	-0,3764	-0,339	-0,938	N
1250	1,59E-02	7,95E-03	0,028	0,0794	1,001E-06	0,11	2,57	4,08E-02	5,03	0,8	-0,328	-0,320	-0,976	0,027	-0,0086	-0,342	-0,3553	-0,329	-0,963	N
1250	1,59E-02	7,95E-03	0,025	0,0710	1,001E-06	0,16	2,57	4,08E-02	6,28	1,0	-0,328	-0,313	-0,954	0,032	-0,0100	-0,342	-0,3553	-0,328	-0,959	N
1250	1,59E-02	7,95E-03	0,023	0,0648	1,001E-06	0,24	2,57	4,08E-02	7,54	1,2	-0,328	-0,319	-0,973	0,05	-0,0160	-0,342	-0,3553	-0,327	-0,956	N
1250	1,59E-02	7,95E-03	0,021	0,0600	1,001E-06	0,32	2,57	4,08E-02	8,80	1,4	-0,328	-0,294	-0,896	0,045	-0,0132	-0,342	-0,3553	-0,326	-0,953	N
1250	1,59E-02	7,95E-03	0,020	0,0561	1,001E-06	0,42	2,57	4,08E-02	10,05	1,6	-0,328	-0,274	-0,835	0,052	-0,0142	-0,342	-0,3553	-0,325	-0,949	N
1250	1,59E-02	7,95E-03	0,019	0,0529	1,001E-06	0,53	2,57	4,08E-02	11,31	1,8	-0,328	-0,267	-0,814	0,053	-0,0142	-0,342	-0,3553	-0,324	-0,946	N
1250	1,59E-02	7,95E-03	0,018	0,0502	1,001E-06	0,66	2,57	4,08E-02	12,57	2,0	-0,328	-0,259	-0,790	0,027	-0,0070	-0,342	-0,3553	-0,322	-0,942	N
1250	1,59E-02	7,95E-03	0,017	0,0479	1,001E-06	0,79	2,57	4,08E-02	13,82	2,2	-0,328	-0,247	-0,753	0,048	-0,0119	-0,342	-0,3553	-0,321	-0,938	N

List of Figures

1 TSHD (http://atozhub.weebly.com/mechanical-engineers/dredging) . . . 1
2 Overflow inside the hopper and dredgeplume behind the THSD 2

2.1 Outline of the entire thesis project 13
2.2 Creating a horizontal density gradient using horizontal non-uniform oscillations . . . 15

3.1 Estimation of articles on the oscillatory motion in translation (Weinstein, 2008) . . . 17
3.2 Visual representation of all the forces in the inviscid model in two directions 18
3.3 Visual representation of all the forces in the BBO-equation in two directions 21
3.4 Correction to the Stokes drag law at high particle Reynolds numbers 23

4.1 Piecewise continuous sawtooth function (Boyce et al., 1969) 28
4.2 Fluid displacement using uniform and non-uniform oscillations $(ki = 1)$ 29
4.3 Fluid displacement using uniform and non-uniform oscillations $(ki = 1.05)$ 30
4.4 Fluid displacement using uniform and non-uniform oscillations $(ki = 21)$ 30
4.5 Fluid velocity using uniform and non-uniform oscillations $(ki = 1.05)$ 31
4.6 Fluid velocity using uniform and non-uniform oscillations $(ki = 21)$ 31
4.7 Fluid acceleration using uniform and non-uniform oscillations $(ki = 1.05)$ 32
4.8 Fluid acceleration using uniform and non-uniform oscillations $(ki = 21)$ 32
4.9 Fourth order Runge-Kutta method 33
4.10 Retardation versus inverse Stokes number (δ), particle density variation 35
4.11 Retardation versus inverse Stokes number (δ), fluid amplitude variation 36
4.12 Fluid density (ρ_f) as function of glycerol fraction with $T \approx 15$ °C 37
4.13 Retardation validation using experimental data 37
4.14 Amplitude ratio validation using experimental data 38
4.15 Phase lag validation using experimental data 39
4.16 Retardation versus inverse Stokes number, particle density variation 40
4.17 Retardation versus inverse Stokes number, standard deviation included 41
4.18 Retardation versus inverse Stokes number, fluid amplitude variation 41
4.19 Retardation versus inverse Stokes number, fluid amplitude variation 42
4.20 Retardation validation using experimental data 43

5.1 Horizontal particle response velocity u_{pot}, uniform oscillations $\gamma > 1$ 46
5.2 Horizontal particle response velocity u_{pot}, uniform oscillations $\gamma < 1$ 46
5.3 Decoupling as function of density ratio (γ) for the inviscid model 47
5.4 Horizontal non-uniform particle response velocity $u_{w,pot}$, $ki = 1.05$ 48
5.5 Horzontal non-uniform particle response velocity $u_{w,pot}$, single wave 49
5.6 Horizontal non-uniform particle response velocity $u_{w,pot}$, $ki = 21$ 49
5.7 Horizontal non-uniform particle response velocity $u_{w,pot}$, single wave 50
5.8 Vertical particle response velocity v_{pot}, $\gamma > 1$ 51
5.9 Vertical particle response velcoity v_{pot}, $\gamma > 1$ 52
5.10 Vertical particle response velcoity v_{pot}, $\gamma < 1$ 52
5.11 Vertical non-uniform particle response velocity $v_{w,pot}$, $ki = 1.05$ 53
5.12 Vertical non-uniform particle response velocity $v_{w,pot}$, $ki = 21$ 54

6.1 Horizontal particle response velocity u, uniform oscillations $\gamma > 1$, $d = 0.1\ mm$ . . . 56
6.2 Horizontal particle response velocity u, uniform oscillations $\gamma > 1$, $d = 2\ mm$ 57
6.3 Horizontal particle response velocity u, uniform oscillations $\gamma < 1$, $d = 2\ mm$ 57
6.4 Horizontal particle response velocity u_w, $\gamma > 1$, $d = 0.1\ mm$ 58
6.5 Horizontal particle response velocity u_w, $\gamma > 1$, $d = 0.1\ mm$ 59
6.6 Decoupling (A_p/A_f) as function of frequency (f) 60
6.7 Decoupled motion for uniform and non-uniform oscillations, $f = 5\ Hz$ 61
6.8 Decoupled motion for uniform and non-uniform oscillations, $f = 80\ Hz$ 61
6.9 Phase angle (φ) as function of frequency (f) 62
6.10 Decoupling (A_p/A_f) as function of viscosity (ν_f), uniform oscillations 63
6.11 Decoupling (A_p/A_f) as function of viscosity (ν_f), non-uniform oscillations 64
6.12 Phase angle (φ) as function of viscosity (ν_f), uniform oscillations 65
6.13 Phase angle (φ) as function of viscosity (ν_f), non-uniform oscillations 66
6.14 Average migration velocities $(\bar{u}$ & $\bar{u_w})$ as function of the inverse Stokes number (δ) . 67
6.15 Relative particle displacement $(u_x$ & $u_{wx})$ at $\delta \approx 3.57$, $A_f = 1\ mm$ 68
6.16 Relative particle displacement u_x & u_{wx} at $\delta \approx 2.52$, $A_f = 5\ mm$ 68
6.17 Relative particle displacement u_x & u_{wx} at $\delta \approx 2.52$, $A_f = 5\ mm$ 69
6.18 Forces due to uniform fluid oscillations at inverse Stokes number, $\delta \approx 3.57$ 70
6.19 Average forces due to uniform fluid oscillations at inverse Stokes number, $\delta \approx 3.57$. 70
6.20 Forces due to non-uniform fluid oscillations, $ki = 1.05$, $\delta \approx 3.57$ 72
6.21 Average forces due to non-uniform fluid oscillations, $ki = 1.05$, $\delta \approx 3.57$ 72
6.22 Forces due to non-uniform fluid oscillations, $ki = 1.05$, $\delta \approx 2.52$ 73
6.23 Average forces due to non-uniform fluid oscillations, $ki = 1.05$, $\delta \approx 2.52$ 73
6.24 Forces due to non-uniform fluid oscillations, $ki = 21$, $\delta \approx 3.57$ 75
6.25 Average forces due to non-uniform fluid oscillations, $ki = 21$, $\delta \approx 3.57$ 75
6.26 Forces due to non-uniform fluid oscillations, $ki = 21$, $\delta \approx 2.52$ 76
6.27 Average forces due to non-uniform fluid oscillations, $ki = 21$, $\delta \approx 2.52$ 76
6.28 Vertical particle response velocity v, uniform oscillations $\gamma > 1$, $d = 0.1\ mm$ 77
6.29 Vertical particle response velocity v, uniform oscillations $\gamma > 1$, $d = 2\ mm$ 78
6.30 Vertical particle displacement v_y & $v_{t,y}$, uniform oscillations $\gamma > 1$ 78
6.31 Vertical particle response velocity v, uniform oscillations $\gamma < 1$, $d = 0.1\ mm$ 79
6.32 Vertical particle response velocity v_w, $\gamma > 1$, $d = 0.1\ mm$, $ki = 1.05$ 80
6.33 Vertical particle response velocity v_w, $\gamma > 1$, $d = 0.1\ mm$, $ki = 1.05$ 81
6.34 Vertical particle response velocity v_w, $\gamma > 1$, $d = 0.1\ mm$, $ki = 21$ 81
6.35 Particle retardation $b0$ & $b1$ as function of the inverse Stokes number (δ) 82

6.36 Forces due to uniform fluid oscillations at inverse Stokes number $\delta \approx 3.57$ 84
6.37 Average forces due to uniform fluid oscillations at inverse Stokes number $\delta \approx 3.57$. 84
6.38 Forces due to non-uniform fluid oscillations, shape factor $ki = 1.05$, $\delta \approx 3.57$ 85
6.39 Average forces due to non-uniform oscillations, shape factor $ki = 1.05$, $\delta \approx 3.57$ . . 85
6.40 Forces due to non-uniform fluid oscillations, shape factor $ki = 1.05$, $\delta \approx 2.52$ 86
6.41 Average forces due to non-uniform oscillations, shape factor $ki = 1.05$, $\delta \approx 2.52$ . . 86
6.42 Forces due to non-uniform fluid oscillations, shape factor $ki = 21$, $\delta \approx 3.57$ 88
6.43 Average forces due to non-uniform oscillations, shape factor $ki = 21$, $\delta \approx 3.57$ 88
6.44 Forces due to non-uniform oscillations, shape factor $ki = 21$, $\delta \approx 2.52$ 89
6.45 Average forces due to non-uniform oscillations, shape factor $ki = 21$, $\delta \approx 2.52$ 89

Bibliography

M. Abbad and M. Souhar. Effects of the history force on an oscillating rigid sphere at low reynolds number. *Experiments in fluids*, 36(5):775–782, 2004a.

M. Abbad and M. Souhar. Experimental investigation on the history force acting on oscillating fluid spheres at low reynolds number. *Physics of Fluids (1994-present)*, 16(10):3808–3817, 2004b.

C.M. Atkinson and H.K. Kytömaa. Acoustic wave speed and attenuation in suspensions. *International Journal of multiphase flow*, 18(4):577–592, 1992.

M.H.I. Baird, M.G. Senior, and R.J. Thompson. Terminal velocities of spherical particles in a vertically oscillating liquid. *Chemical Engineering Science*, 22(4):551–558, 1967.

A. B. Basset. On the motion of a sphere in a viscous liquid. *Philosophical Transactions of the Royal Society of London. A*, 179:43–63, 1888.

E. Benes, M. Gröschl, H. Nowotny, F. Trampler, T. Keijzer, H. Böhm, S. Rade, L. Gherardini, J.J. Hawkes, R. König, et al. Ultrasonic separation of suspended particles. In *Ultrasonics Symposium, 2001 IEEE*, volume 1, pages 649–659. IEEE, 2001.

J.V. Boussinesq. Sur la résistance qu'oppose un liquide indéfini en repos. *CR Acad. Sci. Paris*, 100: 935–937, 1885.

L. Boyadzhiev. On the movement of a spherical particle in vertically oscillating liquid. *Journal of Fluid Mechanics*, 57(03):545–548, 1973.

W.E. Boyce, R.C. DiPrima, and C.W. Haines. *Elementary differential equations and boundary value problems*, volume 9. Wiley New York, 1969.

R. Clift, J.R. Grace, and M.E. Weber. Bubbles, drops and particles. *Academic Press, New York*, 1978.

C.F.M. Coimbra, D. L'ESPERANCE, R.A. Lambert, J.D. Trolinger, and R.H. Rangel. An experimental study on stationary history effects in high-frequency stokes flows. *Journal of Fluid Mechanics*, 504: 353–363, 2004.

P.J.T. Dankers. *On the hindered settling of suspensions of mud and mud-sand mixtures*. PhD thesis, Delft University of Technology, October 2006.

R.I. Ferguson and M. Church. A simple universal equation for grain settling velocity. *Journal of Sedimentary Research*, 74(6):933–937, November 2004.

S. Gupta, R. Sundaram, and S. Gupta. Dynamic compaction to mitigate liquefaction potential. *The Masterbuilder*, pages 190–194, June 2013.

J. J. Hawkes and W. T. Coakley. A continuous flow ultrasonic cell-filtering method. *Enzyme and microbial technology*, 19(1):57–62, 1996.

R.A. Herringe. On the motion of small spheres in oscillating liquids. *The Chemical Engineering Journal*, 11(2):89–99, 1976.

R.A. Herringe. A study of particle motion induced by two-dimensional liquid oscillations. *International Journal of Multiphase Flow*, 3(3):243–253, 1977.

R.A. Herringe and L.R. Flint. Particle motion in vertically oscillated liquids. In *Fifth Australian Conference on Hydraulics and Fluid Mechanics*, pages 103–110, December 1974.

G. Houghton. The behaviour of particles in a sinusoidal velocity field. In *Proceedings of the Royal Society of London A: Mathematical, Physical and Engineering Sciences*, volume 272, pages 33–43. The Royal Society, 1963.

G. Houghton. Particle trajectories and terminal velocities in vertically oscillating fluids. *The Canadian Journal of Chemical Engineering*, 44(2):90–95, 1966.

G. Houghton. Particle retardation in vertically oscillating fluids. *The Canadian Journal of Chemical Engineering*, 46(2):79–81, 1968.

T. Kajishima and S. Takiguchi. Interaction between particle clusters and particle-induced turbulence. *International Journal of Heat and Fluid Flow*, 23(5):639–646, 2002.

S.K. Karanfilian and T.J. Kotas. Drag on a sphere in unsteady motion in a liquid at rest. *Journal of Fluid Mechanics*, 87(01):85–96, 1978.

C. Kranenburg and H.J. Geldof. Concentration effects on settling-tube analysis. Internal report 74 - 1, Delft University of Technology, Department of Civil Engineering, 1974.

Ph. H. Kuenen. Settling convection and grain-size analysis. *Journal of Sedimentary Research*, 38(3): 817–831, 1968.

R.H.A. Kuypers and N. Stam. Hopperbezinkingstests schanulleke 2012. Technical Report D-RKu-13002, IHC Dredgers B.V., Mei 2013a. (in Dutch).

R.H.A. Kuypers and N. Stam. Rapport verificatie shs metingen achteraf. Technical Report R3, IHC Dredgers B.V., April 2013b. (in Dutch).

R.H.A. Kuypers and N. Stam. Hopperbezinkingtests asterix. Technical Report D-RKu-14043, IHC Holland B.V., November 2014. (in Dutch).

R.H.A. Kuypers, N. Stam, and E.C. Van der Blom. Enhanced hopper settling (ehs). Technical Report R3, IHC Dredgers B.V. and Stamsolve B.V., Juli 2011. (in Dutch).

G. J. Kynch. A theory of sedimentation. *Trans. Faraday Soc.*, 48:166–176, 1952.

K. R. Massarsch. Deep soil compaction using vibratory probes. In *American Society for Testing and Material, ASTM, Symposium on Design, Construction, and Testing of Deep Foundation Improvement: Stone Columns and Related Techniques, Philadelphia. Edited by RC Bachus. ASTM Special Technical Publication, STP*, volume 1089, pages 297–319, 1991.

V. Matousek. *Dredge pumps and slurry transport.* Delft, University of Technology, September 2004.

M.R. Maxey and J.J. Riley. Equation of motion for a small rigid sphere in a nonuniform flow. *Physics of Fluids (1958-1988)*, 26(4):883–889, 1983.

P.W. Mayne, J.S. Jones Jr., and J.C. Dumas. Ground response to dynamic compaction. *Journal of Geotechnical Engineering*, 110(6):757–774, June 1984.

L.L. Minkov, Y.O. Stepanova, J. Dueck, and E.V. Pikushchak. On the accelerated settling of fine particles in a bidisperse slurry. *Mathematical Problems in Engineering*, 2015, 2015.

F. Odar. Verification of the proposed equation for calculation of the forces on a sphere accelerating in a viscous fluid. *Journal of Fluid Mechanics*, 25(03):591–592, 1966.

F. Odar and W.S. Hamilton. *Forces on a sphere accelerating in a viscous fluid.* Cambridge Univ Press, 1964.

S.C. Ooijens, A. de Gruijter, A.A.H. van Nieuwenhuijzen, and S. Vandycke. Research on hopper settlement using large-scale modelling.

C.W. Oseen. Hydromechanik. *Leipzig: Akademische Verlag*, 1927.

J.L. Pan and A.R. Selby. Simulation of dynamic compaction of loose granular soils. *Advances in Engineering Software*, 33(7):631–640, 2002.

N.R. Paterson. Seismic wave propagation in porous granular media. *Geophysics*, 21(3):691–714, July 1956.

J. E. Prest, B. J. T. Brown, P. R. Fielden, S. J. Wilkinson, and J. J. Hawkes. Scaling-up ultrasound standing wave enhanced sedimentation filters. *Ultrasonics*, 56:260–270, 2015.

J.F. Richardson and W.N. Zaki. Sedimentation and fluidisation: Part 1. *Transactions of the institution of Chemical Engineers*, 32:35–53, 1954.

P.N. Rowe. A convenient empirical equation for estimation of the richardson-zaki exponent. *Chemical Engineering Science*, 1987.

N. Stam. Verbetering van laadefficiency van sleephopperzuigers door toepassing van smart hopper settling (shs). Technical Report Rev. 3, Stamsolve B.V., Musselkanaal, Maart 2007. (in Dutch).

G.G. Stokes. *On the effect of the internal friction of fluids on the motion of pendulums*, volume 9. Pitt Press, 1851.

K. Takahashi, M. Katayama, and K. Endoh. An approximate method evaluating the particle terminal velocities in accelerating fluid flows. *Memoirs of the Faculty of Engineering, Hokkaido University*, 18(3):15–25, 1992.

S. Te Slaa, D.S. van Maren, and J.C. Winterwerp. On the hindered settling of silt-water mixtures. *Int. Conference on Estuaries and Coasts*, October 2012.

E.B. Tunstall and G. Houghton. Retardation of falling spheres by hydrodynamic oscillations. *Chemical Engineering Science*, 23(9):1067–1081, 1968.

R.G. Van de Wetering. The influence of shock waves on the hindered settling process and the amount of deposited material in time. Technical report, Delft University of Technology, April 2015a. Thesis proposal.

R.G. Van de Wetering. The influence of shock waves on the hindered settling process and the amount of deposited material in time. Technical report, Delft University of Technology, October 2015b. Thesis Literature Study.

R.M. Van Oeveren and G. Houghton. Levitation and counter-gravity motion of spheres by non-uniform hydrodynamic oscillations. *Chemical Engineering Science*, 26(11):1958–1961, 1971.

C. Van Rhee. *On the sedimentation process in a trailing suction hopper dredger*. PhD thesis, Delft, University of Technology, December 2002.

J.M. Van Wijk. Hopperbezinkingtests schanulleke 2012 - analyse en theorievorming rondom shs proeven. Technical Report M13-107, MTI Holland B.V., April 2013. (in Dutch).

A. Verruijt. *Soil Mechanics*. Delft University of Technology, November 2011.

J.A. Weinstein. *The motion of bubbles and particles in oscillating liquids with applications to multiphase flow in Coriolis meters*. PhD thesis, University of Colorado, 2008.

H. Wenliang, D. Zengnan, and C. Hong. Water hammer in pipelines with hyperconcentrated slurry flows carrying solid particles. *SCIENCE CHINA Technological Sciences*, 41(4):337 – 347, 1998.

G. Whitworth and W. T. Coakley. Particle column formation in a stationary ultrasonic field. *The Journal of the Acoustical Society of America*, 91(1):79–85, 1992.

G. Whitworth, M.A. Grundy, and W.T. Coakley. Transport and harvesting of suspended particles using modulated ultrasound. *Ultrasonics*, 29(6):439–444, 1991.

J.C. Winterwerp. On the flocculation and settling velocity of estuarine mud. *Continental Shelf Research*, 22:1339 – 1360, 2002.